NAVAL POSTGRADUATE SCHOOL
Monterey, California

THESIS

THE EFFECT OF WESTERLY WIND BURSTS ON A TROPICAL OCEAN GENERAL CIRCULATION MODEL

by

Charles A. Weddle

December, 1993

Thesis Advisor: James Thomas Murphree
Co-Advisor: Roland W. Garwood,JR.

REPORT DOCUMENTATION PAGE

Form Approved
OMB No. 0704-0188

1. AGENCY USE ONLY (Leave blank)	2. REPORT DATE	3. REPORT TYPE AND DATES COVERED
	16 Dec 93	Master's Thesis

4. TITLE AND SUBTITLE
THE EFFECTS OF WESTERLY WIND BURSTS ON A TROPICAL OCEAN GENERAL CIRCULATION MODEL.

5. FUNDING NUMBERS

6. AUTHOR(S)
Weddle, Charles Alan

7. PERFORMING ORGANIZATION NAME(S) AND ADDRESS(ES)
Naval Postgraduate School
Montery, CA 93943-5000

8. PERFORMING ORGANIZATION REPORT NUMBER

9. SPONSORING/MONITORING AGENCY NAME(S) AND ADDRESS(ES)
Naval Postgraduate School
Monterey, CA 93943-5000

10. SPONSORING/MONITORING AGENCY REPORT NUMBER

11. SUPPLEMENTARY NOTES
The views expressed in this thesis are those of the author and do not reflect the official policy or position of the Department of Defense or the U. S. Navy

12a. DISTRIBUTION/AVAILABILITY STATEMENT
Unclassified/Unlinited

12b. DISTRIBUTION CODE
A

13. ABSTRACT *(Maximum 200 words)*

A primitive equation general circulation model with imbedded mixed layer physics has been used to investigate the response of the equatorial Pacific ocean to daily varying winds and westerly wind bursts. The major issue addressed by this study is the impact of daily varying winds, including westerly wind bursts, in the modeling of the tropical Pacific ocean and El Nino.

In the developmental phase, the sensitivity of the model to the integration time step and the domain size were investigated. The results of this work were used to determine the optimal time step and model domain size for the main experimental runs.

In the experimental phase, the model was spun-up using time averaged wind stresses. The model ocean was then exposed to two-years of realistic daily varying wind stresses covering the period of 1991 and 1992. The model developed an El Nino like response that corresponded in several respects with observed features of the 1991-92 El Nino. The model alsc developed tropical instability waves in the

14. SUBJECT TERMS	15. NUMBER OF PAGES
El Nino, westerly wind burst, OGCM, mixed layer depth	141
	16. PRICE CODE

17. SECURITY CLASSIFICATION OF REPORT	18. SECURITY CLASSIFICATION OF THIS PAGE	19. SECURITY CLASSIFICATION OF ABSTRACT	20. LIMITATION OF ABSTRACT
UNCLASSIFIED	UNCLASSIFIED	UNCLASSIFIED	UL

Continuation page of SF298 block 13 abstract

eastern Pacific similar to those observed in situ and in satellite SST images. The model's responses to the tropical cyclones that occurred during 1991-92 were also consistent in several ways with observations.

Approved for public release; distribution is unlimited.

The Effect of Westerly Wind Bursts on a Tropical Ocean General Circulation Model

by

Charles A. Weddle
Lieutenant United States Navy
B.S., East Texas State University, 1984

Submitted in partial fulfillment
of the requirements for the degree of

MASTER OF SCIENCE IN METEOROLOGY
and
MASTER OF SCIENCE IN PHYSICAL OCEANOGRAPHY

from the

NAVAL POSTGRADUATE SCHOOL
December 1993

Author: _____
Charles A. Weddle

Approved by: _____
James Thomas Murphree, Thesis Advisor

_____
Roland W. Garwood, Jr., Co-Advisor

_____
Robert L. Haney, Chairman
Department of Meteorology

_____
Curtis A. Collins, Chairman
Department of Oceanography

ABSTRACT

A primitive equation general circulation model with imbedded mixed layer physics has been used to investigate the response of the equatorial Pacific ocean to daily varying winds and westerly wind bursts. The major issue addressed by this study is the impact of daily varying winds, including westerly wind bursts, in the modeling of the tropical Pacific ocean and El Niño.

In the developmental phase, the sensitivity of the model to the integration time step and the domain size were investigated. The results of this work were used to determine the optimal time step and model domain size for the main experimental model runs.

In the experimental phase, the model was spun-up using time averaged wind stresses. The model ocean was then exposed to two years of realistic daily varying wind stresses covering the period of 1991 and 1992. The model developed an El Niño like response that corresponded in several respects with observed features of the 1991-92 El Niño. The model also developed tropical instability waves in the eastern Pacific similar to those observed in situ and in satellite SST images. The model's responses to the tropical cyclones that occurred during 1991-92 were also consistent in several ways with observations.

TABLE OF CONTENTS

LIST OF FIGURES

LIST OF SYMBOLS

EUC	Equatorial Undercurrent
SECC	South Equatorial Countercurrent
NECC	North Equatorial Countercurrent
NEC	North Equatorial Current
SEC	South Equatorial Current
OTIS	Optimal Thermal Interpolation Scheme
NOGAPS	Navy Operational Global Atmospheric Prediction System
TOGA	Tropical Ocean-Global Atmosphere
COARE	Coupled Ocean-Atmosphere Response Experiment
SOI	Southern Oscillation Index
ITCZ	Intertropical Convergence Zone
OGCM	Ocean General Circulation Model
NRL	Naval Research Laboratory

I. INTRODUCTION

A. EL NIÑO AND WESTERLY WIND BURSTS

The El Niño/Southern Oscillation (ENSO) phenomenon has received much scientific interest due to its global impact on the oceans and the atmosphere. The Tropical Ocean Global Atmosphere Coupled Ocean Atmosphere Response Experiment (TOGA-COARE) has as one of its major goals to provide additional detailed information to better understand the air-sea interaction in the tropics and ENSO (Webster and Lukas 1992). Although much is known about ENSO events and the changes that take place in the Pacific during these events, no single theory can yet explain all of the factors leading to an El Niño or what causes the ocean to return to its pre-El Niño state.

Prior to the onset of an El Niño event, the atmospheric sea level pressure gradient weakens between Darwin and Tahiti, with the pressure at Darwin rising and the pressure at Tahiti falling. This pressure change is measured by the Southern Oscillation Index (SOI). El Niño events are associated with negative SOI values. A change in the atmospheric sea level pressure gradient can decrease the trade wind easterlies allowing warm water to flow to the east, which contributes to large scale warming in the eastern Pacific. However, we can

also follow the opposite path to get to the same result. Warm water flowing to the east can cause warming which will change the pressure gradient and weaken the trade wind easterlies. This feedback mechanism between the ocean and the atmosphere makes the prediction, modeling, and understanding of El Niño extremely difficult. Obviously, the complex interactions between the atmosphere and ocean are of crucial importance to the understanding of the problem (Philander et al. 1989). This study focuses on the importance of the forcing applied to the ocean by the wind.

Several theories have been proposed on the role that westerly wind bursts play in the weakening of the trade winds (e.g., McPhaden 1988; Wyrtki 1975; Giese and Harrison 1991; Philander 1981). Keen (1982) proposed that sea surface temperature (SST) changes in the tropical Pacific at the start of an ENSO create favorable conditions for the formation of westerly winds and, specifically, for the development of tropical cyclone pairs that lead to large westerly wind bursts. Giese and Harrison (1990) suggested that a series of westerly wind bursts timed to have an additive effect could be the trigger for an El Niño and/or help to maintain an El Niño. Thus, westerly wind bursts may play an important role in both the onset and maintenance of El Niño events.

Definitions of a westerly wind event or burst vary. Riehl (1979) used the term to describe anomalous low-level synoptic scale westerly winds. This definition includes the relaxation

of normal easterly flow. Thus, for example, a sudden decrease from normally strong easterly flow to weak easterly flow would be considered a westerly wind burst (Luther et al. 1983). I will use Riehl's definition in this paper.

Numerous sources of westerly wind bursts in the tropics have been found. If, during the northern winter, the Siberian anticyclone shifts south, sea level pressure in the tropical western Pacific may rise and lead to westerly winds (Chu 1988). A surge of the trade winds in the northern hemisphere that pushes the intertropical convergence zone (ITCZ) south of 10°S can lead to westerly winds at the equator (Riehl 1979). Also, the formation of a pair of tropical cyclones, with one north and one south of the equator, can cause intense westerly winds for extended periods of time (Keen 1982). A single tropical cyclone can also cause westerly wind bursts and may cause westerly wind bursts that precede or lag the time the storm intensifies to strength T4 (32 m/s) by up to seven days (Harrison and Giese 1991).

Westerly wind bursts occur frequently in the tropical Pacific. Rasmusson and Carpenter (1982) have developed a classification scheme of westerly wind bursts based on the latitude of the wind burst. Their study showed that there is an increase in the number of events just prior to and during an El Niño event and that most of the wind events at the start of an event are either centered on or just south of the equator. They found that wind events to the north of the

equator, or to the far south of the equator, are not as closely linked to the start of an El Niño.

Westerly wind bursts are probably not sufficient in and of themselves to cause an El Niño. Wyrtki (1975) proposed that the Pacific must be preconditioned in order for an El Niño event to occur. He found that before most El Niño events there was an increase in strength of the southeasterly winds for up to two years. These stronger winds would increase the amount of warm water piling up in the tropical western Pacific and set the stage for the warm water to surge back to the east. This combination of a preconditioned ocean with strong westerly wind bursts is more likely to cause an El Niño than the westerlies alone.

Philander (1981) suggested that the warming of the equatorial central Pacific during an El Niño event causes westerly wind bursts by weakening the easterly winds. These changes in the winds will tend to maintain the event.

Westerly wind bursts may initiate or enhance an El Niño by several processes. In an observational study, Cooper (1992) found that a westerly wind burst can have a local as well as a remote response. Locally it can cause a reversal of the South Equatorial Current (SEC), downwelling, and a deepening of the thermocline. Some extremely strong events can even cause an eastward surface current (a Yoshida jet) to develop (McPhaden et al. 1988). The remote response is in the form of an equatorially trapped Kelvin wave that can travel across the

entire Pacific (e.g., Delcroix 1991, Cooper 1992). These eastward currents and the currents associated with the Kelvin wave can lead to the advection of warm sea surface temperatures (SSTs) thus contributing to the warming in the tropical eastern Pacific (Harrison and Schopf 1984). These Kelvin waves also cause a rise in the ocean surface and a deepening of the thermocline.

Due to the small amount of data that has been collected in the tropical Pacific that can be used to study El Niño, models are needed to fill in the gaps. These models can not only provide insight into what is observed in the oceans, they can also point out areas where more observation is needed.

B. NUMERICAL MODELING IN THE TROPICS

A wide variety of models with varying complexity have been used to simulate the ENSO phenomenon. The earliest attempts to model the ENSO phenomenon used very simple conceptual models. These types of models are useful for determining the types of waves and instabilities that may play a role in El Niño. McCreary and Anderson (1991) provide a good review of these models.

Models of intermediate complexity have also been useful. These models use detailed physics but are limited in some way. For example, they may use a limited domain, or they may prescribe the atmosphere in terms of specified atmospheric

parameters, and then evaluate the ocean's response as these parameters are varied.

The most complex kind of model is the coupled global circulation model. These models combine an atmospheric model with an ocean model and use the solutions from each model to force the other one. Presently many problems still exist with coupled models. These problems include climate drifts that slowly cool the atmosphere and the ocean, and nonlinear instabilities. For a good review of several coupled models and the problems inherent in them, see McCreary and Anderson (1991) or Charnock and Philander (1989).

To lay the groundwork for the work done in this paper, this review will concentrate on work with ocean models having specified atmospheric forcing. These models have received considerable attention and have greatly enhanced our understanding of the ENSO process.

McCreary (1976) used a simple analytical model with two layers to simulate the tropical Pacific circulation. Although this model did not attempt to accurately duplicate the structure of the Pacific, it did show that changes in the winds near the equator caused a greater response than do winds some distance away (±5° of latitude). The model also was able to produce a response which resembled an El Niño in many ways. Later efforts with the same model, after some improvements, showed that if the winds are linked to the sea surface temperature so that a warming in the east weakens the winds,

the model oscillated on time scales similar to observed El Niño scales (McCreary and Anderson 1984). An example of attempts to use more realistic physics in the modeling problem can be seen in Semtner and Holland's (1980) work using a primitive equation model with 14 levels. Although this model was limited in basin size and had a constant wind stress, it did develop many of the features of the tropical Pacific ocean.

The next step toward investigating El Niño came when these models were exposed to realistic forcings. Latif (1986) ran a primitive equation model forced with real wind data for several decades. Although the wind fields he used had all been smoothed or were interpolated from monthly mean values, he did obtain relatively realistic simulations of the climatologic currents and temperature fields for the Pacific. The model was also used to simulate the 1982-83 El Niño. The model developed an El Niño-like response, with tropical eastern Pacific SST anomalies as large as 4°C. A weakened equatorial undercurrent and eastward surface currents were also produced. Philander et al. (1987) used a primitive equation model of the tropical Pacific with a 33 km meridional grid near the equator increasing to 200 km at about 27° (the northern boundary was at 50°N and the southern boundary was at 28°S) and a fixed 100 km spacing in the longitudinal direction. This model included land masses if they projected into the area of interest; otherwise, solid boundaries were

used to close the domain. The model was integrated for several years with monthly mean winds. The model developed all of the major currents of the Pacific equatorial region and showed the seasonal dependence of these currents.

Miller et al. (1992) used a primitive equation model in isopycnic coordinates with an imbedded bulk mixed layer model and prescribed climatologic monthly mean atmospheric temperature, humidity, cloudiness, and turbulent kinetic energy in the form of u* (surface friction velocity). The wind stresses were smoothed monthly means interpolated to daily values. Although the model did develop the major currents and was within one degree of the real sea surface temperature for most of the domain, the speeds of the currents were only about 50% of those observed.

Whitney (1992) used an ocean model with an imbedded mixed layer model to evaluate the importance of detailed modeling of the upper layers of the ocean. She exposed her model to a highly smoothed time varying wind to evaluate the model's response to westerly wind events. Her results showed that detailed modeling of the mixed layer of the ocean is very important in correctly modeling El Niño.

These models have succeeded in simulating several, but not all, of the major ocean features of El Niño.

C. UNRESOLVED PROBLEMS

Most of the modeling efforts to date have looked at the responses to long term or monthly changes in the winds, while the observational studies (Cooper 1992, Chen et al. 1988) indicate that the daily and weekly fluctuations of the wind can play an important part in the structure of the ocean currents.

The focus of this study is on the effects of the daily to weekly variations in wind forcing and the role they play in an El Niño event and in the development of the temperature and current patterns in the tropical Pacific ocean. In this study, I test the hypothesis that the inclusion of the short term variability in the winds over the Pacific is extremely important in the development of a realistic El Niño response, and in developing a realistic model of the tropics.

Since the effect of the wind is initially at the surface, the model used for this study is a general circulation model with explicit mixed layer physics to enhance the modeling of the changes due to wind forcing. This model was first used by Whitney (1992) to examine the response of the tropical Pacific Ocean to fixed and variable winds. The relatively simple atmospheric forcing used in this model allows for the isolation of independent forcing terms to study their individual effects on the model ocean.

The wind stresses used for this study were developed from the U. S. Navy's Operational Global Atmospheric Prediction

System (NOGAPS) daily average surface wind analyses without any spatial smoothing. In the final model runs, the model was initially spun-up with a two-year time mean wind stress calculated from the daily NOGAPS winds for 1 January 1991 through 31 December 1992. The model was then run out for two years using the actual daily average wind stresses, in an attempt to model the 1991-92 El Niño.

The goals of this study are:

1. To further refine the model first used by Whitney (1992) to study the tropical Pacific.
2. To test the model with realistic daily wind stress forcing.
3. To examine the model's waves and currents created by westerly wind bursts.
4. To perform sensitivity studies to identify ways to improve the model.

Chapter II contains a description of the model and the wind stress fields used in this experiment. Chapter III contains the results of some of the developmental and the experimental model runs. Chapter IV is a discussion of the results of the model runs, some conclusions, and suggestions for further improvements to the model and areas needing further investigation.

II. THE MODEL

A. MODEL FUNDAMENTALS

The model used for this study is a 15-level primitive equation ocean general circulation model (OGCM) with an imbedded bulk mixed layer model. The model was originally developed in radial coordinates and used to study the ocean response to a hurricane (Adamec et al. 1981). The model has since been reformulated in cartesian coordinates and has proven to be extremely versatile. Whitney (1992) adapted the model for use in the equatorial region and performed much of the initial developmental work for application to the tropical oceans. The model for this study is basically the same as that developed and tested by Whitney (1992). However, a few minor modifications have been made to improve the dynamics and response of the model.

The OGCM portion of the model was originally developed by Haney (1974) as a 6-level primitive equation model used to study oceanic responses to large-scale heat and momentum fluxes.

The mixed layer model was developed by Garwood (1977) and is based on the turbulent kinetic energy equation. The model assumes that the water column below the mixed layer is dynamically stable, and the mixed layer is dynamically

unstable. Thus, the mixed layer depth is the depth to which turbulent mixing penetrates. The temperature and horizontal velocity in the mixed layer are assumed to be vertically homogeneous. Mixed layer conditions are allowed to change due to surface fluxes, advection, and entrainment.

Adamec et al. (1981) incorporated the Garwood mixed layer model into Haney's OGCM to give an OGCM with realistic surface layer physics. Interaction between the fixed level OGCM and the mixed layer portion occurs in two steps. First, the dynamic portion of the model calculates advective and diffusive changes for the mixed layer model. The mixed layer model then computes changes in mixed layer depth, velocity, and temperature due to surface fluxes and entrainment and passes the information back to the dynamic part of the model. For more information on the coupling of the two models, see Adamec et al. (1981).

The basic assumptions of the model are as follows:

1. The ocean is hydrostatic and incompressible.
2. Density is a function of temperature only.
3. Vertical velocity is zero at the ocean surface and at the bottom.
4. All of the boundaries (other than the ocean surface) are treated as free slip surfaces.
5. Heat is allowed to diffuse through the north and south boundaries.

These conditions do not allow a barotropic mode. Laplacian diffusion is used in the horizontal momentum and temperature tendency equations to simulate subgrid scale horizontal fluxes of heat and momentum. Vertical turbulent fluxes below the mixed layer are also parameterized in the same manner. Table 1 gives the values of the model coefficients.

The model domain is rectangular in the horizontal and vertical, with the longitudinal extent exceeding the latitudinal extent in all cases for this study. The model is symmetric about the equator, with the middle line of grid points located on the equator. The 15 levels in the vertical are concentrated in the upper ocean to provide for better resolution of the mixed layer and seasonal thermocline. All of the boundaries are considered to be solid (no flow normal to the boundary) and flat (no topography). Figure 1 provides a schematic of the model domain and shows the distribution of levels in the vertical. The upper level of the model is at 10 meters; however, this level will be treated as representing the sea surface temperature (SST). This is not a bad assumption, except in the case of rapid heating of the surface or a mixed layer depth shallower than 10 meters.

Several different model domains were used in the developmental stages and in the final experiments. Figure 2 shows the location of the different model domains in the Pacific and the grid sizes and number of grid points in each direction for each of the model runs. Five different model

domains were used during this study, the smallest of which extends from 10°N to 10°S and covers 30°in longitude from 170°W to 140°W. The next model had twice as many grid points in both directions and extended from 20°N to 20°S and covered approximately 60° of longitude from 175°E to 125°W. A larger version of this model was used that had the same latitudinal extent as the previous model but had a larger longitudinal grid spacing so that it covered 120° of longitude from 150°E to 90°W. A later version of this same model was used with 15 more grid points in the longitudinal direction to increase the basin length to 135°. This model was also centered further to the west than the 120° wide basin, with its western boundary at 135°E and extending to 90°W. The final model domain extended from 45°N to 45°S and covered 90° of longitude from 160°E to 110°W. This domain used a variable meridional grid spacing to achieve the larger north south boundaries. These domains are referred to as the small, medium, large, large2, and variable grid domains in Figure 2.

The model is initiated from rest with the temperature profile uniform in the horizontal and a vertical profile as illustrated in Figure 3. This temperature profile was chosen to match the profile used by Semtner and Holland (1980) so that the initial model runs could be compared to their work. The model is integrated forward in time using a leapfrog scheme with an Euler backward scheme applied every eleven time steps to prevent the solutions from separating in time. The

finite is differencing done on an Arakawa B grid (Haltiner et al. 1980). The grid spacing, time step, and other parameters are given in Table 1.

The two surface forcings required for the model are wind stress and the surface heat flux. The surface heat flux is computed using the method of Haney (1971) and is proportional to the air-sea temperature difference, where the net downward heat flux is given by:

$$Q=\gamma\,(T_a-T_s)$$

Where

γ = heat flux coefficient (W m^{-2} $°C^{-1}$)

T_a = air temperature (°C)

T_s = sea surface temperature (°C)

All of the model runs in this study used a fixed air temperature of 25°C over the entire domain. The wind stresses used for the experimental model runs are described in detail in the next section. For the developmental runs, a constant westward wind stress of 0.6 dynes/cm^2 was used.

B. WIND STRESS FIELDS

Wind stress is the only forcing term that was varied while the model was running. Initial model development was carried out using a spatially and temporally constant wind stress to provide a baseline for comparison with previous efforts (e.g., Semtner and Holland 1980). This also helped in finding

numerical instabilities in the model (cf. Whitney 1992). Next, wind stresses that varied in space but not in time were used to produce a temperature and current pattern that more closely simulated the equatorial Pacific. Whitney (1992) added an observed time varying wind stress anomaly to a constant analytic wind stress field to test the model's response to time varying wind stress. The results she obtained were encouraging and led to the current work. For this study, we applied full-strength time varying wind stresses to the model.

The wind stresses chosen for this study were derived from daily averages of the NOGAPS analyzed 10 meter wind fields for 1991 and 1992. Goerss and Phoebus (1993) describe the NOGAPS analysis procedure. The original data set, provided by Dr. R. Gelaro at the Naval Research Laboratory (NRL) in Monterey, California, contained global wind values at 10 m above the surface twice daily at every 2.5 degrees of longitude and latitude. These winds were averaged in time to provide single daily average values. The winds were then linearly interpolated to the various model grids. The wind stress was calculated from these winds at each grid point using the formulas:

$$\tau_x = \rho_a C_D u_{10} \left| \sqrt{u_{10}^2 + v_{10}^2} \right|$$

where

$$\tau_y = \rho_a C_D u_{10} \left| \sqrt{u_{10}^2 + v_{10}^2} \right|$$

ρ_a= the density of air (1.2 kg-m^{-3})

C_D= drag coefficient (1.2 x10^{-3})

u_{10} and v_{10} = the u and v components of the wind at 10 m above the surface in (m/s)

The wind stresses were then converted to dynes/cm^2.

The wind stresses were also averaged over the entire two-year period to provide a mean wind stress field for use in initializing the model during spin-up. Several of the early model runs were performed using an average wind stress field created from the December 1991, January 1992, and February 1992 wind stresses. This wind stress field was used to determine how important preconditioning the model ocean with pre-El Niño wind stresses was in developing a realistic response. Figures 4 and 5 show the three month average wind stress fields used during spin-up of the early runs. Figures 6-10 show the two year average wind stress fields used during the one year spin-up period of each of the different domain sizes. These figures show that, in general, these wind stresses decrease in strength from east to west and from high latitudes to low latitudes. This general pattern in the strength of the wind stress was also found in the analytic wind stresses used by Whitney (1992) in her final experimental runs.

The last form of wind stresses used in this study were created by calculating the average wind stress for each month. These monthly values were interpolated to provide smoothed daily values. This was done by applying the monthly average wind stress to the 15th of the month. Values of the wind

stress between the 15ths of each month were found by linearly interpolating between the mid-month values. Since the data for December 1990 was not available, I applied the January 1991 monthly average for the first 15 days of this month. The same technique was used to obtain values for the last 16 days of December 1992. These time varying wind stresses based on the monthly averages were used to develop a baseline model run to determine the importance of daily wind stress variations.

The 1991-1992 time period was chosen because of the well observed El Niño from the end of 1991 to May 1992, and the resurgence of the El Niño that took place at the end of 1992.

C. DATA ANALYSIS TOOLS

The analysis of the model data was greatly simplified with the use of the VIS5D graphics visualization software developed at the University of Wisconsin - Madison (Hibbard et al. 1993). Running this software on a Silicon Graphics workstation attached to a SGI 4D/380 VGX system, with 256 MB of RAM and 8 processors and graphics capable of displaying 10^6 shaded polygons/sec, allowed for easy and rapid animation of all the model output fields using contours, vectors, and color shading. Animations of the model fields were used to determine when the model had reached a steady state during the spin-up stage. The determination of when the model had reached a steady state was done by animating the model's output fields and observing when the temperature and currents

had stopped changing with time. This software was also used to verify the realism of the model predictions. VIS5D was an invaluable tool in the analysis of the data. However, the figures shown in this thesis were generated with simpler graphics tools.

TABLE 1. MODEL PARAMETERS

Parameter	Symbol	Value	Units
East-west grid spacing	dx	50/75/100	km
North south grid spacing	dy	25/var.	km
Time step	dt	600,1800	s
Heat flux coefficient	γ	6.9×10^{-4}	$Wm^{-2}{}^{\circ}C^{-1}$
Horizontal eddy viscosity	A_m	5.0×10^{7}	cm^2s^{-1}
Vertical eddy viscosity	k_m	1.0	cm^2s^{-1}
Horizontal eddy conductivity	A_h	1.0×10^{7}	cm^2s^{-1}
Vertical eddy conductivity	k_h	1.0	cm^2s^{-1}
Thermal expansion coefficient	α	3.0×10^{-4}	cm^2s^{-1}
Reference density	ρ	1.0276	$gm\ cm^{-3}$

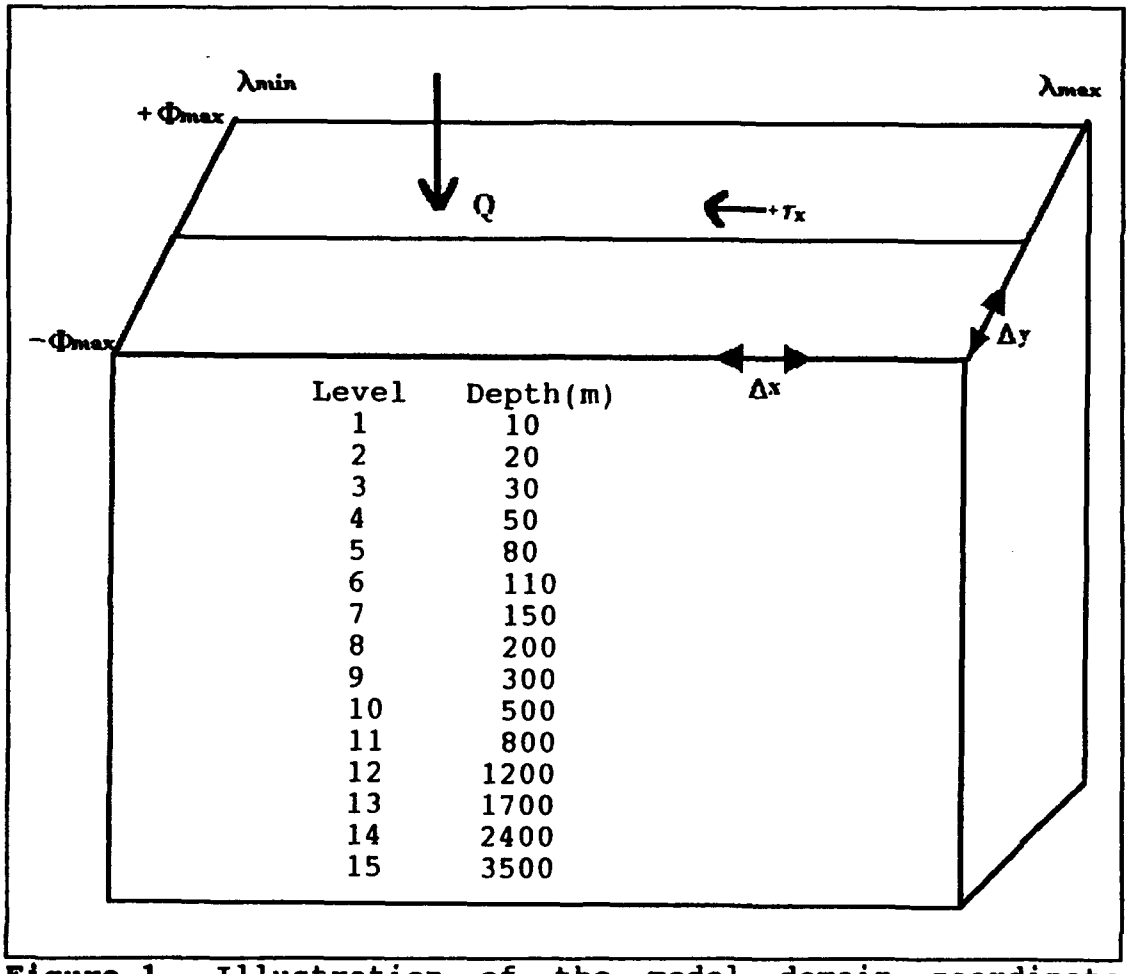

Level	Depth(m)
1	10
2	20
3	30
4	50
5	80
6	110
7	150
8	200
9	300
10	500
11	800
12	1200
13	1700
14	2400
15	3500

Figure 1. Illustration of the model domain coordinate system.

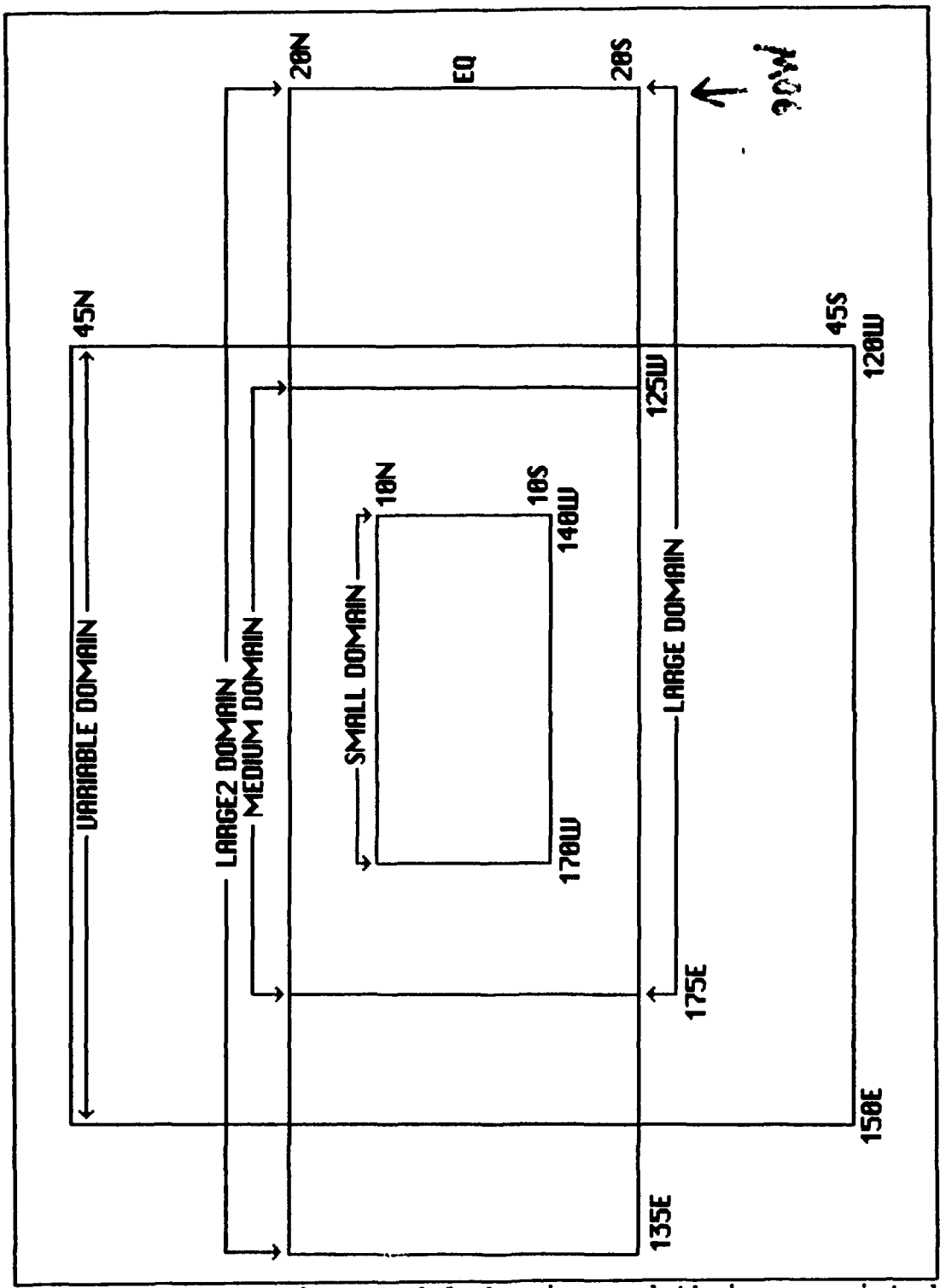

Figure 2. The various model domains and their associated dimensions.

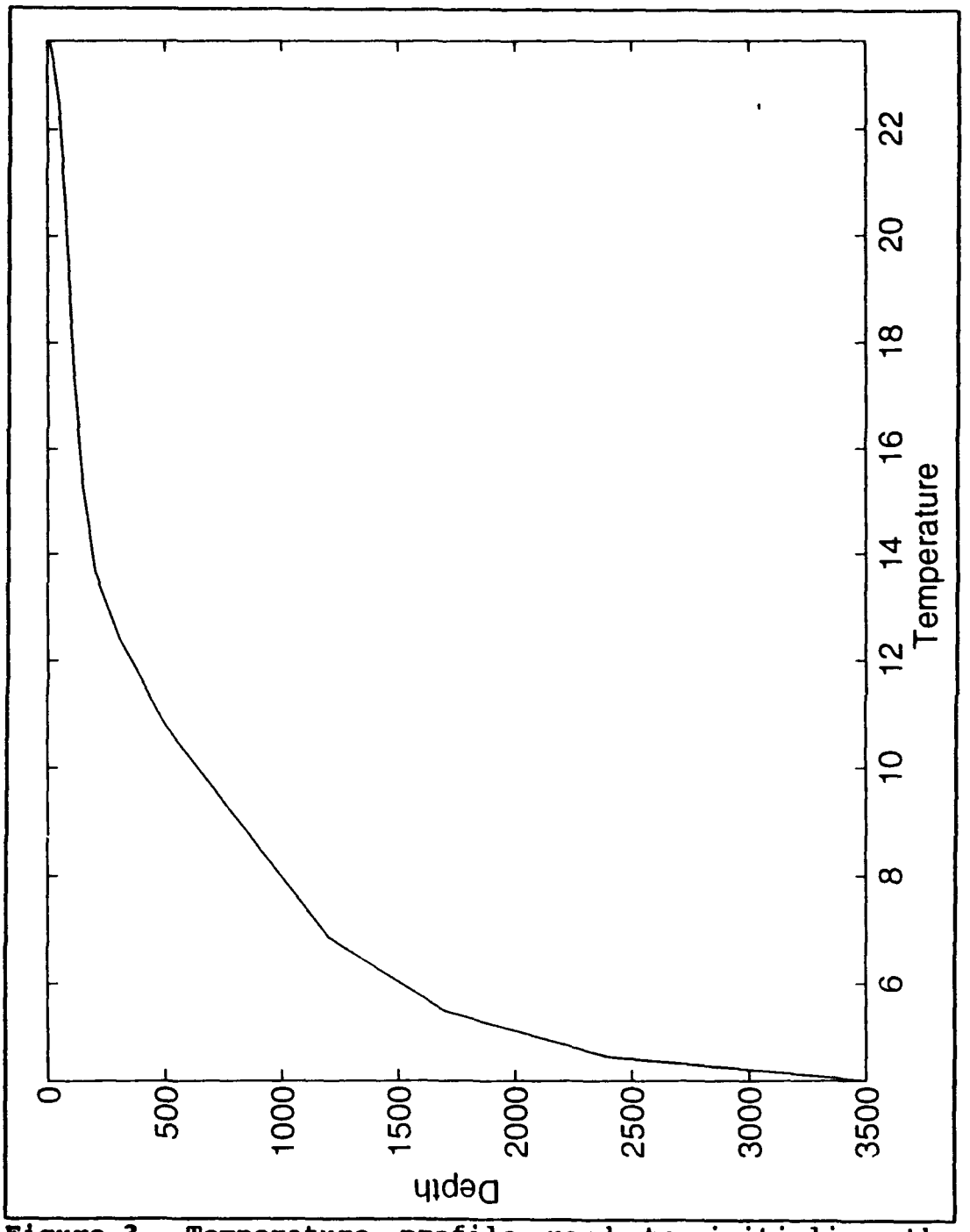

Figure 3. Temperature profile used to initialize the model.

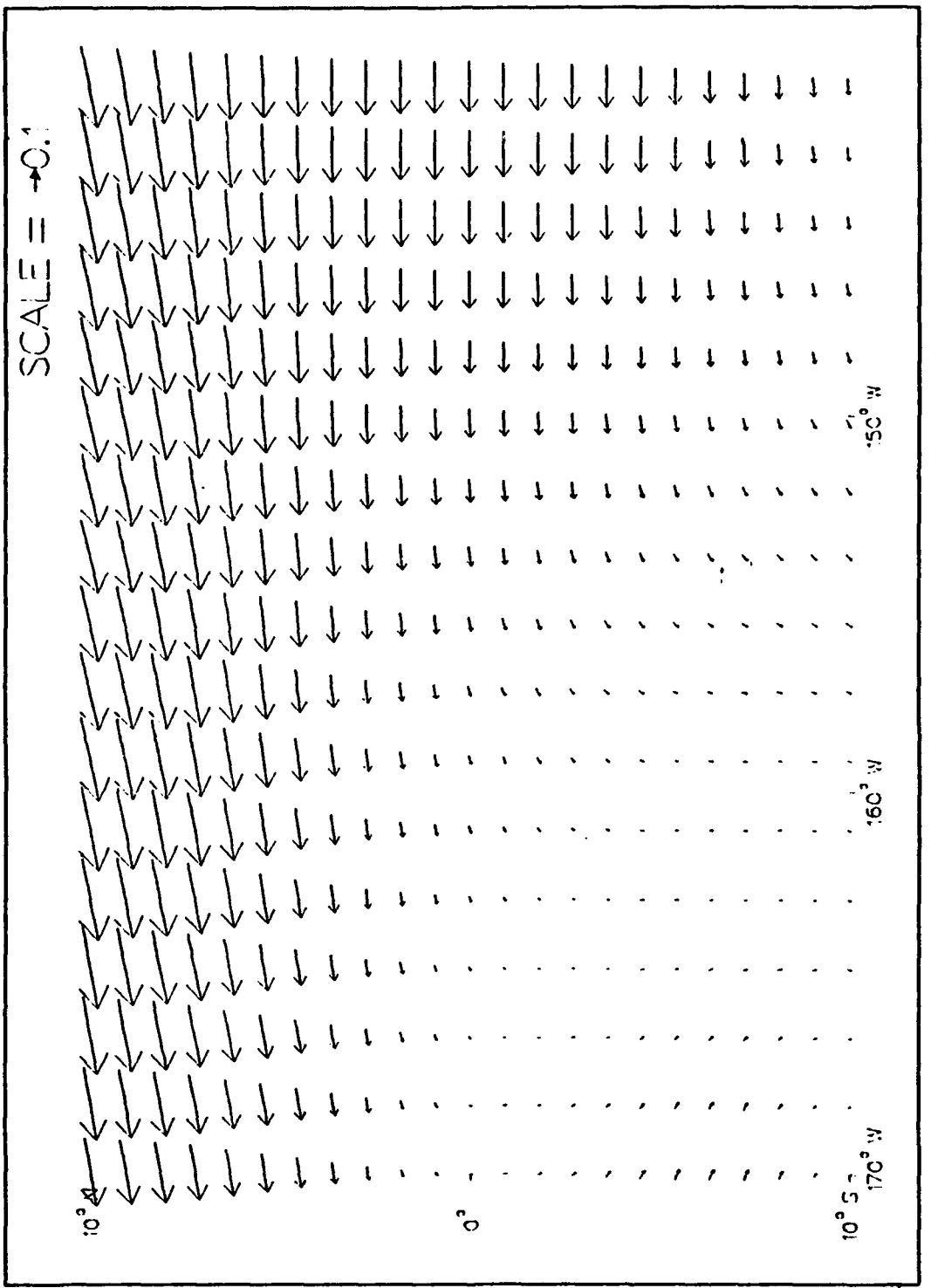

Figure 4. Three month average wind stresses (dynes/cm^2) used to spin-up the model for the small domain runs.

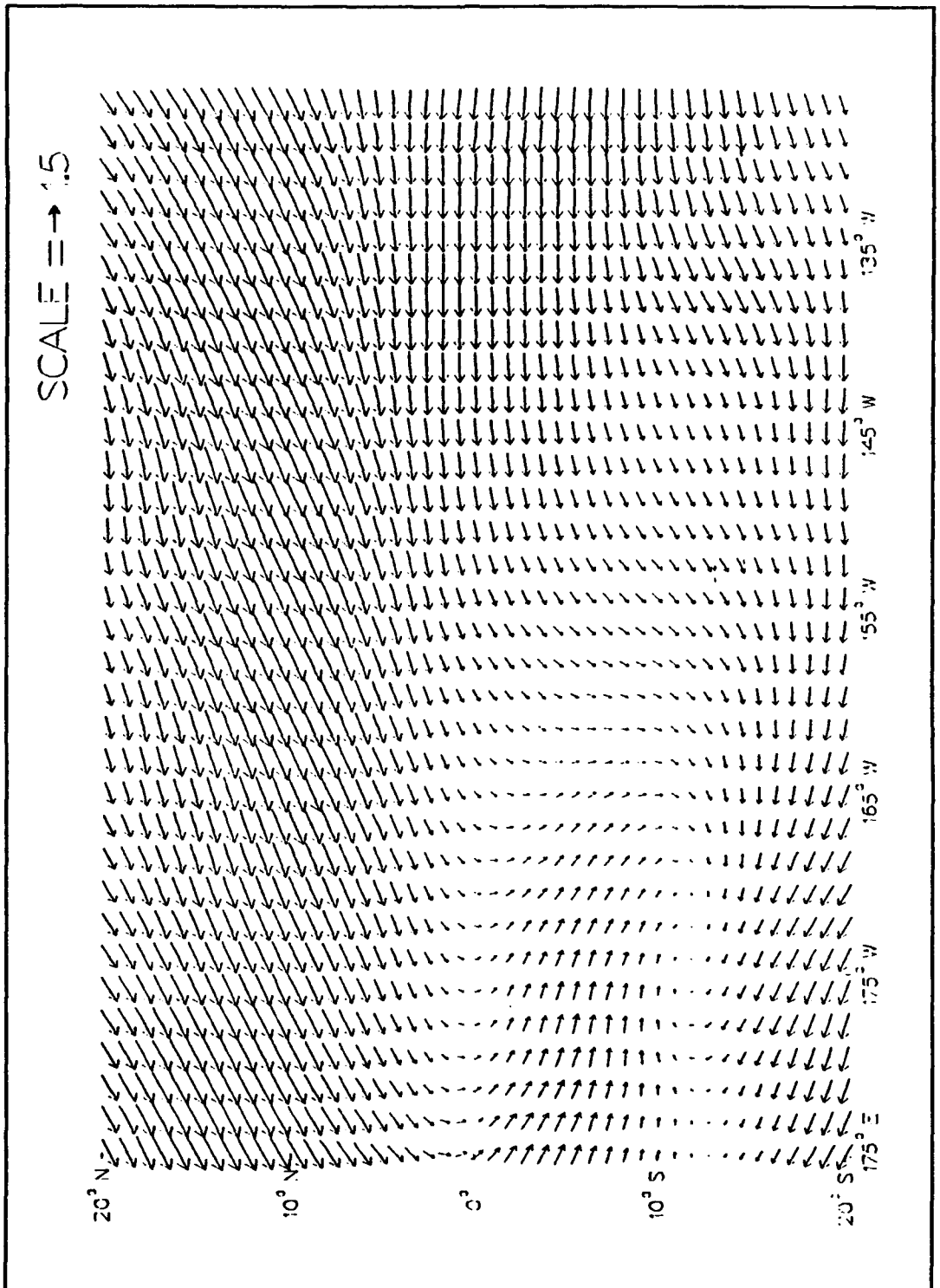

Figure 5. Three month average wind stresses (dynes/cm^2) used to spin-up the model for the medium domain runs.

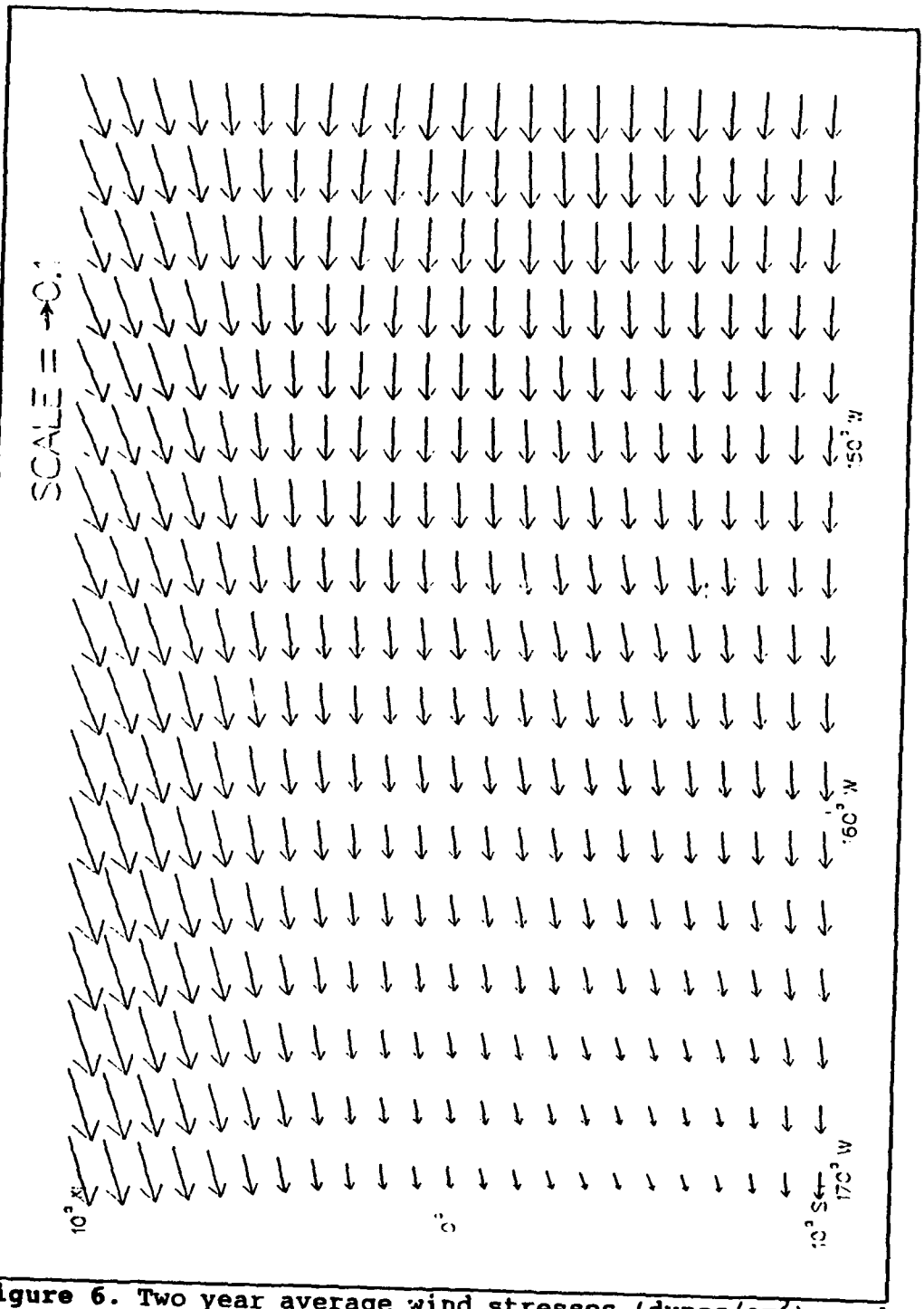

Figure 6. Two year average wind stresses (dynes/cm^2) used to spin-up the model for the small domain runs.

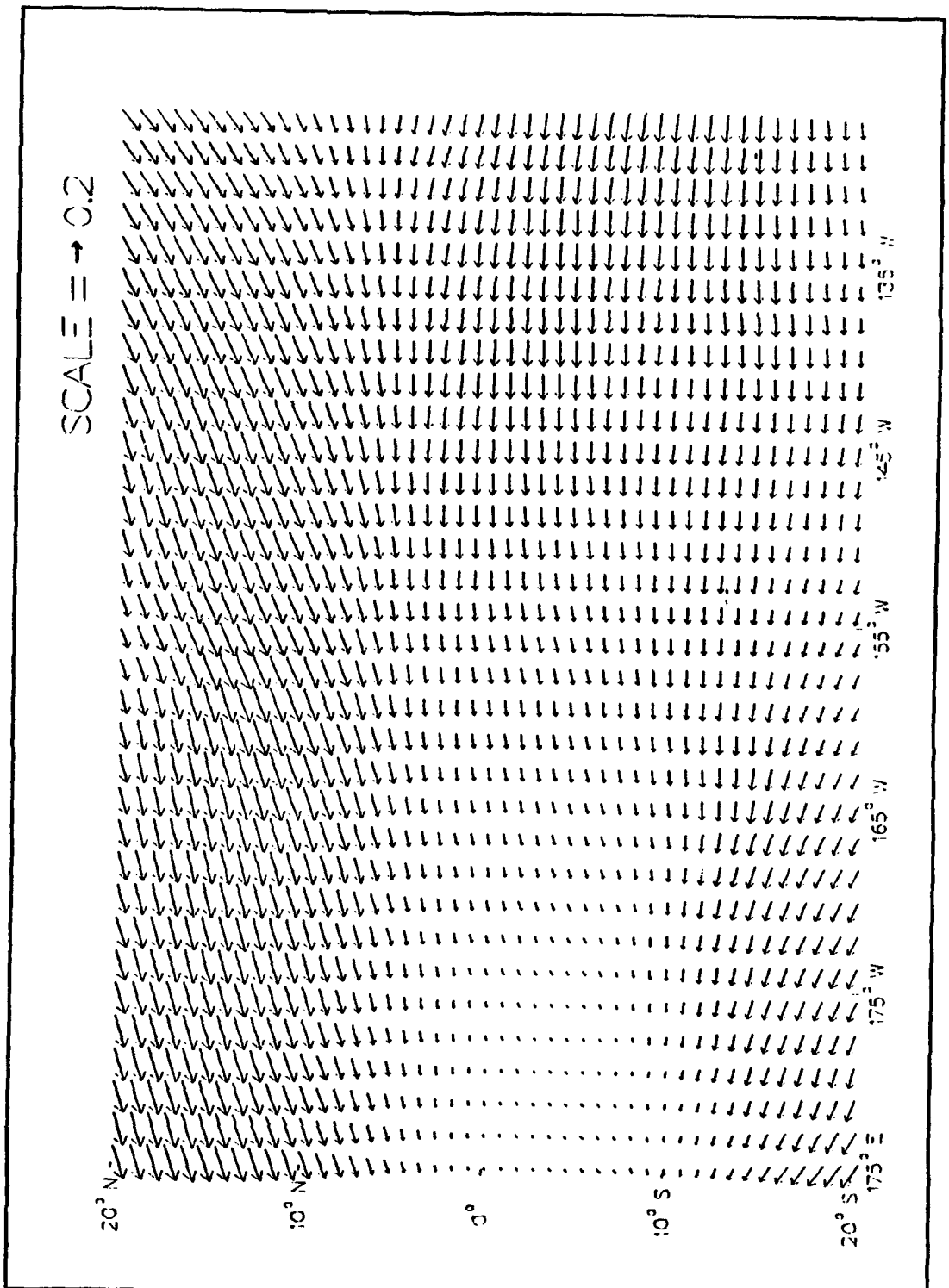

Figure 7. Two year average wind stresses (dynes/cm^2) used to spin-up the model for the medium domain runs.

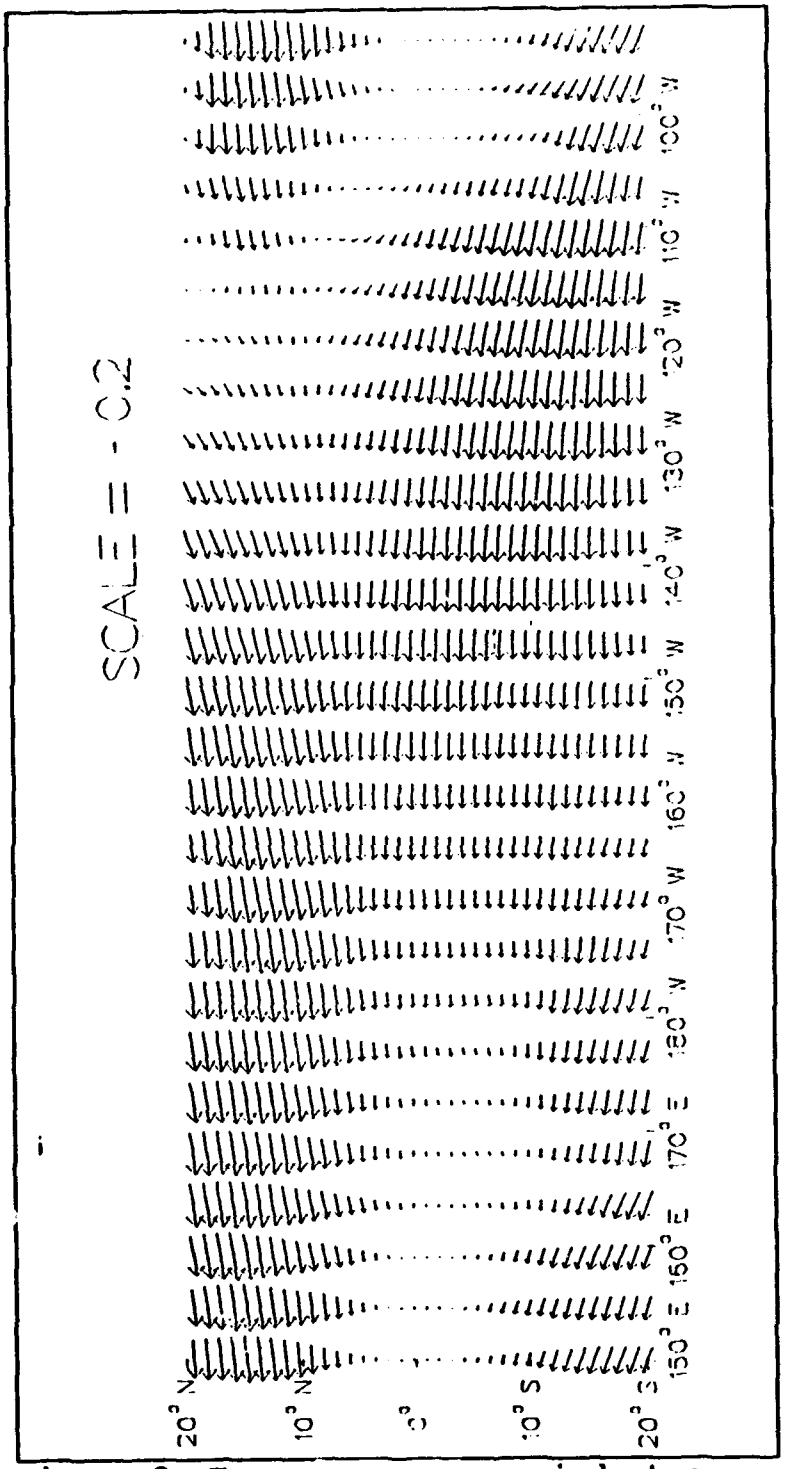

Figure 8. Two year average wind stresses (dynes/cm^2) used to spin-up the model for the large domain runs.

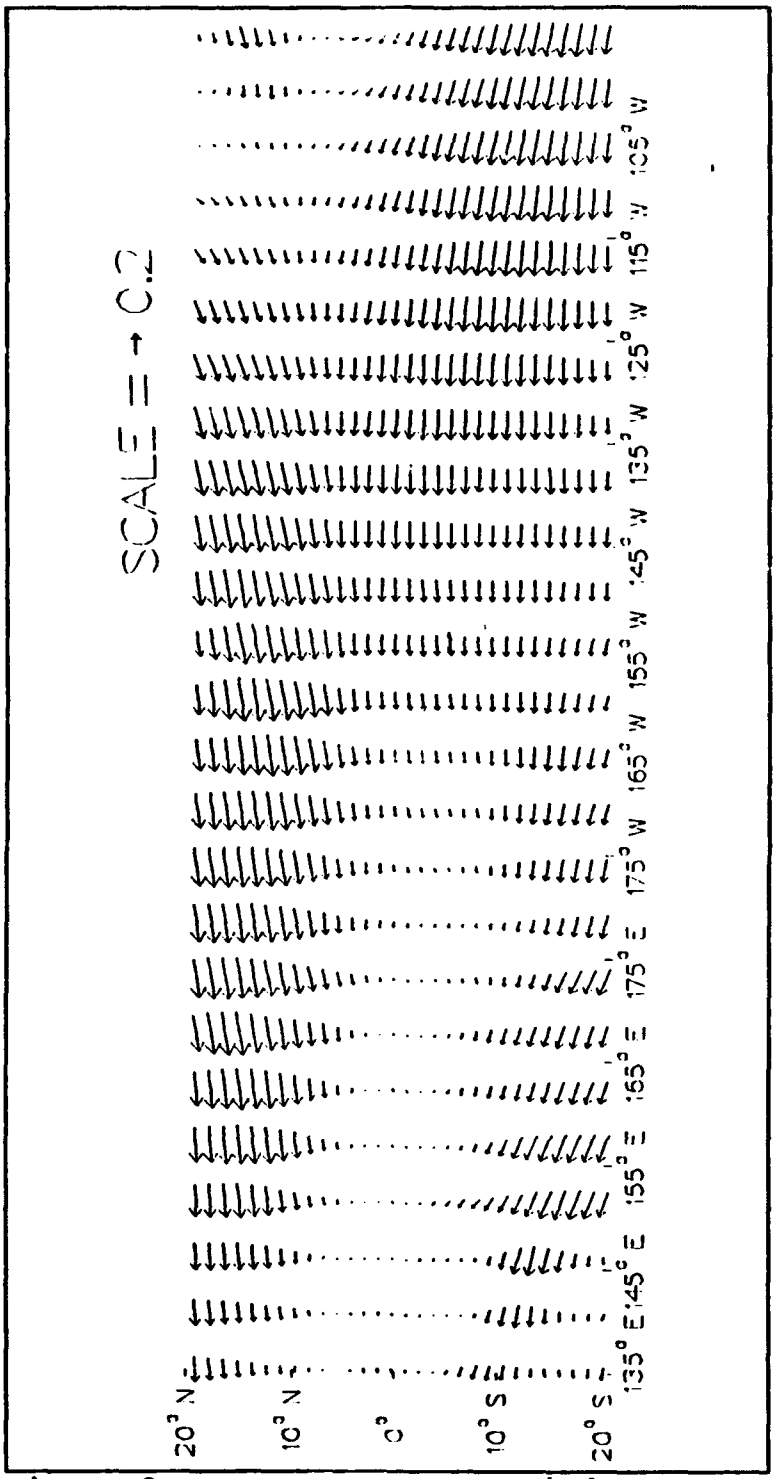

Figure 9. Two year average wind stresses (dynes/cm^2) used to spin-up the model for the large2 domain runs.

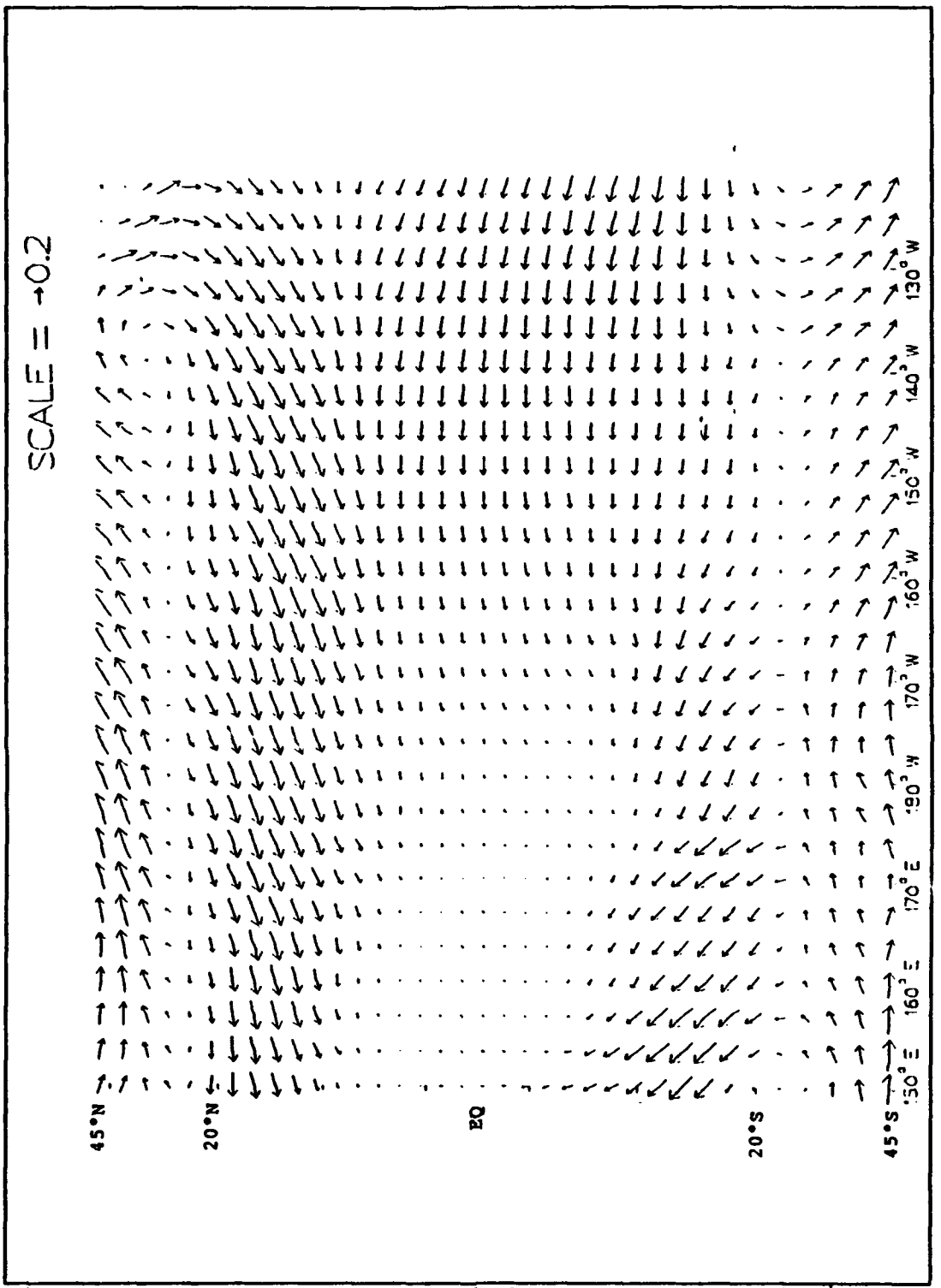

Figure 10. Two year average wind stresses (dynes/cm^2) used to spin-up the model for the variable domain run.

III. MODELING RESULTS

A. DEVELOPMENTAL MODEL RUNS

Several developmental runs were performed to determine the dependence of the model's response to variable wind stress forcing, basin size, grid size, and time step. Table 2 gives a listing of the different developmental runs performed. The major results from each of these runs are discussed in the following subsections in order to provide a basis for understanding the results from the experimental runs presented in the next section of this chapter. For most of the model runs, the surface (10 meter) temperature and currents, and a vertical cross section of the zonal velocity field along the equator are the only fields shown. These fields represent the major features of the model extremely well.

1. Developmental run S1

This model run used a three-month average wind stress field based on twice daily NOGAPS winds for December 1991 - February 1992 (Figure 4). The 1991-92 El Niño was near its mature phase during this period (Rasmusson and Carpenter 1982, Kousky 1992a). The model was spun-up for 360 days until all the model fields appeared to have reached a steady state. Figure 11 shows the steady state currents and temperature structure in the upper (10 meters) level of the model. The

TABLE 2. DEVELOPMENTAL MODEL RUNS

RUN NAME	DOMAIN SIZE	WIND STRESS FORCING	RUN TIME (days)	Δt (s)	Δx/Δy (km)	APPROXIMATE RESOLUTION (degrees)	SIZE (degrees)	WEST/EAST BOUNDARIES
S1	SMALL	DJF 91/2 A	R+360	600	50/25	.45x.23	30x20	170W/140W
S2	SMALL	DJF 91/2 V	S1+91	600	50/25	.45x.23	30x20	170W/140W
S3	SMALL	DJF 91/2 A	R+360	1800	50/25	.45x.23	30x20	170W/140W
S4	SMALL	DJF 91/2 A	R+360	2400	50/25	.45x.23	30x20	170W/140W
S5	SMALL	DJF 91/2 A	R+360	3600	50/25	.45x.23	30x20	170W/140W
S6	SMALL	DJF 91/2 V	S3+91	1800	50/25	.45x.23	30x20	170W/140W
S7	SMALL	DJF 91/2 V	S4+91	2400	50/25	.45x.23	30x20	170W/140W
S8	SMALL	DJF 91/2 V	S5+91	3600	50/25	.45x.23	30x20	170W/140W
M1	MEDIUM	DJF 91/2 A	R+360	600	50/25	.45x.23	60x40	175E/125W
M2	MEDIUM	DJF 91/2 V	M1+91	600	50/25	.45x.23	60x40	175E/125W
X1	LARGE	NOGAPS A	R+390	600	100/25	.9x.23	120x40	150E/90W
X2	LARGE	NOGAPS V	X1+731	1800	100/25	.9x.23	120x40	150E/90W

Table key: A=Time Average wind stress. V=Time Varying wind stress. DJF=NOGAPS Dec, Jan, Feb 1991-92 wind stress only. NOGAPS= 1991-1992 NOGAPS wind stress. Run Time indicates starting point plus length of the model run. R indicates run was started from rest. See Ch. 2 for a full description of domains and wind forcing fields.

strong meridional currents at the western boundary may be the result of the small basin size and the closed boundaries that prevent a realistic poleward outflow in the northwest and southwest corners of the domain. A cross section of the model's zonal velocity field along the equator (Figure 12) shows the vertical structure of the equatorial undercurrent (EUC). The model's EUC has a strong core in the eastern portion of the domain with the strongest flow having a maximum speed exceeding 20 cm/s at a depth between 50 and 80 meters. This is much less than the observed speed of the undercurrent (about 100-180 cm/s, Pond and Pickard 1983). Other models have also had problems in correctly representing the undercurrent speed maximum (e.g., Miller et al. 1992).

2. Developmental Run S2

The initial state for this model run was the final state of run S1. The model was forced with the daily varying wind stresses for December 1991 through February 1992 in an attempt to develop an El Niño-like response. The model's initial response to the varying stresses was a slow strengthening of the cold tongue at the equator. Figure 13 shows the temperature and currents in the upper level of the model at the time of maximum extent of the cold tongue. Figure 14 is a cross section at the equator of the model's zonal velocity field, at the same date as Figure 13. A comparison of Figures 11 and 13, and of Figures 12 and 14,

shows that the EUC slope has decreased but that the EUC still sholes to the west. Notice also that the EUC core has weakened slightly. Figures 15 and 16 show the same fields as Figures 13 and 14 at a time 24 days later when the cold tongue has retreated and an eastward surface current has developed between about 157°W and 170°W. The initial lengthening of the cold tongue during the first 40 days of the S2 run may indicate that some type of preconditioning in preparation for the retreat of the cold tongue is taking place. This tendency for the cold tongue to lengthen and narrow slightly can be seen in all of the model runs prior to a retreat of the cold tongue. Figures 17 and 18 from the end of the S2 run show a weak cold tongue at the end of the 91 day run.

3. Developmental Runs S3 through S5

The purpose of these runs was to investigate the sensitivity of the model to changes in the time step of integration. The time step was increased from an initial value of 600 seconds in increments of 1200 seconds until the model became unstable. At a time step of 3600 seconds the model was still stable and showed no signs of instability. At a time step of 4800 seconds the model was numerically unstable. No effort was made to determine the exact point at which the model would become unstable.

The wind stress forcing for these runs was chosen so that the results could be compared to model run S1. Figures 19-24

show the temperature and currents for the model's upper level for each run, paired with cross sections along the equator of the model's zonal velocity field. Comparisons of Figures 19, 21 and 23 with Figure 11 show that increasing the time step led to a general decrease in the 10 meter temperature, but a qualitatively similar temperature pattern. The 10 meter currents show little change with increasing time step. The cross sections of zonal currents (Figures 20, 22, and 24 compared with Figure 12) show a slight decrease in the current speeds at all depths, however, this decrease is not enough to indicate that the time step tested should not be used. These results indicated that time steps ranging from 600 to 3600 seconds would be suitable for use in the later model runs.

4. Developmental Runs S6 through S8

Time steps of 1800, 2400, and 3600 seconds were used in model runs S6, S7, and S8 in order to ensure that the results obtained in model runs S3 through S5 would also apply to runs with variable wind stresses. These model runs are the same as run S2 but with larger time steps. Figures 25-30 show the temperature and currents for the model's upper level on 2 February 1992 for runs S6, S7, and S8 paired with the corresponding cross sections along the equator of the model's zonal velocity field. Comparisons of Figures 25 and 27 with Figure 15 show that increasing the time step cooled the 10 meter temperatures and strengthened the 10 meter currents.

Figures 26 and 28 show little difference in the zonal currents with depth compared to Figure 16. Figure 29 shows a small westward current in the midst of the eastward flow in the western portion of the domain. Figure 30 shows that this surface current is the manifestation of a large region of westward flow beneath the surface.

Run S8 with a time step of 3600 seconds (Figures 23 and 24) was stable. However, the region of westward currents that developed in the western portion of the domain (Figure 24) was not observed in runs S6 or S7. This is probably an indication that under variable wind forcing this time step might be to close to the point of model instability. Even though Run S7 with a time step of 2400 seconds, (Figures 21 and 22) gave results that compared reasonably well with runs S2 and S6 (time steps of 600 and 1800 seconds respectively), a time step of 1800 seconds was chosen for subsequent runs to ensure that the model would remain stable under variable forcing.

5. Developmental Runs M1 and M2

Runs M1 and M2 were performed in order to determine the effects of basin size on the model's results. For these runs, the grid spacing used in the previous runs was maintained, but the number of grid points in both x and y was doubled, which quadrupled the area of the model domain. For run M1 the December 1991 through February 1992 three-month

average wind stress field (Figure 5) was used to spin the model up for 360 days. Due to the large region of cyclonic wind stress near the southwest boundaries of the domain, (Figure 5) the model was unstable for integration time steps greater than 600 seconds. Model run M2 used the final state of model run M1 as a initial state. In model run M2, the model became unstable when it was exposed to the time varying wind stresses no matter what time step was used. No attempts were made to correct the instability in this model run by relocating the domain, since the two-year average wind stress data was available, and it did not have this large cyclonic region.

6. Developmental Run X1

This model run was completed after experimental model runs M3 and M4 (described in Chapter III, Section B) had shown that use of the two-year average wind stress (Figure 7) corrected the instability problems of model runs M1 and M2. Based on the results of model runs M3 and M4, another effort to increase the model's domain was made. Increasing the number of grid points in the model was not feasible due to computational run time limits. Therefore, the longitudinal grid spacing, Δx, was doubled to 100 km, which increased the domain size to 120°x40°. This domain was large enough to study the remote effects of wind anomalies in the western Pacific on the eastern Pacific. The 1991-92 NOGAPS average

wind stress field was used to spin the model up for 390 days, at which time the model fields had reached a steady state. An error in the wind stress field used for the forcing of this run and run X2 was discovered near the end of model run X2. This error caused the results in the extreme eastern portion of the domain to be incorrect, and it also increased the $2\Delta x$ scale noise near the equator. However, the results for the rest of the domain were good and gave the information needed to determine the best position of the model domain for the final experimental run.

Figure 31 shows the final temperature and current pattern in the upper level of model for this run. Figure 32 shows a cross section of zonal velocity along the equator. There is a small area of weak eastward surface flow in the far western portion of the domain. This current is probably due to the extremely weak average winds at the equator in this region (Figure 8). Increasing the domain size also increased the strength of the equatorial undercurrent.

Also of interest is the development of waves in the temperature field, which are most noticeable on the flanks of the cold tongue in the eastern Pacific. Figure 33 shows an example of the temperature waves along the middle of the cold tongue. The waves in this model run tend to be stronger along the northern flank of the cold tongue. This asymmetry is consistent with the observations of Legeckis (1977) and Harvey and Patzert (1976). The model's waves propagate to the west

at a speed of approximately 18-24 cm/sec, which is about half of the speed observed by Legeckis (1977). This difference may be due in part to the model's weak westward currents which are about half the speed of the observed currents. Semtner and Holland (1979) observed these waves in the steady state of their model but noted that the waves were too symmetric about the equator and were too strong in the southern hemisphere. This could be due to the constant wind stress field they used in contrast to the space and time varying field used in this model run.

7. Developmental Run X2

Run X2 was started from the final state of run X1. The model was forced with the daily varying wind stress for the entire two year period. The equatorial cold tongue of the model retreated to the east three times during the two-year period. The first retreat of the cold tongue occurred between April 1991 and July 1991. This event was extremely small and was probably due to a few strong westerly wind bursts in the western Pacific. The second occurrence was in early November 1991 and lasted for a period of 5 months. The third retreat was much weaker and occurred at the end of November 1992 and was still in progress at the end of the run. Figures 34 and 36, respectively, show the temperature and currents associated with the greatest deviations from the initial state of the model for each of these events. Figures 35 and 37,

respectively, show the zonal currents in cross section along the equator for the same time periods. Figures 38 and 39 show these same fields at the point between the second and third retreats when the temperature and current structure had returned to almost the same State that was present at the beginning of the run. The second event showed a maximum retreat of the cold tongue of approximately 30° of longitude in late March 1992. In the third retreat, the cold tongue had moved only about 11° to the east by the end of the run. The wind stress fields for 1993 were not available to determine if the third event would have reached the same strength as the second event or if it would have remained weaker throughout its duration. Figures 35 and 37 show that not only did a eastward surface current develop during the retreats, but a westward equatorial undercurrent developed at about 100 meters in the western Pacific. This pattern appears to have split the equatorial region into two separate zonal circulations, one in the western Pacific and one in the central and eastern Pacific, instead of one large circulation across the entire basin (Figures 35 and 37). The two zonal circulations met at the surface in the vicinity of the dateline, where the surface horizontal flow was strongly convergent.

B. EXPERIMENTAL MODEL RUNS

Based on the results obtained in the developmental runs, three major experimental runs were performed. The three

domain sizes for these experiments were the ones labeled small, medium, and large2 in Figure 2. Table 3 lists the experimental runs in pairs, with the first run being the spin-up phase, and the second run being the run in which variable wind forcing was used. This section provides information and observations on all of the runs. However, the X3 and X4 runs, and comparisons with the X5 run, are the main focus of this section. The X3 and X4 runs gave the best simulation of the mean temperature and velocity fields and showed the most realistic responses to the variable wind forcing.

1. Experimental run S9

The model for this run was spun-up from rest for 360 days using the two year average wind stress forcing. The location of the model domain (Figure 2) was chosen so that some westerly wind bursts in the western Pacific would be contained in the model domain. Figure 40 shows the final temperatures and currents in the model's upper level. Figure 41 shows a cross section along the equator of the zonal velocity to show the equatorial undercurrent structure. The general structure of the fields is similar to that obtained by Semtner and Holland (1979), although this model shows less symmetry across the equator, probably due to the use of spatially and temporally varying wind stress fields. A comparison of this run (Figures 40 and 41) with run S1

TABLE 3. EXPERIMENTAL MODEL RUNS

RUN NAME	DOMAIN SIZE	WIND STRESS FORCING	RUN TIME (days)	Δt (s)	$\Delta x/\Delta y$ (km)	SIZE (degrees)	WEST/EAST BOUNDARIES	APPROXIMATE RESOLUTION (degrees)
S9	SMALL	NOGAPS A	R+360	600	50/25	30x20	170W/140W	.45x.23
S10	SMALL	NOGAPS V	S9+731	600	50/25	30x20	170W/140W	.45x.23
M3	MEDIUM	NOGAPS A	R+390	1800	50/25	60x40	175E/125W	.45x.23
M4	MEDIUM	NOGAPS V	M3+731	1800	50/25	60x40	175E/125W	.45x.23
X3	LARGE2	NOGAPS A	R+360	1800	100/25	135x40	135E/90W	.9x.23
X4	LARGE2	NOGAPS A	X3+731	1800	100/25	135x40	135E/90W	.9x.23
X5	LARGE2	NOGAPS M	X3+365	1800	100/25	135x40	135E/90W	.9x.23

Table key: A=Time Average wind stress. V=Time Varying wind stress. M=Monthly average wind stress interpolated to daily. NOGAPS= 1991-1992 NOGAPS wind stress. Run Time indicates starting point plus length of the model run. R indicates run was started from rest. See Ch. 2 for a complete description of the Model domains and wind forcing fields.

(Figures 11 and 12) shows a colder and larger cold tongue and a more elongated EUC.

2. Experimental run S10

Starting from the final state of model run S9, the model was forced with the daily varying wind stresses for all of 1991-92. The model showed several realistic responses to these winds. The cold tongue retreated to the east on three different occasions. The first model retreat was a weak event that lasted from May 1991 through July 1991. During this retreat, the model showed a mild surface warming, probably in response to westerly wind stresses in the western and central Pacific early in 1991. Animations of the model's temperature and velocity fields showed some indications of a Kelvin wave associated with this retreat of the cold tongue. Another study that used daily varying NOGAPS winds to force a 2 1/2 layer ocean model has shown the passage of a Kelvin wave through the equatorial Pacific during the middle of 1991 (Phoebus and Kindle 1993). In this study the model Kelvin wave had a very weak temperature and height anomaly signature compared to the Kelvin wave associated with the 1991-92 El Niño. According to the Climate Diagnostic Bulletin (Kousky 1991), a weak warm event and negative values of the SOI were observed during this time frame. The real ocean and atmosphere didn't recover from this warm event as quickly as did the model. In the observations the warm event in mid 1991

blended directly into the large warm event at the end of 1991 with only a small cooling and weakening of the SOI in between the two.

The last two S10 model run retreats coincided with the observed retreats at the end of 1991 (Kousky 1992a) and again at the end of 1992 (Kousky 1992b). Figure 42 shows the temperature and currents at the point of maximum retreat for the second retreat that started near the end of 1991. A cross section along the equator of the zonal velocity component (Figure 43) shows the corresponding equatorial undercurrent structure. In Figures 42 and 43 the reversal of the SEC associated with the cold tongue retreat has already dissipated. The EUC has reestablished itself across the entire domain but is tilted down from west to east, a reversal of its normal tilt. During this period, observations show the 1991-92 El Niño became firmly established (Kousky 1992a). However, in the model, the cold tongue tended to move rapidly back to its original position instead of remaining in a retreated state through May 1992, as was observed. Thus the westerly wind bursts that extended into this model's domain were capable of initiating an El Niño-like response in the model, but they were not able to sustain this pattern long enough. This suggests that westerly wind bursts to the west of the model domain (i.e. in the western Pacific) may be important to the development and maintenance of an El Niño.

Figures 44 and 45 show the S10 model run temperatures and currents at the end of the 1992. These figures represent the third cold tongue retreat that was developing in December 1992.

Before each of the three periods of retreat, the model SEC strengthens and the cold tongue tended to narrow and lengthen slightly. This is consistent with Wyrtki's (1975) hypothesis that the ocean must be preconditioned before an El Niño by the piling up of more warm water in the western Pacific.

In the model's retreat of the cold tongue at the end of 1991, a strong reversal of the SEC occurred in the equatorial western Pacific. This strong eastward current had dissipated by the point of maximum retreat of the cold tongue, so it is not visible in Figures 42 and 43. Animations of the model's output fields showed that this eastward flow developed initially from a southward extension of the NECC. Below the surface the NECC also extended south and merged with the northern flank of the EUC. Then the NECC continued to extend equatorward as the EUC core sholed. This region of eastward flow then developed into a full reversal of the SEC in the equatorial western Pacific. Several aspects of this eastward equatorial flow can be seen in Figure 46, which shows the structure of the currents in a meridional cross section in the western portion of the domain on 13 November 1991, at the beginning of this merging of the currents. Figure 47 shows

the same field one day later when the currents have almost completely merged at the equator. This merging of the currents only occurred during the large retreat of the cold tongue at the end of 1991. Several strong reversals of the SEC in the western Pacific were observed during 1991-1992, including a reversal during June of 1992 that dissipated before the one associated with the 1992 El Niño (Kousky 1992c).

Tropical instability waves like those observed in model runs X1 and X2 were observed in this model run and in S9 although the waves were much weaker. The model waves tended to weaken during the retreats of the cold tongue as seen in observations of these waves (Halpern 1988).

3. Experimental Run M3

Run M3 was done to better investigate the effects of westerly wind bursts in the western Pacific and to determine the effects of the small basin size on the results obtained in runs S9 and S10. Run M3 is a repeat of run S9 but with the next larger basin size and a larger time step (cf. Table 3). The longer time step was used to minimize the increase in run time arising from the larger domain. The developmental runs showed that although this time step increase might change the results quantitatively, it should not change the results qualitatively. The medium size domain model was spun-up from rest for 390 days to ensure that it had reached a steady

state. Figure 48 shows the temperature and currents of the model in its steady state. Figure 49 shows the zonal currents in cross section along the equator. Although the EUC is very weak and diffuse in the western portion of the domain, it is stronger and has a very well defined core over most of the domain. The model's EUC also developed a more realistic tilt in this run as compared to model run S9 (Figure 41), with the core of the undercurrent rising from west to east. The model also developed a narrower more well defined cold tongue than in model run S9 (Figure 40).

4. Experimental Run M4

The final state of model run M3 was used as an initial state for model run M4. This run is the larger domain and longer time step version of run S10. Due to the larger domain which extended further into the western Pacific, run M4 had more westerly wind bursts in the wind stresses than did run S10. In addition, the direct effects of the boundary conditions on the interior of the model basin were smaller. The M4 run showed the same cold tongue retreats seen in run S10. However, the retreat at the end of 1991, lasted about 2 months longer, ending in March of 1992. By July 1992, the model had returned to a state resembling the steady state of run M3.

Figures 50 and 52 show the temperature and currents at the point of greatest retreat for the second and third

retreats. Figures 51 and 53 show the zonal currents in a longitudinal cross section along the equator for the same periods. The model's upper level temperature tended to increase throughout this model run, indicating that perhaps a longer spin-up time was needed in model run M3. Although the cold tongue does not appear to have retreated much in Figure 52, the beginnings of an eastward surface current can be seen that would probably have led to a cold tongue retreat if the model run had been continued.

The tropical instability waves seen in runs X1 and X2 were evident in this model run. The M4 run waves also had a strong seasonal cycle with the waves being strongest during August and September of 1991 and 1992 when the cold tongue was well developed. The waves could be seen throughout the model run; however, they were weaker during the strong cold tongue retreats at the ends of 1991 and 1992.

5. Experimental Run X3

Based on the results of run X2, the large model domain was altered slightly to include more area in the western Pacific. This put the western boundary at 135°E and the eastern boundary at 90°W. This alteration was done because an examination of the NOGAPS winds for 1991 and 1992 showed that a shift in the model domain further to the west (see Figure 2) would include almost every westerly wind burst that occurred in the Pacific during the period of interest. This westward

shift of the model domain also placed a region of generally weak wind stresses near the western boundary (Figure 9). This meant that the wind forcing in the western part of the domain was generally too weak to directly force strong currents. This tended to reduce the magnitude of the problematic western boundary currents and seemed to improve the model results for the entire western basin. After making these changes, model run X3 was spun-up from rest for 360 days, using the two year average wind stress field. At this time the model circulation had achieved a steady state.

Figure 54 shows the temperature and currents in the upper level once model run X3 reached a steady state. Figure 55 shows the zonal currents in a cross section along the equator. Figures 54 and 55 show an equatorial surface current in the western Pacific. The relaxation of the wind stress near the equator in the western portion of the domain yielded a negative wind stress curl which forced an eastward equatorial current. This current was much stronger than in the X1 model run, probably due to the larger portion of the X3 model domain in the western Pacific area of weak wind stresses. If a climatological value of the wind stress had been used, this eastward current would probably have developed more to the north at the latitude of the NECC.

Figure 56 shows the model's mixed layer depth which is about 10 meters over most of the equatorial western Pacific, with the mixed layer depth getting deeper to the north and the

south. As discussed in Chapter II, the mixed layer depth is not allowed to go above the top model level (10 meters). Thus the mixed layer depth in Figure 56 may be an overestimate of the actual depth of turbulent mixing. Figure 57 is a cross section along the equator of the model's temperature field. This Figure shows that the model's thermocline is between 80 and 110 meters in the east and between 30 and 50 meters in the western portion of the domain.

6. Experimental Run X4

In run X4, the final state of run X3 was used as a starting point from which the model was forced with the 1991 - 1992 NOGAPS daily wind stresses. During the X4 run, the model ocean was exposed to strong westerly and easterly wind bursts in the western portion of the domain, and the eastward equatorial surface current seen in the western Pacific in run X3 (Figures 54 and 55) weakened and eventually disappeared (not shown). Figure 58 shows the temperature and currents in the upper level of the model on 29 August 1991, after the eastward current on the equator had completely disappeared. Figure 59 shows the zonal currents in a cross section along the equator at the same time.

The three retreats of the equatorial cold tongue seen in runs S10 and M4 were also seen in this model run although their structures were slightly different. The first and weakest retreat occurred before the eastward equatorial

surface current in the western Pacific had completely disappeared. Figures 60 and 61 show the upper level temperature and currents of the model at the point before this weak retreat began (26 March 1991) and at the time when this retreat was at a maximum (12 July 1991).

Figures 62 shows the model's temperature and currents in the upper level on 16 October 1991. At this time, the equatorial cold tongue had reached its maximum extent. Figure 63 shows the corresponding cross section of the zonal velocity component. This figure shows that, compared to run X3 (Figure 55), the eastward equatorial surface current had diminished greatly, and the EUC had become better organized. Figure 64 shows the model's mixed layer depth on 16 October 1991. Figure 65 shows a cross section of the temperature field along the equator for the same day. These figures provide a good basis for assessing the model's evolution during the first major retreat of the cold tongue.

The second retreat of the model cold tongue began in the late October 1991. Figure 66 shows the temperature and currents on 11 December 1991 when a strong eastward equatorial surface current had formed in the western Pacific. Figure 67 shows a cross section of the zonal currents along the equator for this same time. The source of this eastward current was similar to that in previous runs (eg. run S10). That is, the NECC in the western Pacific slowly extended southward toward the equator. The NECC then merged with the large reversal of

the SEC that developed in the model. In the spin-up run (X3), and in this run the equatorial undercurrent did not extend into the western Pacific (Figure 67). Thus, there was no strong eastward EUC in the western Pacific for the NECC to merge with, as in model run S10. If wind stresses from 1990 were used to force the model, so that it was in a more realistic state at the start of the retreat of the cold tongue, a western Pacific EUC might have formed and merged with the NECC as in model run S10. Figures 68 and 69 show the zonal currents in a meridional cross section at 165°E during the period when the NECC current was moving onto the equator.

An unusual feature that developed in the model during the second cold tongue retreat was a tongue of warm water that extended eastward into the cold tongue (Figure 66). This warm tongue was produced at the strong eastward equatorial surface current in the western and central Pacific rapidly advected warm water to the east along the equator. It is difficult to compare this feature to anything seen in the observations of the 1991-1992 El Niño, since the model does not actually represent the true surface temperature but a 10 meter temperature. I examined data from the TOGA buoys near the equator to see if they showed a comparable signal. However, the few buoys that did exist in the region where this feature was strongest in the model had several gaps in their data to provide a useful comparison. An examination of SST analyses from the U.S. Navy's optimal thermal interpolation scheme

(OTIS, Figure 70) shows that the SST tended to increase on the equator during the last 40 days of 1991, while the temperatures to the north and the south decreased slightly or stayed the same. Since the OTIS SST data is derived to a large extent from satellite data, surface heating and cooling may have masked the actual strength of the SST warming on the equator. The OTIS data is also spatially smoothed, and this would tend to mask the strength of this very narrow feature. This data does suggest that the model's eastward equatorial warm water intrusion may be realistic. However, the model may overdevelop the temperature gradients associated with the warm water intrusion, due to the extremely strong cold tongue that developed in the model.

Figures 71 through 74 show the same model fields as Figures 62 through 65 but at the time of maximum retreat of the cold tongue on 13 March 1992. During the retreat of the cold tongue, the equatorial portion of the SEC had reversed in the western and central Pacific. The resulting strong eastward current advected warm water to the east. By mid-March 1992, this eastward current had begun to weaken, and the SEC was beginning to reestablish itself (Figures 71 and 72).

Although the restoration of the cold tongue in the model was mostly completed by 30 August 1992, the maximum extent of the cold tongue was not reached until 27 October 1992 (not shown). The cold tongue then began to retreat again. This third retreat was not nearly as strong as the second

event. At the end of 1992, the cold tongue had retreated about 10° of longitude, compared to a retreat of approximately 20° at the end of 1991. Figure 75 shows the upper level temperature and currents on 31 December 1992 which was the end of run X4. Figure 76 shows a cross section at the equator of the zonal velocity for the same time. The development of the cold tongue retreat seen in Figures 75 and 76 is comparable to that on 11 December 1991 (Figures 66 and 67), prior to the mature phase of the second cold tongue retreat.

By using daily varying wind stresses instead of temporally averaged wind stresses, I was able to observe the model's response to numerous typhoons that passed through the model domain. The expected response would be a swath of colder water in the region that the typhoon has just passed over (Ginis 1993). Observing the animated model output showed this effect in the wake of every typhoon that passed through the region. Although some of the typhoon cooling events were obscured by the large cold tongue in the model, several events were quite clear.

Figures 77 through 82 show the wind stresses between the western boundary and 180°E every two days during the period 13-23 November 1992. Typhoons Hunt and Gay can be seen intensifying and moving westward across this portion of the model domain. Figures 77-79 show that these typhoons are in a broad band of cyclonic flow in the northern hemisphere. In Figure 80, typhoon Hunt can be seen moving out of the area in

the upper right corner of the figure, and typhoon Gay continuing to move west northwestward across the domain. The most intense westerly winds on the equator in Figures 77-82 are associated with typhoons Hunt and Gay and are part of the westerly wind bursts that forced the retreat of the cold tongue at the end of 1992.

Figure 83 shows the X4 model run upper level temperatures and currents for 13 November 1992. Figures 84 through 88 show the upper level temperature anomalies and currents for 15-23 November 1992, corresponding to the days represented in Figures 78-82. The temperature anomaly (TA) on a given day is calculated by subtracting the 10 meter temperature on 13 November 1992 from the 10 meter temperature on that day. For example the TA on 15 November 1992 is:

$$TA_{15Nov} = T_{15Nov} - T_{13Nov}$$

Figures 84-88 show negative TA's (i.e., cooling) in the wakes of typhoons Hunt and Gay. The TAs for 23 November 1992 (Figure 88) show a large region of cooling in the wake of typhoon Gay of about 0.5° C with a maximum cooling of 2.5°C. The maximum cooling agrees well with observed temperature drops (e.g., 2-3°C, Ginis 1993), but should cover a larger region than is seen in the model. However, this model does not allow for factors such as reduced insolation due to clouds and the addition of fresh cool water in the form of

precipitation. The model's cooling is mainly due to mixing, upwelling, and advection.

Figures 84-88 also show a region of cyclonic flow in typhoon Gay's wake. This cyclonic flow tends to be slightly west of the cooling region. This is consistent with cooling due to upwelling, with the maximum cooling lagging the maximum cyclonic flow by a few degrees of longitude and a day or two. Figure 89 shows a north-south cross section through this divergent region on 21 November 1992. This figure shows that the model produced strong upwelling in this region down to 500 meters, with an extremely strong signature down to 150 meters.

The model's mixed layer depth deepened with the storm's passage (not shown). The region of colder water in the wake of the typhoon slowly returned to normal but was still visible 10 days after the storm (not shown). This strong response to the realistic wind forcing shows the ability of the model to handle real winds and the importance of realistic daily varying wind stresses in forcing the ocean.

The tropical instability waves on the equator were quite distinct in model run X4 (not shown). The seasonal cycle to these waves developed as in runs X2, S10, and M4. The waves were observed throughout the duration of the model run, although their intensity and the number of waves varied with the season. The waves were not as strong in late 1991 and early 1992 when the cold tongue was quite weak. The waves were stronger during July-September, when the NECC and SEC

were relatively strong and the cold tongue had extended well into the central Pacific. The waves propagated to the west at about 20 cm/s, which is about half the observed speed (Legeckis 1977). The model's weaker and slower propagation speed may be due to the weak SEC and NECC which had about half the observed speed (12 cm/s versus the observed 25 cm/s for the NECC, and 40 cm/s versus the observed 60 cm/s for the SEC Pickard and Emery 1990). This would result in a weaker shear environment in which to develop the waves and a slower westward motion of the waves.

7. Experimental Run X5

Model run X5 was performed to provide a comparison to model run X4 that would highlight the role of the daily varying winds. Run X5 repeated X4 but used smoothed wind stresses instead of the daily fluctuating wind stresses. Chapter II, section B, page 17, describes the procedure used to obtain these smoothed wind stresses.

This model run was started late, so the results are only available through the end of 1991. The model's response to the smoothed winds is similar to that of model run X4 in general structure and response. However, several differences developed in run X5. As expected, these differences are largest at later dates in the model runs. The absence of strong typhoons in run X5 kept the temperatures warmer in

general, probably due to the lack of the intense mixing and upwelling associated with these wind events.

Figures 90 and 91 show the upper level temperature and currents on 26 March 1991 and 12 July 1991. Comparing runs X4 and X5 (Figures 90 and 60) shows that the basic current patterns are the same, but many of the small scale current variations are missing from the smoothed run. This is consistent with the lack of rapid variations in the wind stress. At the later date, a comparison of runs X4 and X5 (Figures 91 and 61) shows that although no westerly winds existed in the smoothed fields for the summer of 1991, the easterly winds did relax enough for the model to develop the weak retreat of the cold tongue that had been observed in previous runs.

Figure 92 shows temperature anomalies calculated by subtracting the fields of model run X4 from those of X5 for 1 October 1991 (just before a retreat of the cold tongue). This figure shows that the western equatorial Pacific is generally warmer, and the eastern equatorial Pacific is generally cooler in model run X5 than in X4. The warmer west Pacific and cooler east Pacific regions in run X5 may be due to a reduction in eastward warm water advection from the west Pacific resulting from a reduction in westerly wind bursts in run X5. The cooler eastern Pacific in run X5 also may be due to increased upwelling caused by the more constant easterly winds resulting from the smoothing of westerly wind bursts in

the run X5 wind stresses. Figure 93 shows a cross section along the equator of the run X5 temperature anomalies. This figure shows that the strong anomalies are limited to the upper 150 meters of the model domain.

Figure 94 shows the upper level current anomalies for run X5 on 1 October 1991. The differences between the current patterns of the two models is small, but numerous small anomalies do exist. The mixed layer depth of model run X5 is on average 5-10 meters shallower than that of model run X4, due to a decrease in the turbulent mixing (not shown). The anomaly fields became quite complex for the period corresponding to the retreat of the cold tongue (not shown). This is because a difference in position of the cold tongue of a degree of longitude is enough to generate extremely large temperature and current anomalies.

Figure 95 shows the upper level temperatures and currents for 11 December 1991. Figure 96 shows a cross section along the equator of the zonal velocity field. These figures can be compared with Figures 66 and 67 which show the same fields on 11 December 1991 in model run X4. Comparisons of these figures show similar major features exist in both model runs. The SEC has reversed, and warm water has been advected to the east. The large scale changes in the model tend to dominate the figures, and so the small scale differences in the two models are not as apparent as they are when the cold tongue is well established. The speeds of the

major currents (EUC, SEC, and reversed SEC) are all faster in this model run than in X4. This is probably due to the more constant wind forcing throughout model run X5. The cold tongue also retreated slightly farther to the east by the end of 1991 in run X5 than in X4. This is again probably due to the weaker, but more constant, westerly wind forcing that existed near the equator when all of the westerly wind bursts were smoothed together.

In general, although the results of model run X5 were similar to those of X4, numerous differences developed due to the lack of the daily varying winds. The major current speeds were 10-20 cm/s higher when using smoothed wind stresses instead of daily varying wind stresses. Based on the results obtained by the end of 1991, the differences between the two model runs would probably continue growing through the rest of the X5 run, with large differences developing during the retreat of the cold tongue at the end of 1992.

C. SUMMARY OF RESULTS

The model's response to the variable wind forcing used in this study was excellent. The model remained stable and developed realistic responses to wind forcing events on time scales of a few days to years. The increases in basin size allowed the model to develop more realistic current and temperature patterns. This also reduced the problems due to large anomalous currents that tended to develop on the western

boundary in the small basin runs, and reduced problems with wave reflections off the model's closed boundaries. The daily varying wind field was extremely important in the development of the model's temperature and current patterns. Experimental run X5 shows that the absence of daily variations in wind stress may lead to large basin scale temperature and current anomalies.

One area of concern in the early developmental work on this model (Whitney 1992) was the extremely noisy mixed layer depth field. The increase of the basin size has tended to reduce the development oı pockets of extremely shallow or deep mixed layer depths. Some of the remaining small scale variations in the mixed layer depth may be explained by the mixed layer depth definition used in this model. The mixed layer depth is defined by the depth of turbulent mixing, which can have large variations over short horizontal scales due to changes in surface currents and wind forcing.

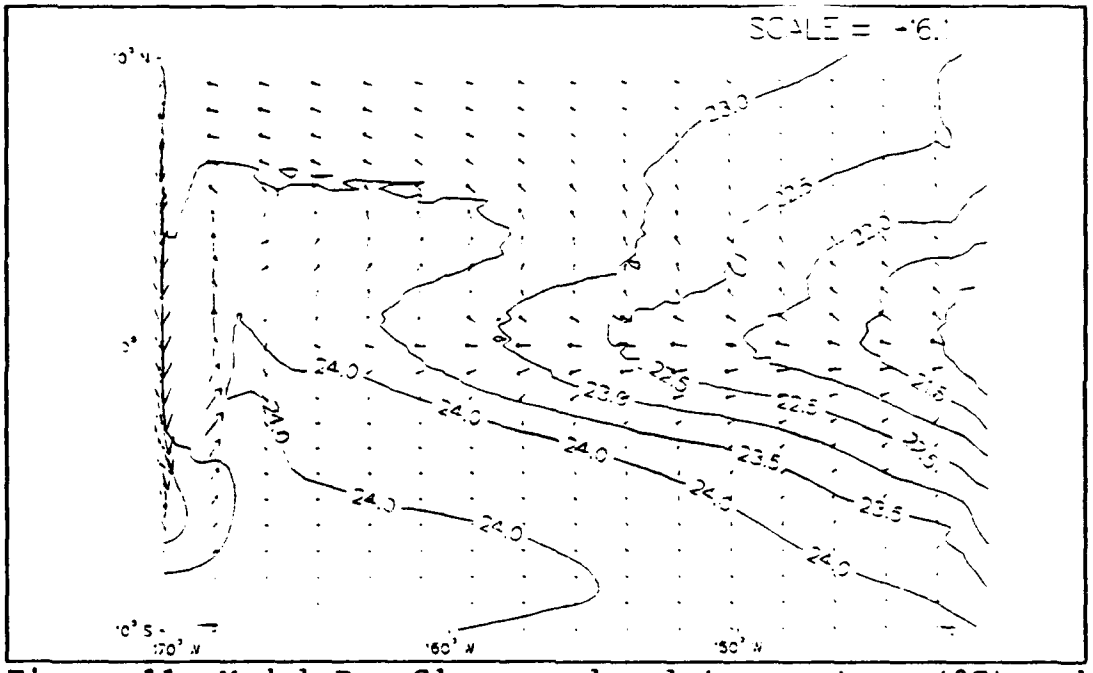

Figure 11. Model Run S1 upper level temperature (°C) and currents (cm/s) at the end of the model run.

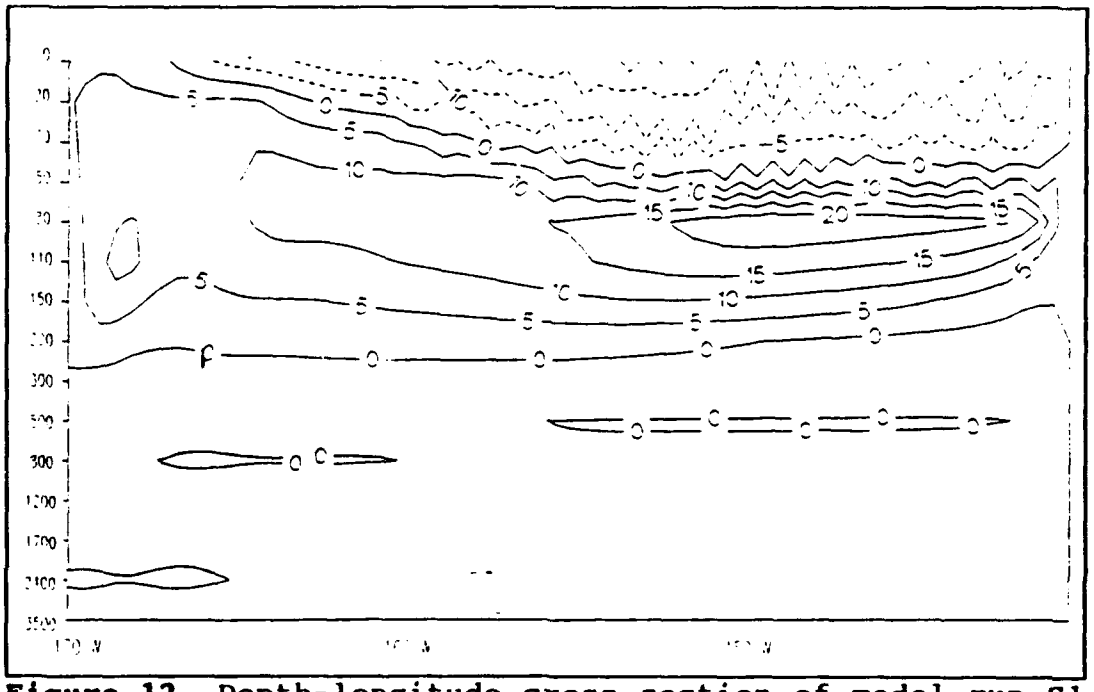

Figure 12. Depth-longitude cross section of model run S1 zonal currents (cm/s) along the equator at the end of the model run. Dashed (solid) contours indicate westward (eastward) flow.

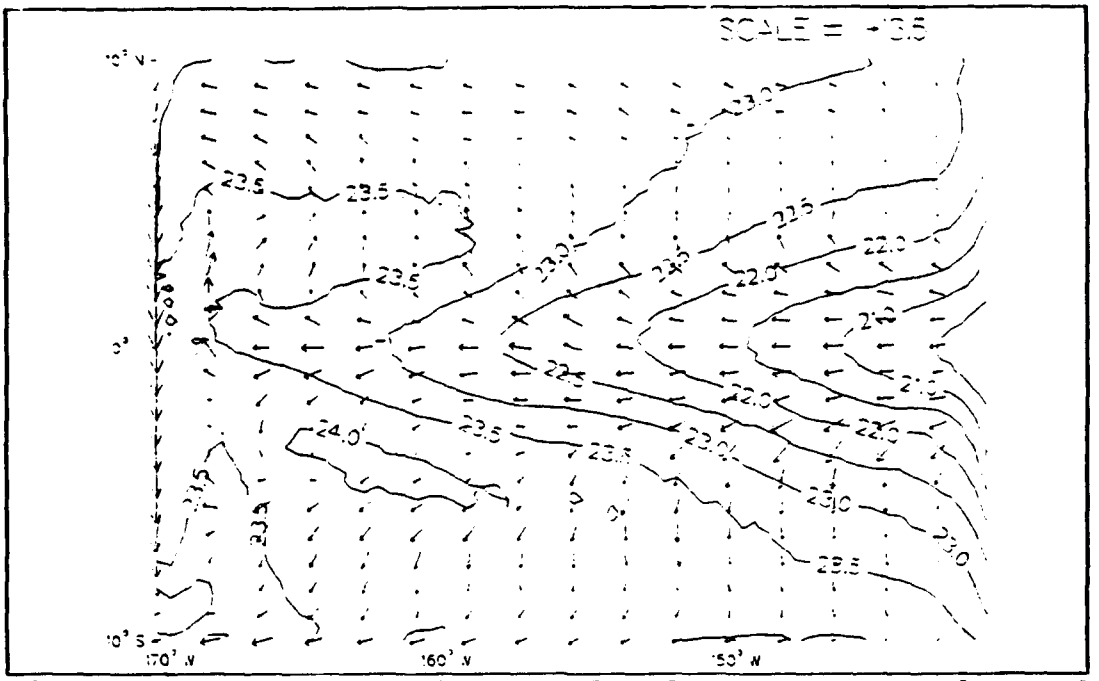

Figure 13. Model run S2 upper level temperature (°C) and currents (cm/s) on 9 January 1992, showing the maximum extent of the cold tongue.

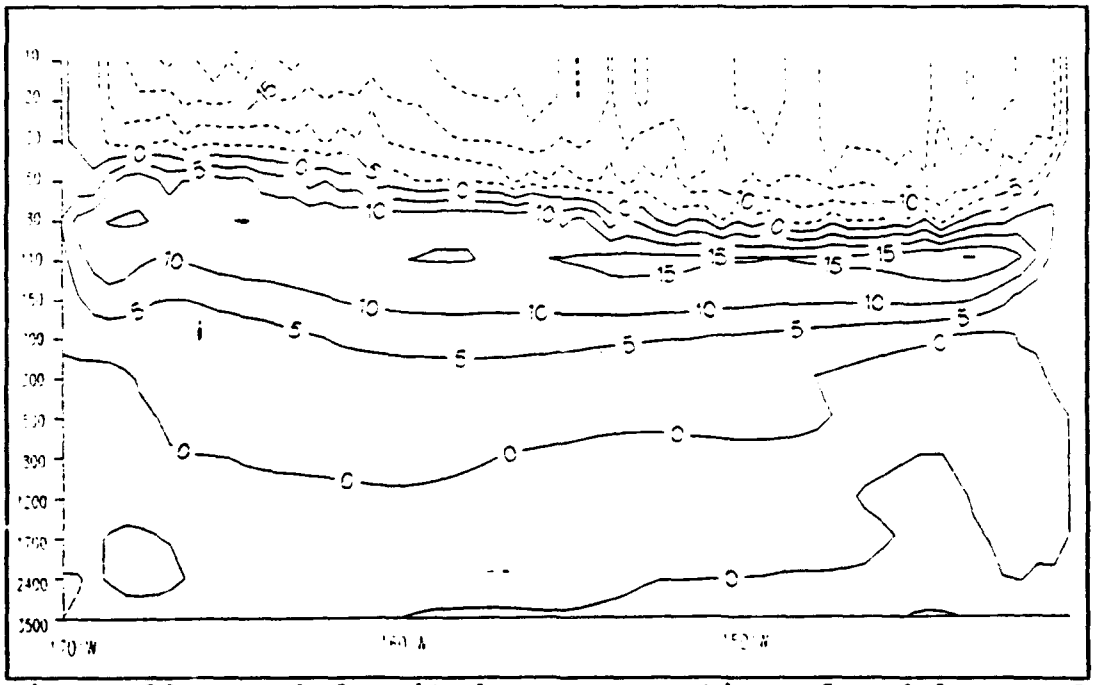

Figure 14. Depth-longitude cross section of model run S2 zonal currents (cm/s) along the equator on 9 January 1992. Dashed (solid) contours indicate westward (eastward) flow.

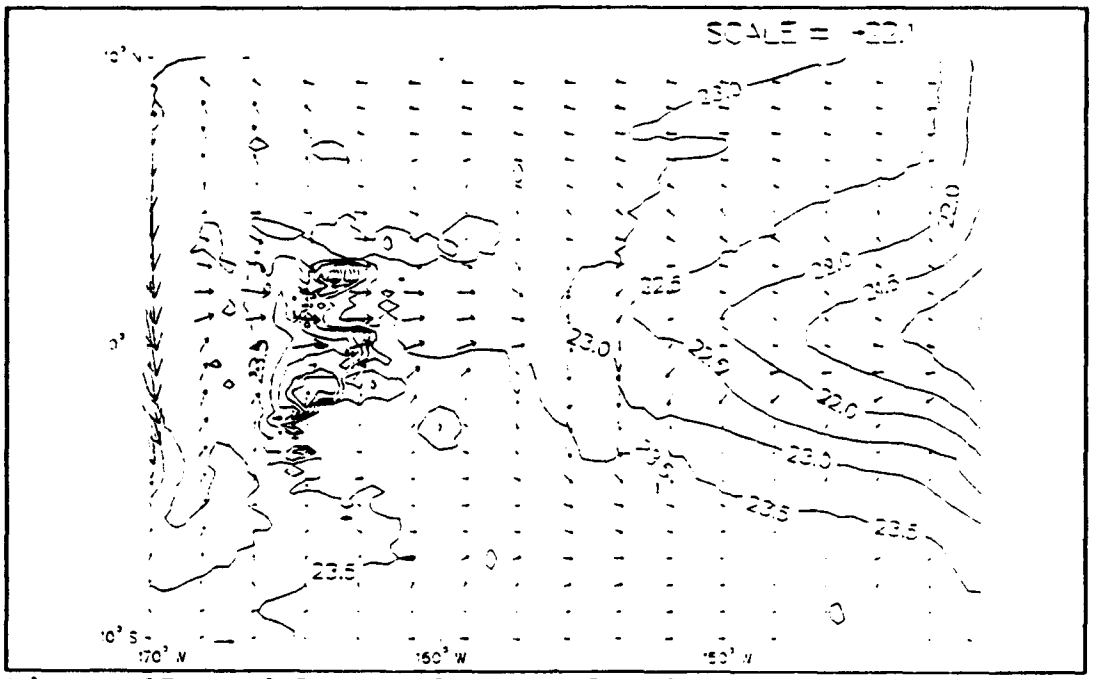

Figure 15. Model run S2 upper level temperature (°C) and currents (cm/s) on 2 February 1992, when the cold tongue has retreated to the east.

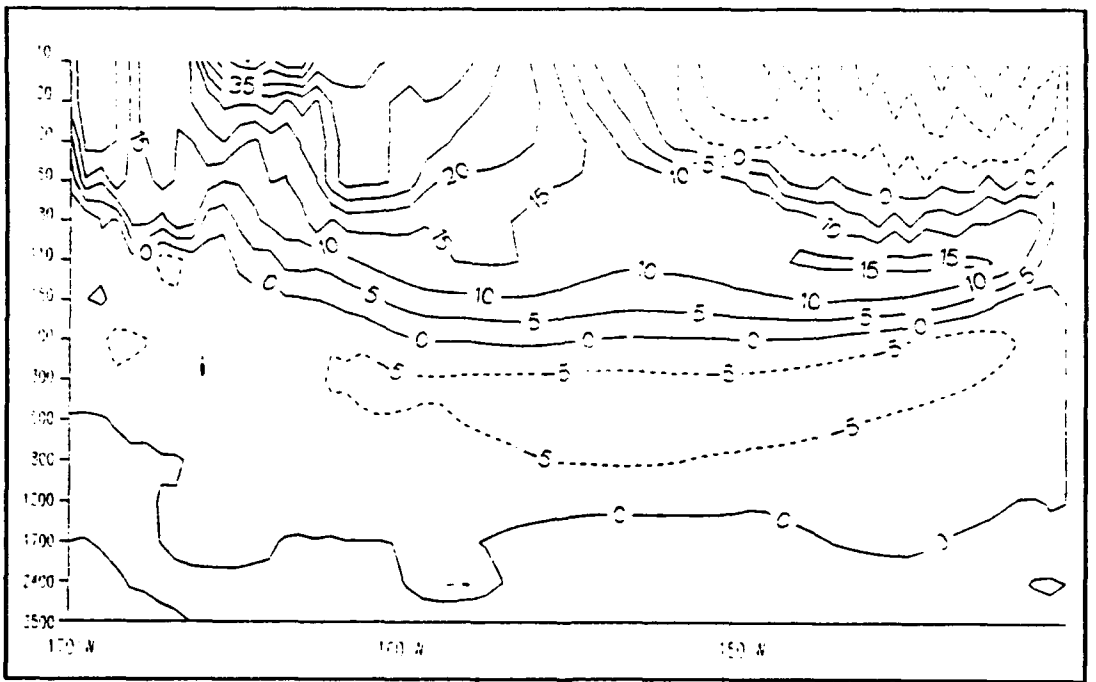

Figure 16. Depth-longitude cross section of model run S2 zonal currents (cm/s) along the equator on 2 February 1992. Dashed (solid) contours indicate westward (eastward) flow.

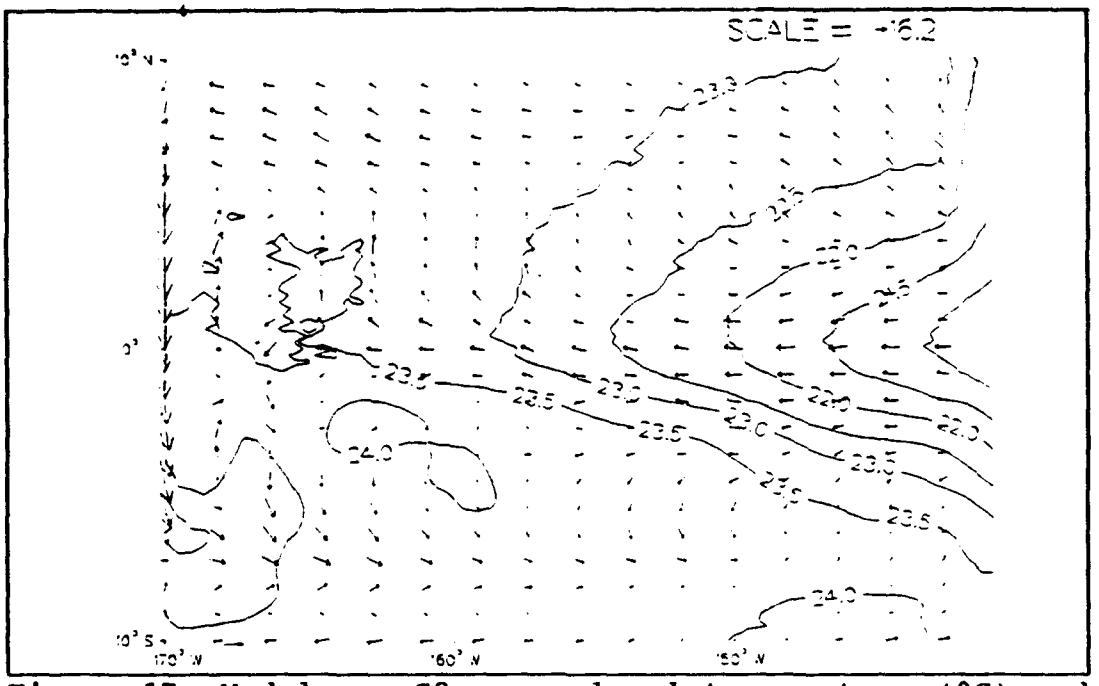

Figure 17. Model run S2 upper level temperature (°C) and currents (cm/s) at the end of the model run (29 February 1992) as the cold tongue extends back to the west.

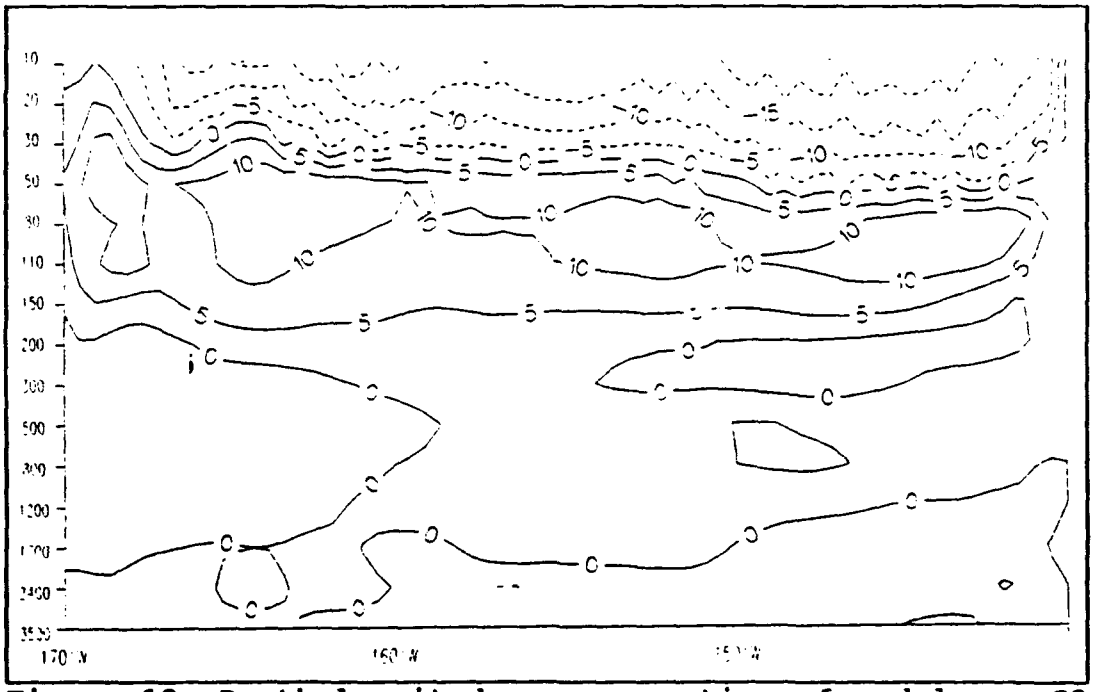

Figure 18. Depth-longitude cross section of model run S2 zonal currents (cm/s) along the equator at the end of the model run (29 February 1992). Dashed (solid) contours indicate westward (eastward) flow.

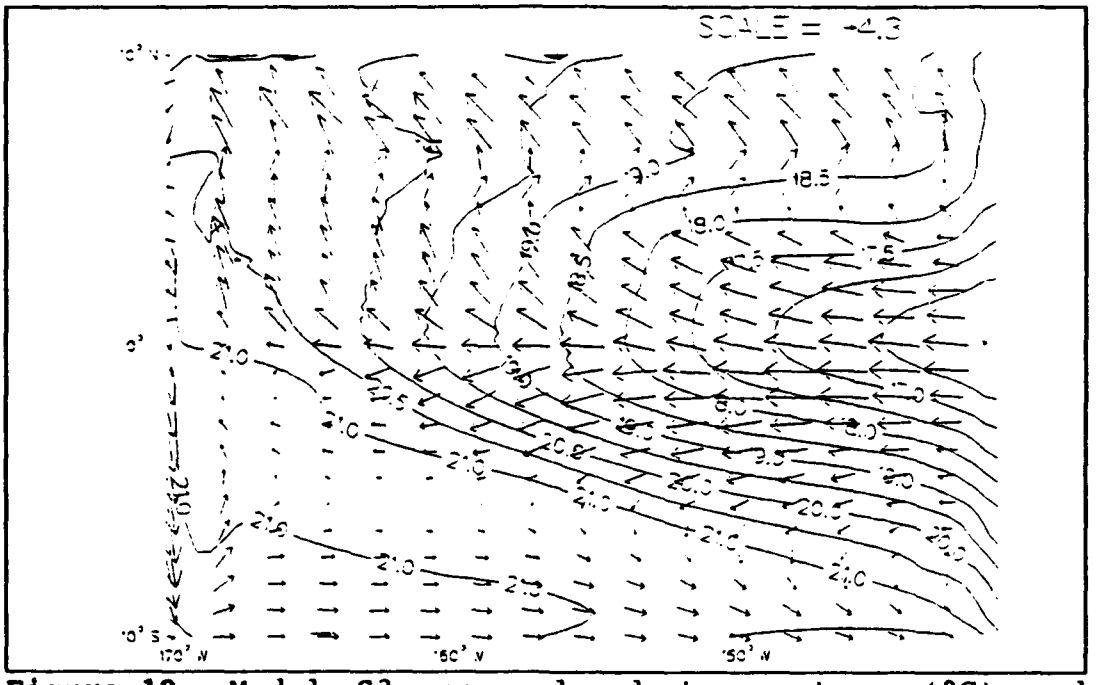

Figure 19. Model S3 upper level temperature (°C) and currents (cm/s) at the end of the model run with a Δt of 1800s.

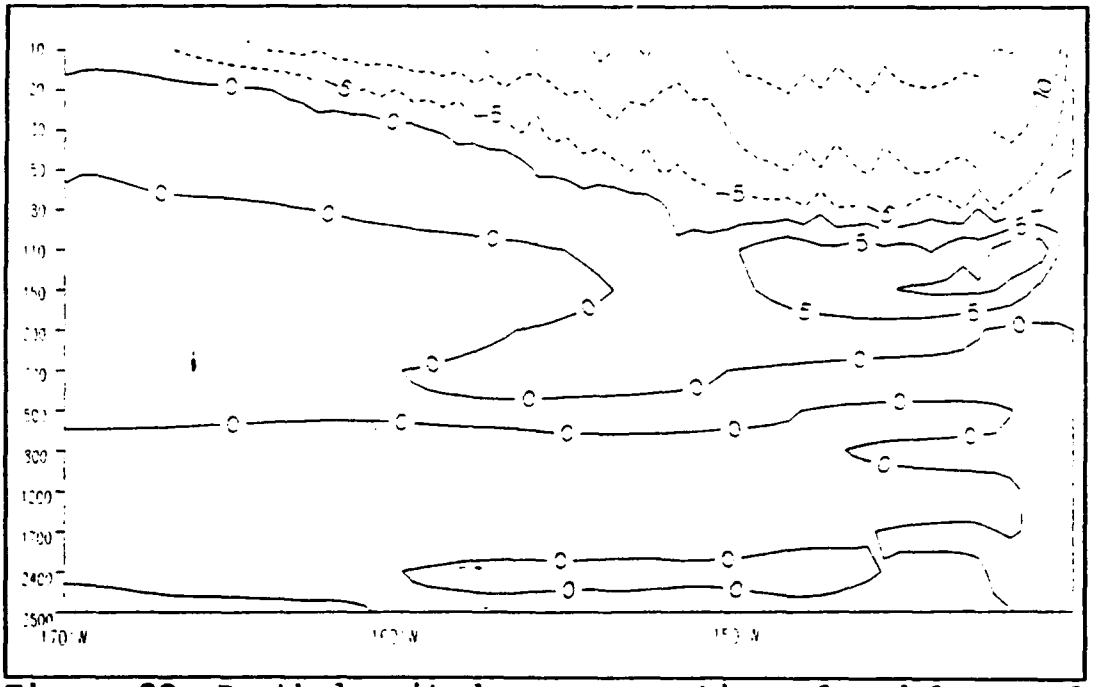

Figure 20. Depth-longitude cross section of model run S3 zonal currents (cm/s) along the equator at the end of the model run with a Δt of 1800s. Dashed (solid) contours indicate westward (eastward) flow.

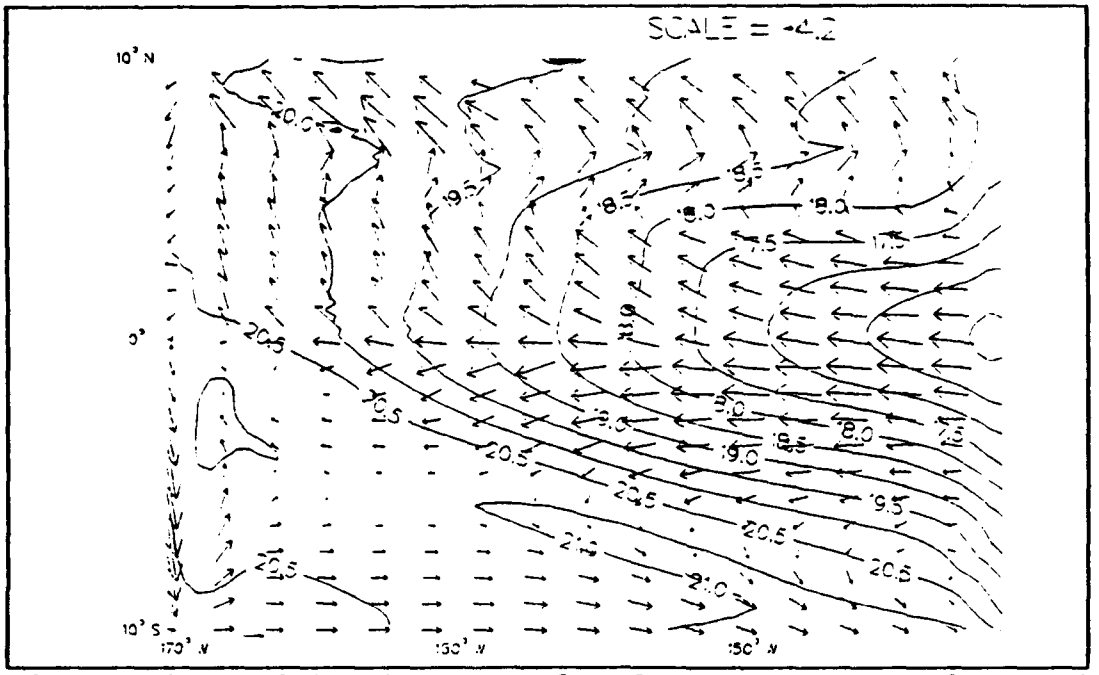

Figure 21. Model S4 upper level temperature (°C) and currents (cm/s) at the end of the model run with a Δt of 2400s.

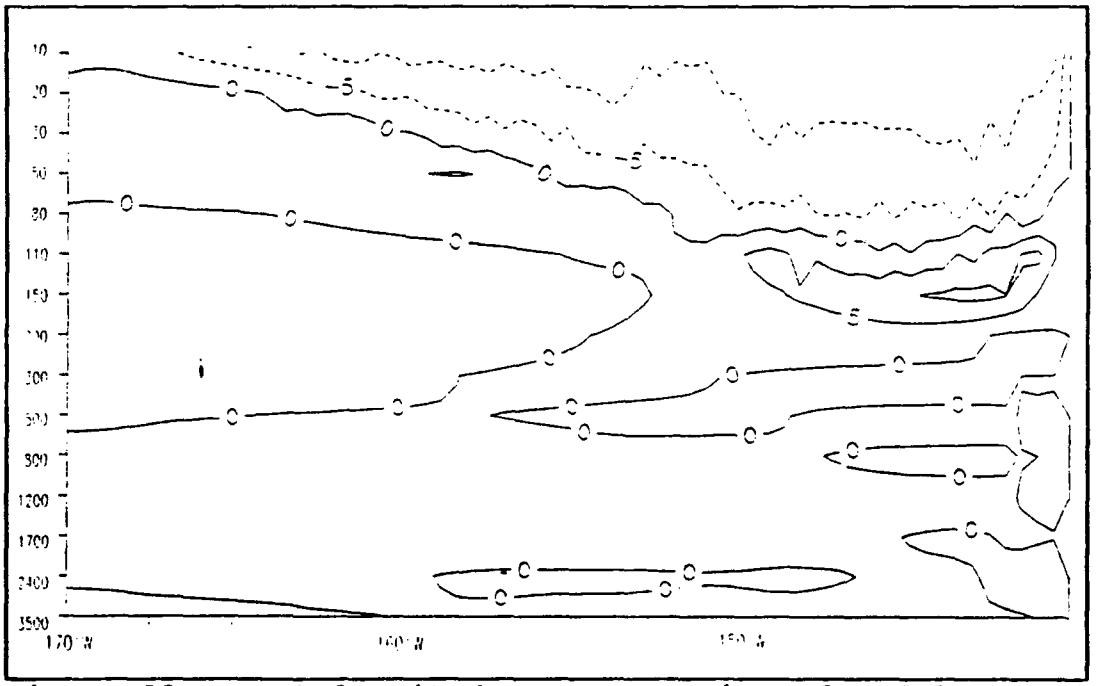

Figure 22. Depth-longitude cross section of model run S4 zonal currents (cm/s) along the equator at the end of the model run with a Δt of 2400s. Dashed (solid) contours indicate westward (eastward) flow.

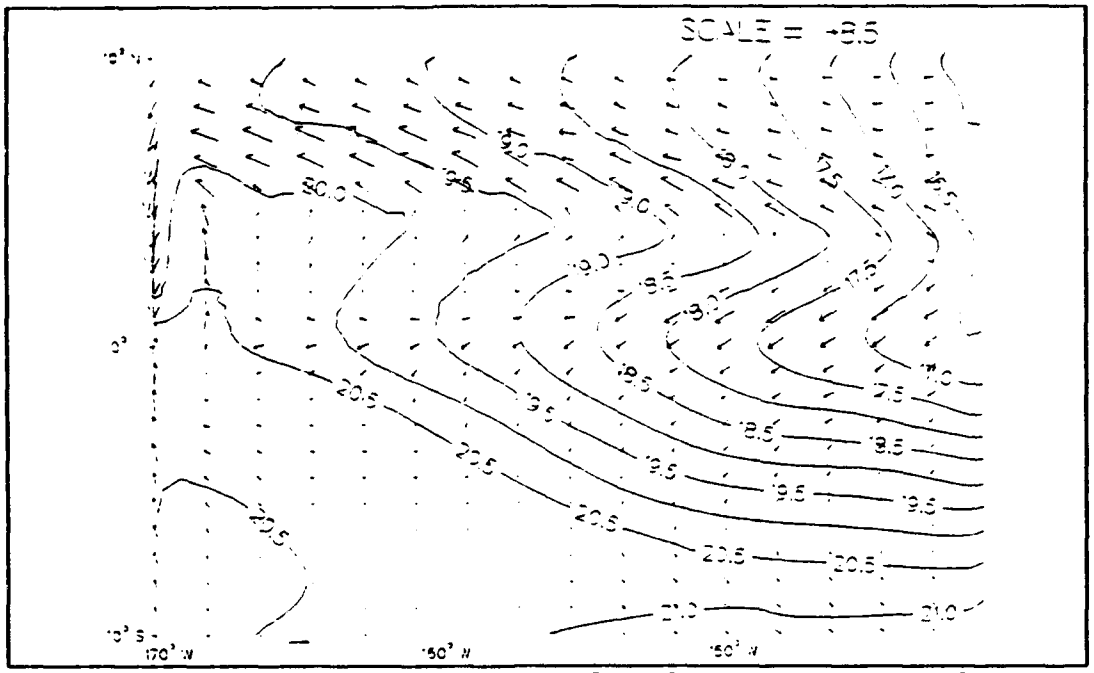

Figure 23. Model run S5 upper level temperature (°C) and currents (cm/s) at the end of the model run with a Δt of 3600s.

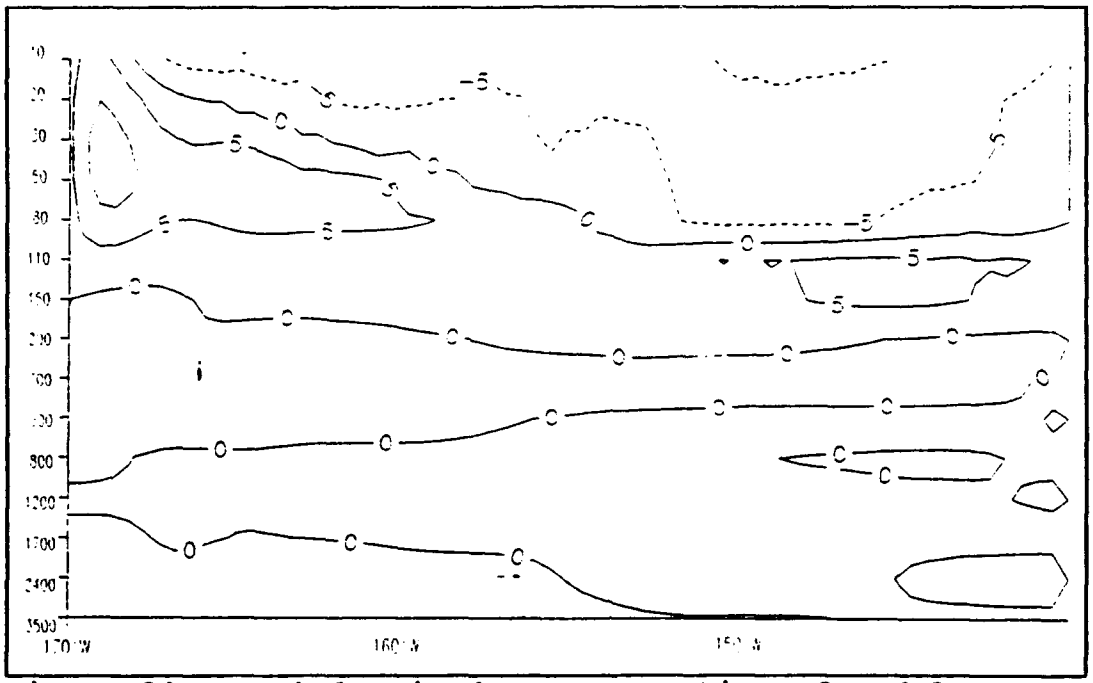

Figure 24. Depth-longitude cross section of model run S5 zonal currents (cm/s) along the equator at the end of the model run with a Δt of 3600s. Dashed (solid) contours indicate westward (eastward) flow.

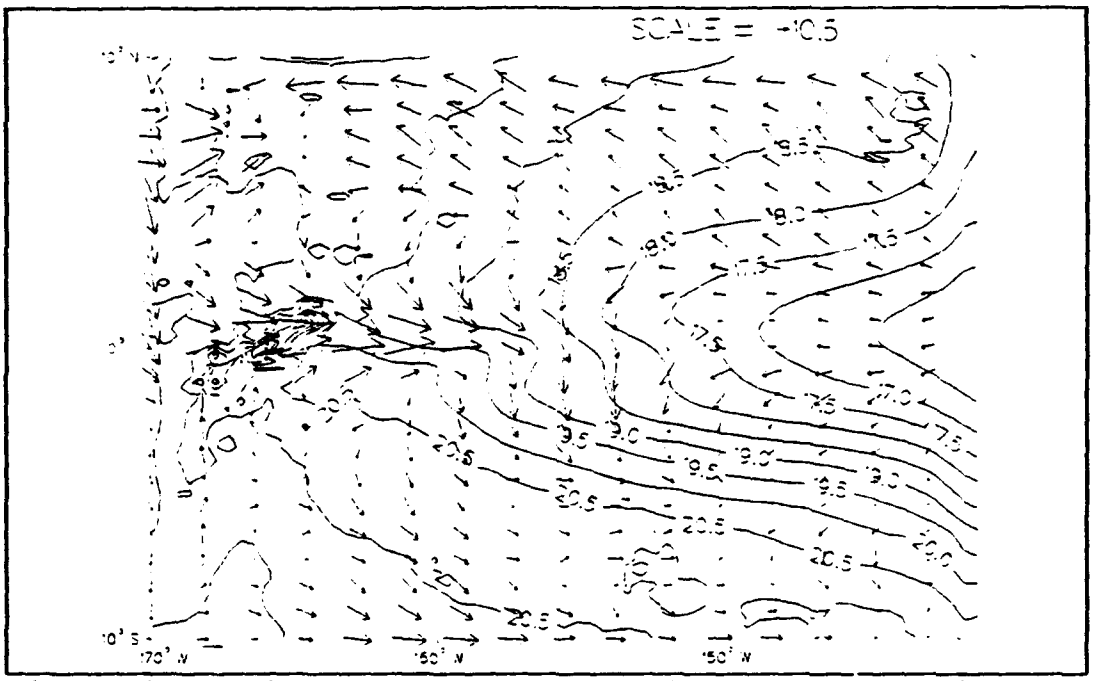

Figure 25. Model run S6 upper level temperature (°C) and currents (cm/s) on 2 February 1992, with a Δt of 1800s.

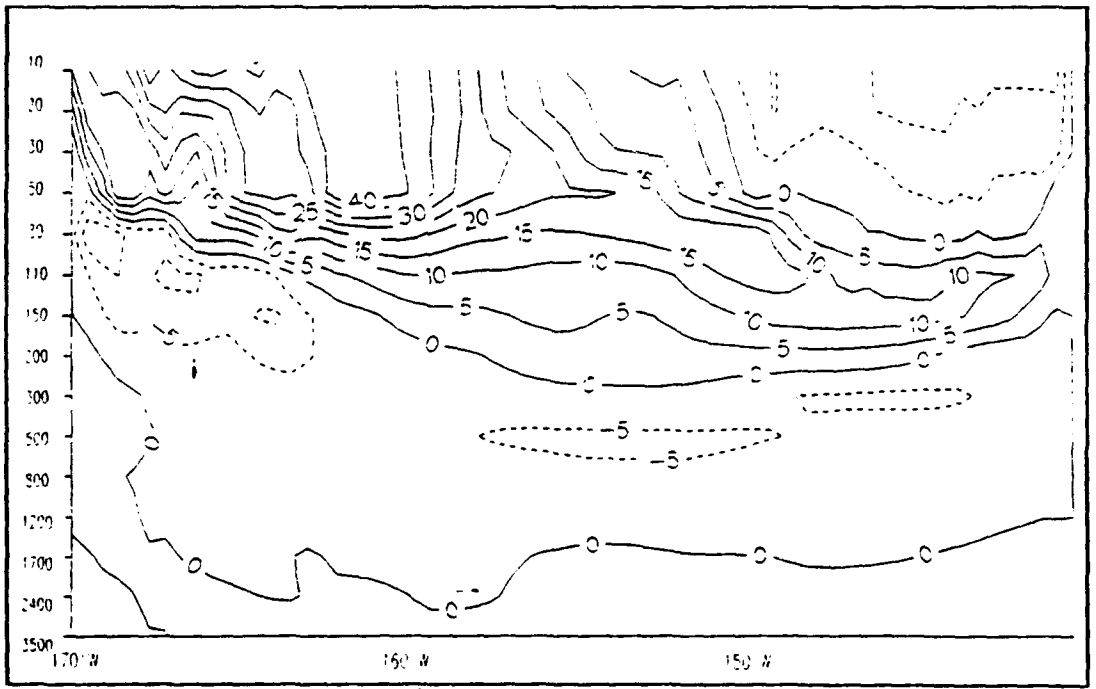

Figure 26. Depth-longitude cross section of model run S6 zonal currents (cm/s) along the equator on 2 February 1992, with a Δt of 1800s. Dashed (solid) contours indicate westward (eastward) flow.

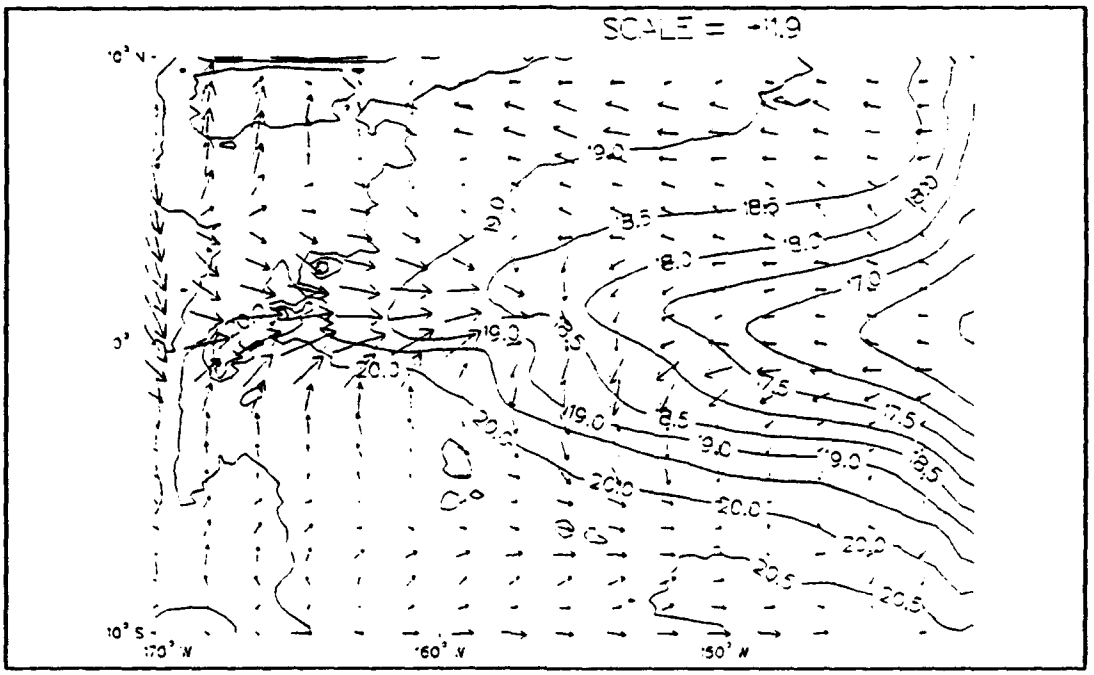

Figure 27. Model run S7 upper level temperature (°C) and currents (cm/s) on 2 February 1992, with a Δt of 2400s.

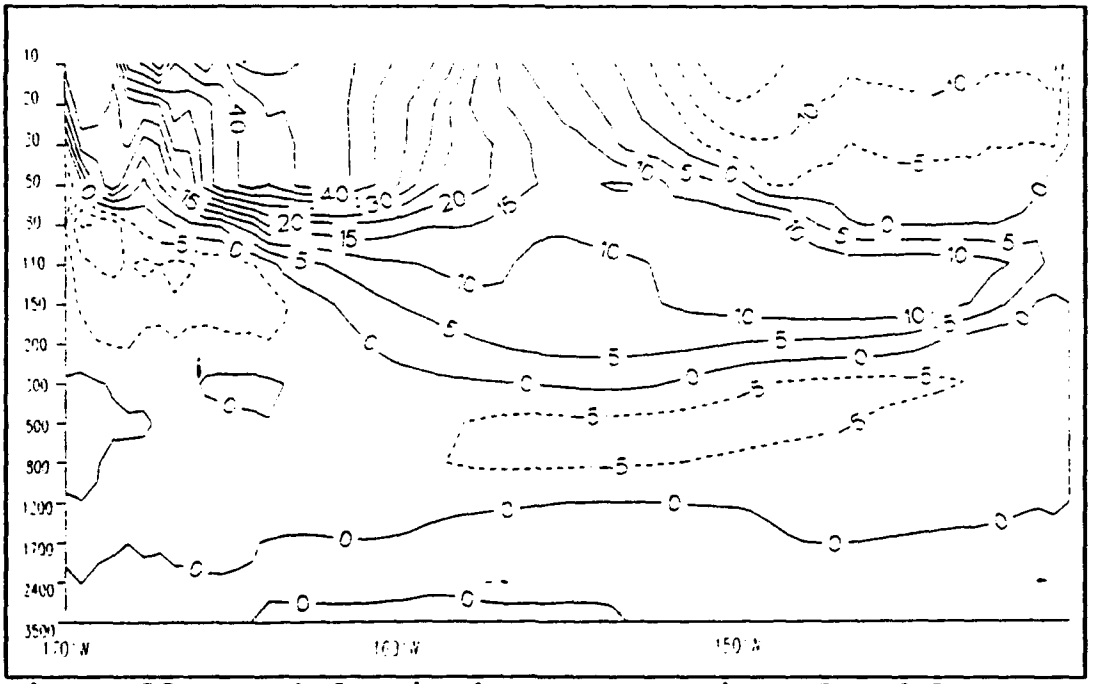

Figure 28. Depth-longitude cross section of model run S7 zonal currents (cm/s) along the equator on 2 February 1992, with a Δt of 2400s. Dashed (solid) contours indicate westward (eastward) flow.

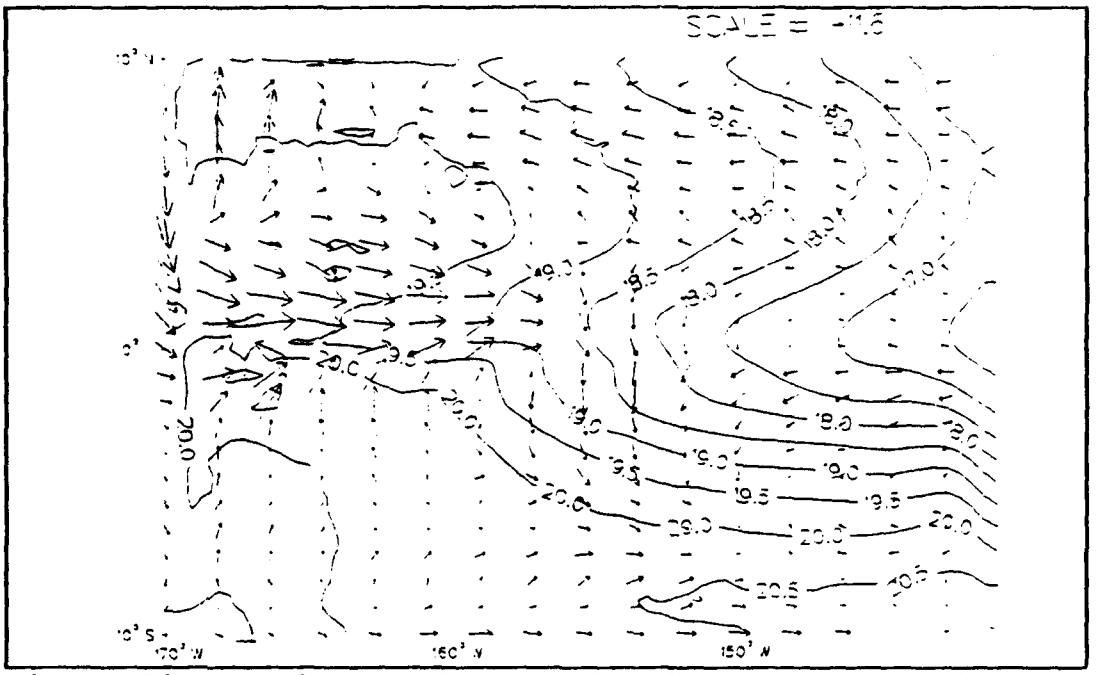

Figure 29. Model run S8 upper level temperature (°C) and currents (cm/s) on 2 February 1992, with a Δt of 3600s.

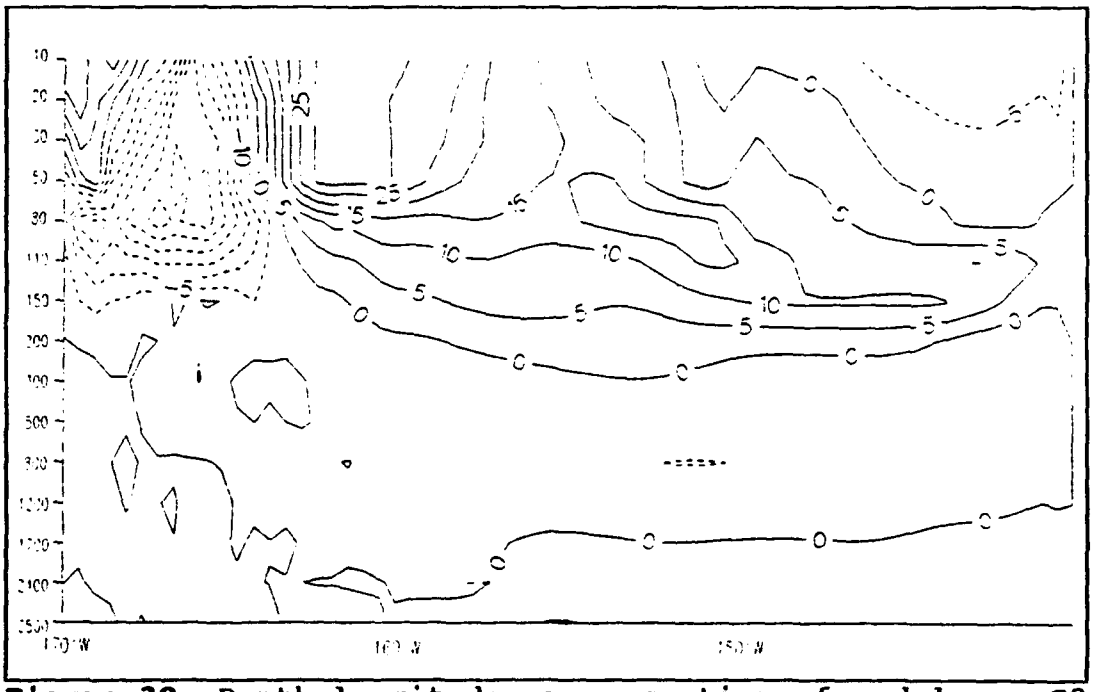

Figure 30. Depth-longitude cross section of model run S8 zonal currents (cm/s) along the equator on 2 February 1992, with a Δt of 3600s. Dashed (solid) contours indicate westward (eastward) flow.

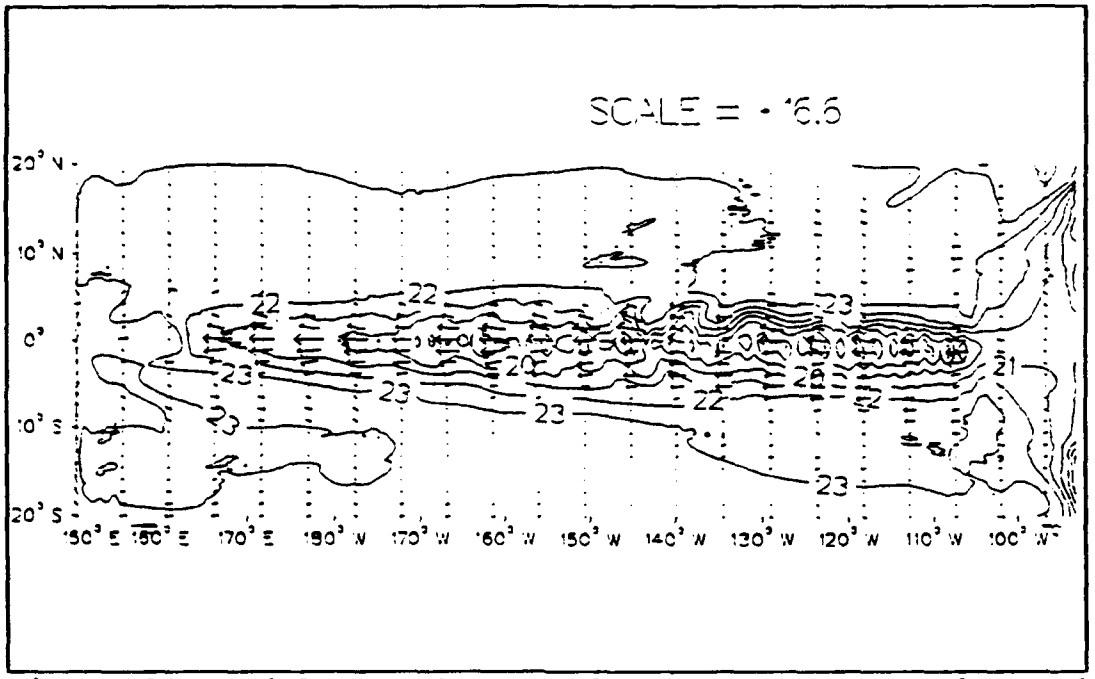

Figure 31. Model run X1 upper level temperature (°C) and currents (cm/s) at the end of the model run.

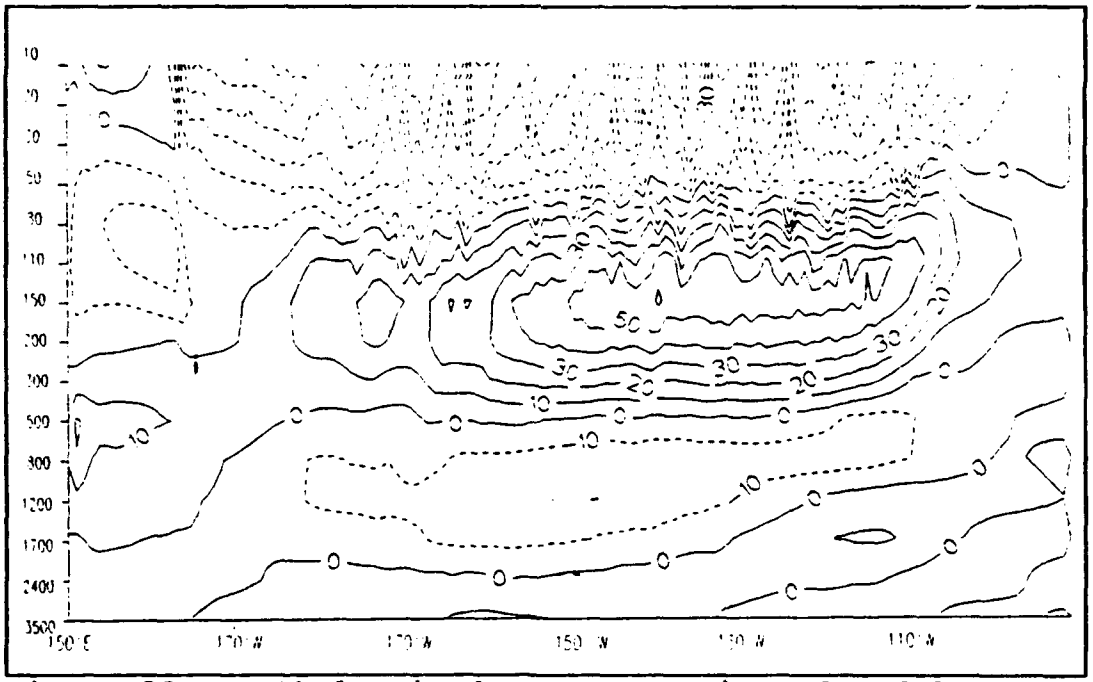

Figure 32. Depth-longitude cross section of model run X1 zonal currents (cm/s) along the equator at the end of the model run. Dashed (solid) contours indicate westward (eastward) flow.

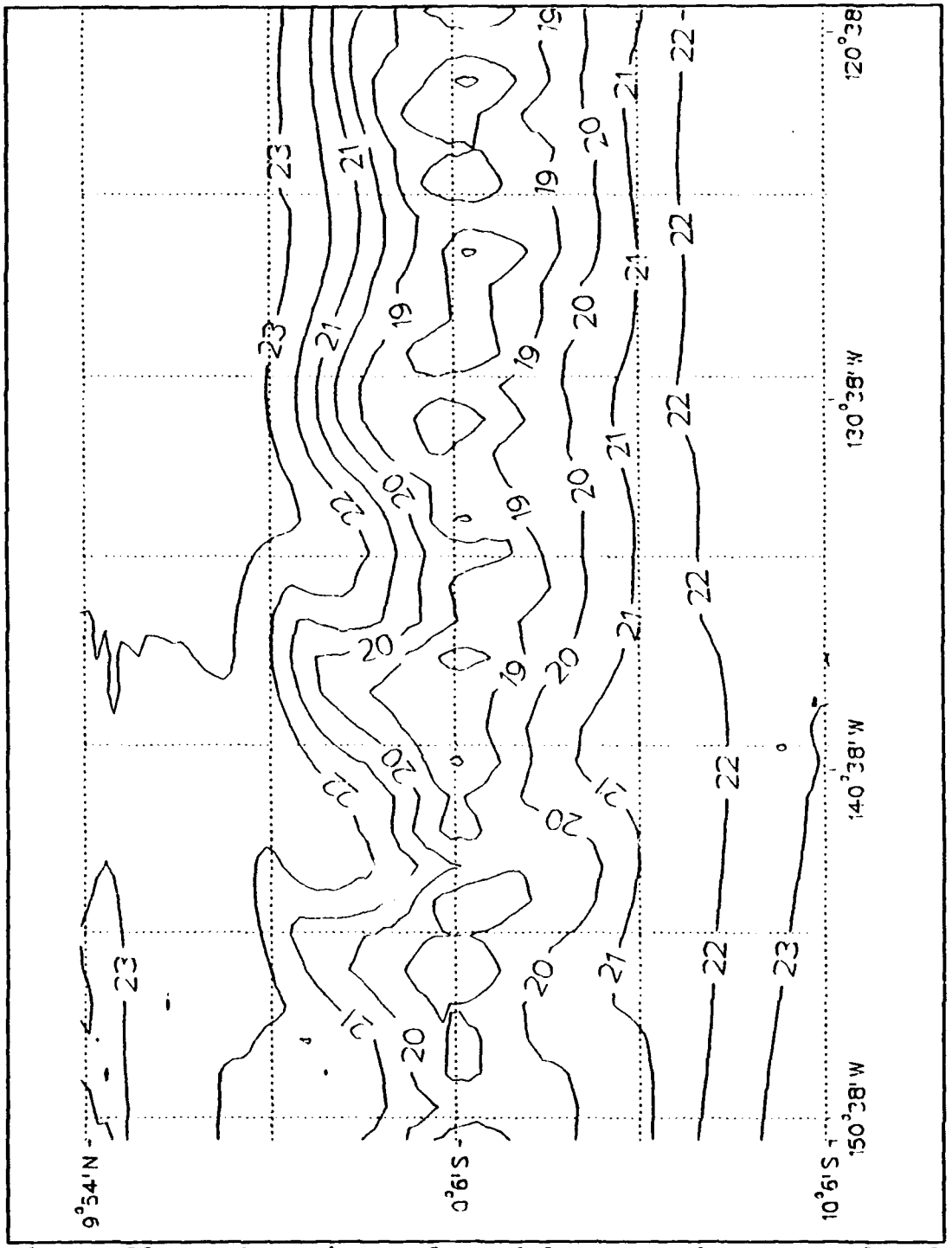

Figure 33. Subsection of model run X1 upper level temperature, showing waves observed along the north and south boundaries of the eastern portion of the cold tongue at the end of model run.

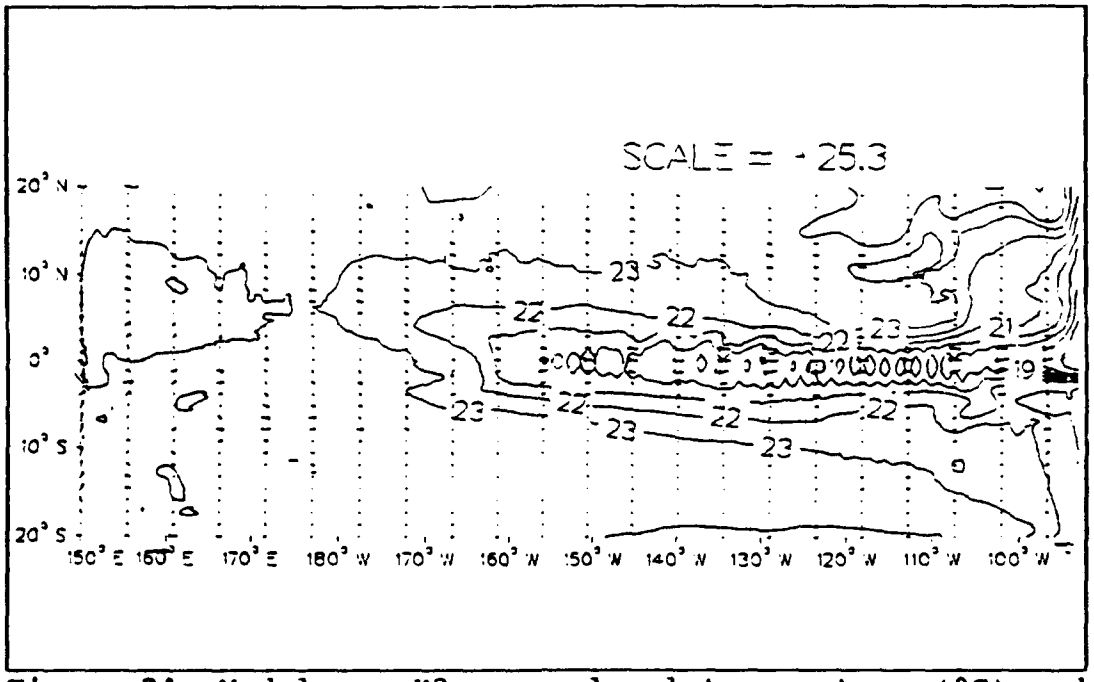

Figure 34. Model run X2 upper level temperature (°C) and currents (cm/s) on 21 March 1992. During the second cold tongue retreat.

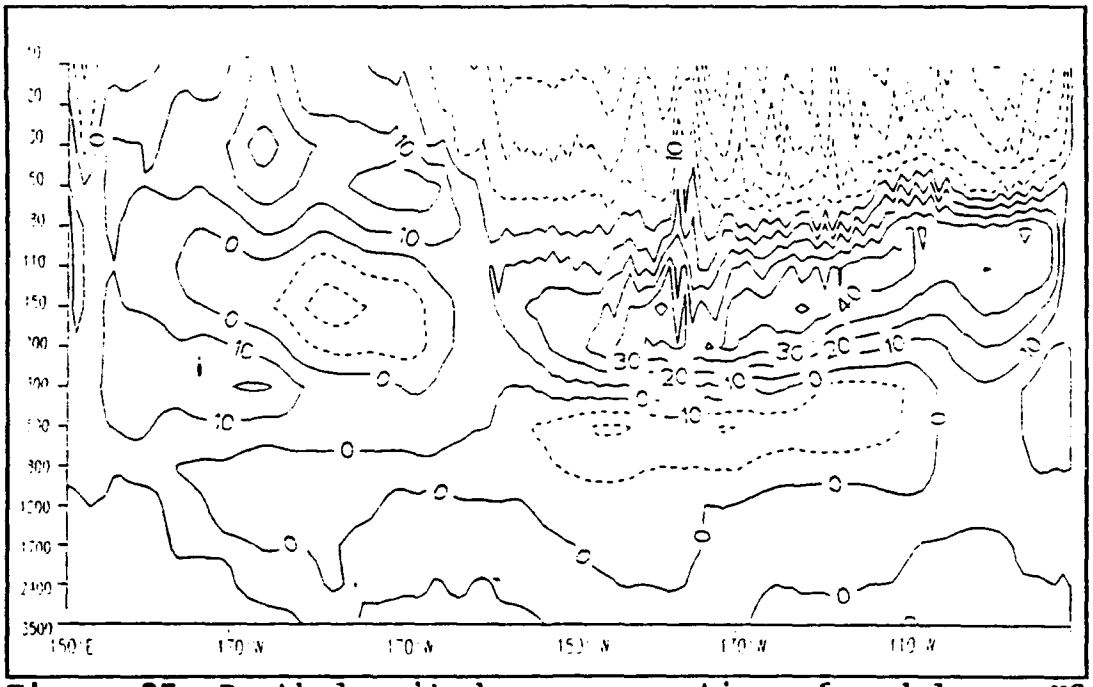

Figure 35. Depth-longitude cross section of model run X2 zonal currents (cm/s) along the equator on 21 March 1992. During the second cold tongue retreat. Dashed (solid) contours indicate westward (eastward) flow.

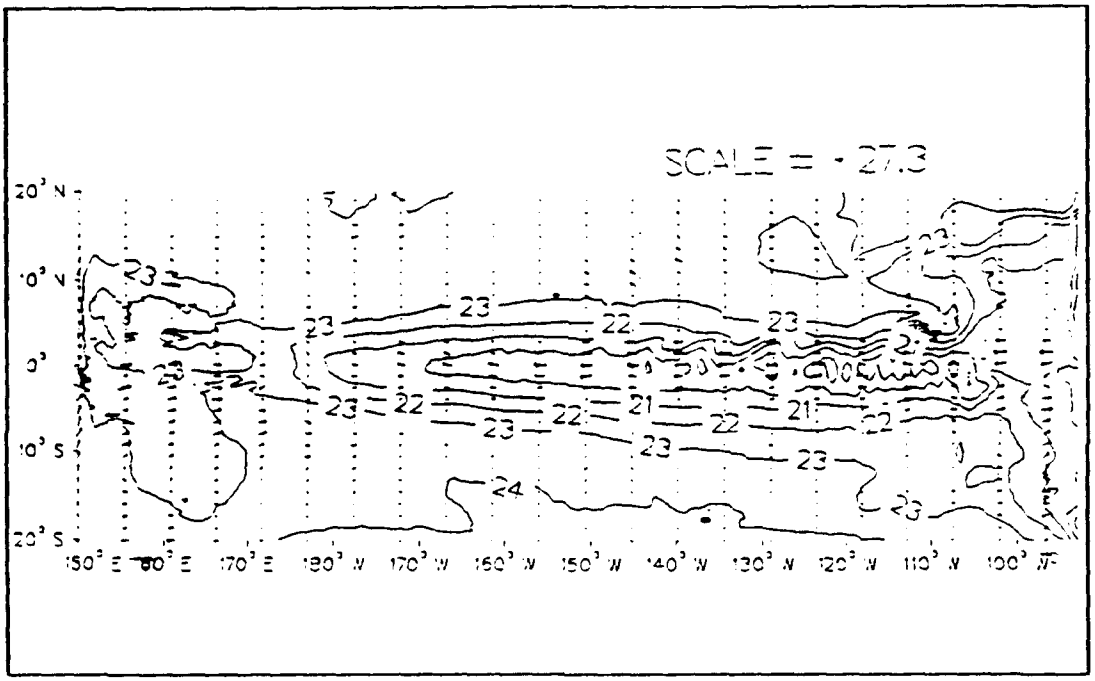

Figure 36. Model run X2 upper level temperature (°C) and currents (cm/s) on 31 December 1992. During the second cold tongue retreat.

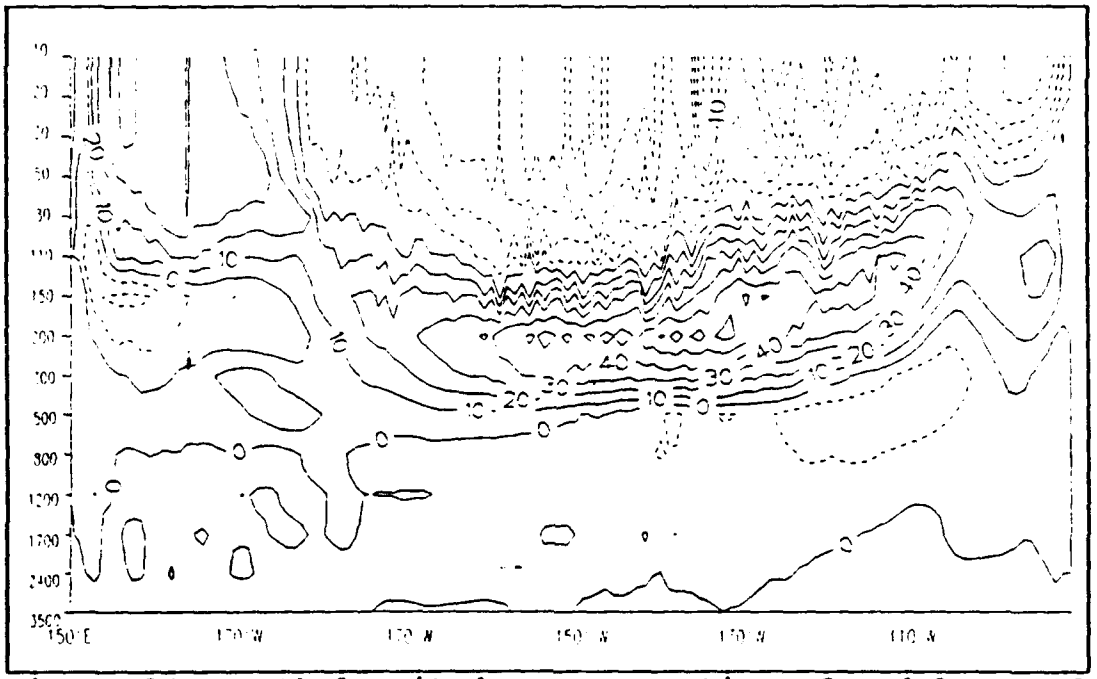

Figure 37. Depth-longitude cross section of model run X2 zonal currents (cm/s) along the equator on 31 December 1992. During the third cold tongue retreat. Dashed (solid) contours indicate westward (eastward) flow.

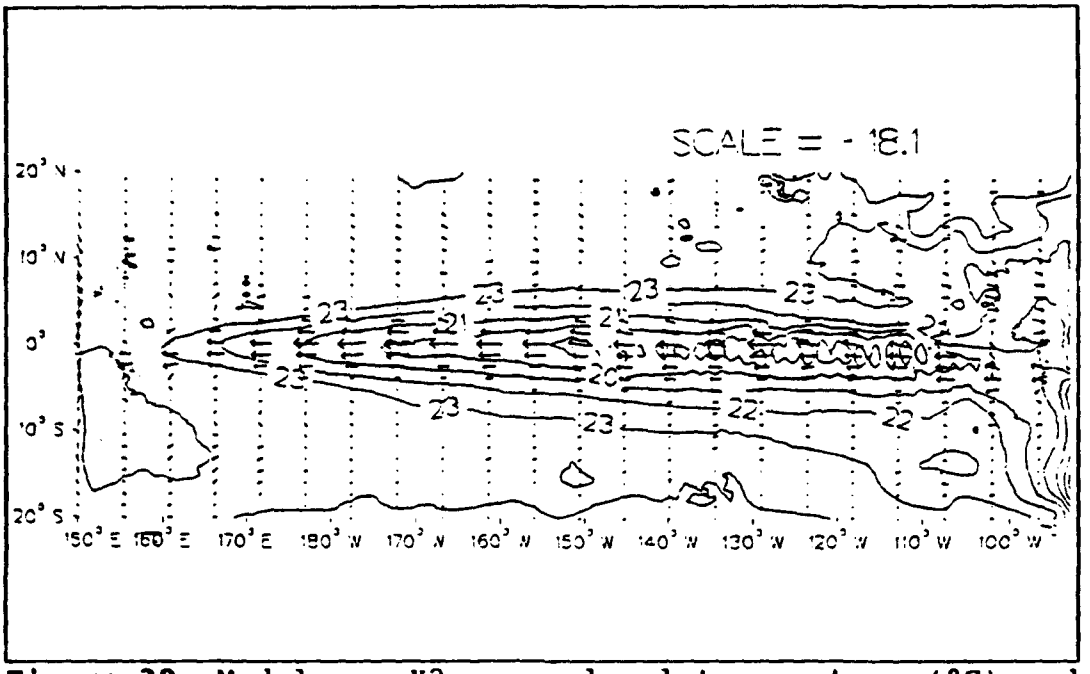

Figure 38. Model run X2 upper level temperature (°C) and currents (cm/s) on 25 September 1992. In between the second and third cold tongue retreats.

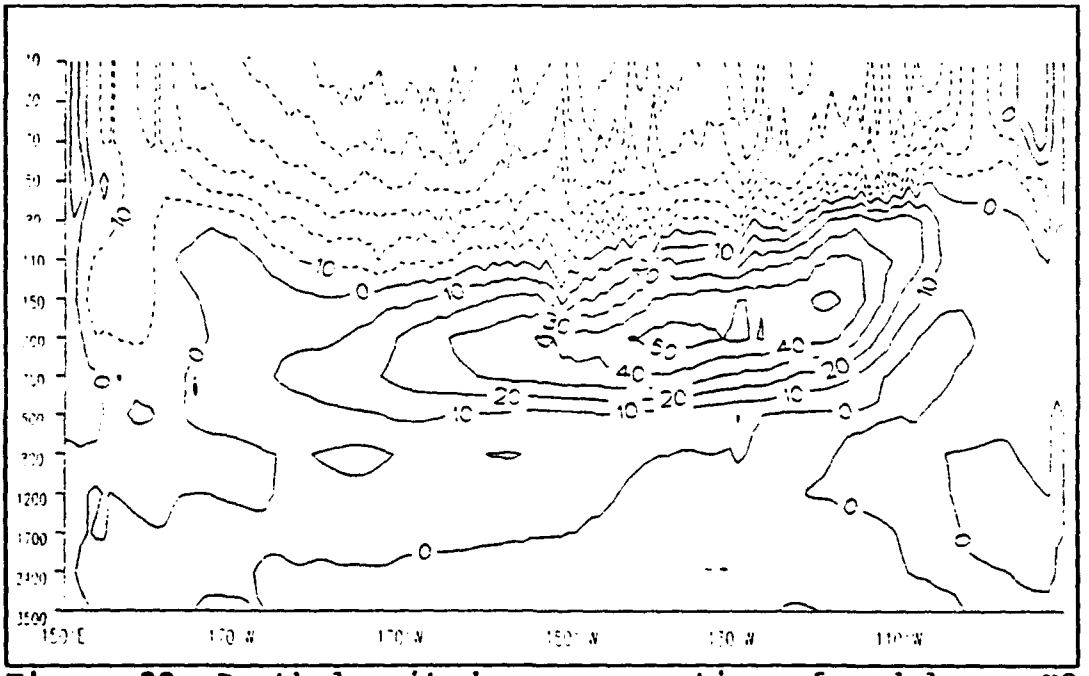

Figure 39. Depth-longitude cross section of model run X2 zonal currents (cm/s) along the equator on 25 September 1992. In between the second and third cold tongue retreats. Dashed (solid) contours indicate westward (eastward) flow.

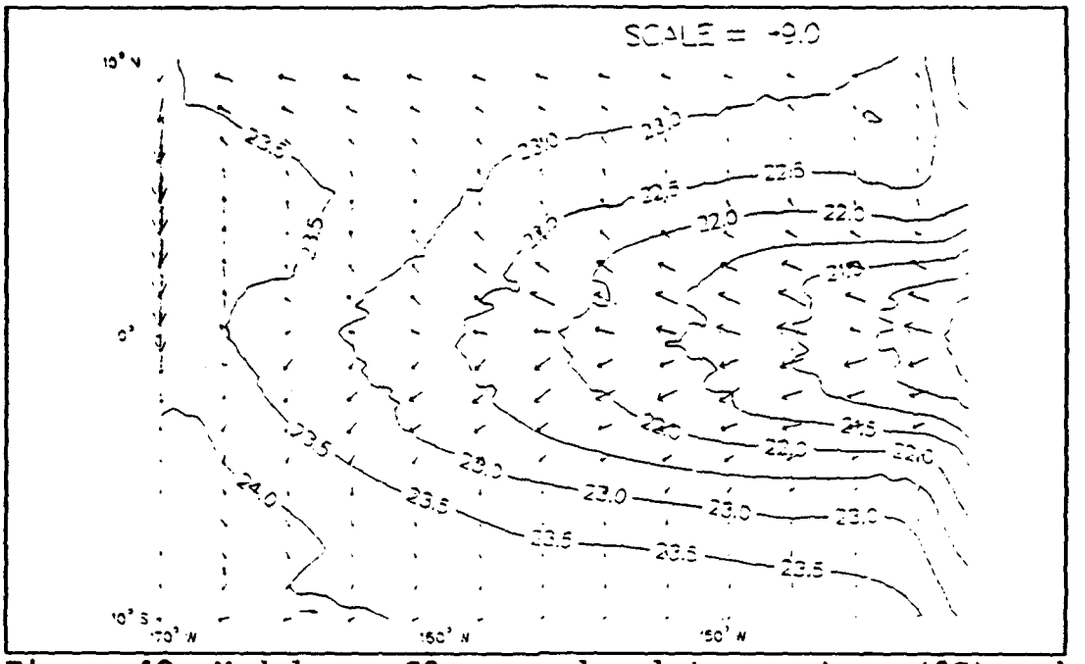

Figure 40. Model run S9 upper level temperature (°C) and currents (cm/s) at the end of the model run.

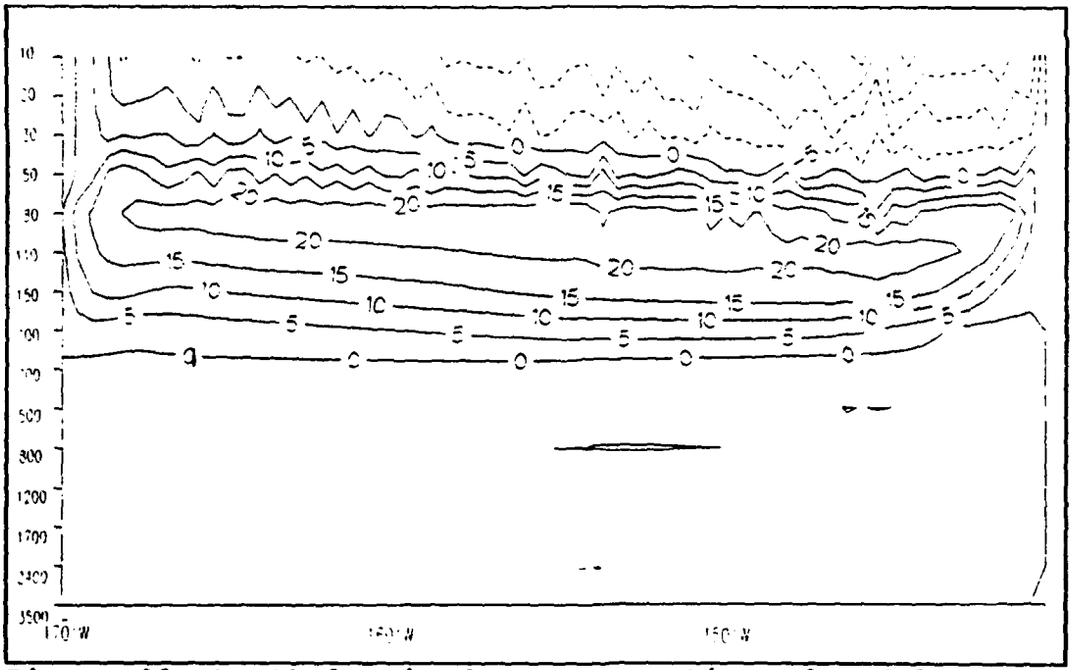

Figure 41. Depth-longitude cross section of model run S9 zonal currents (cm/s) along the equator at the end of the model run. Dashed (solid) contours indicate westward (eastward) flow.

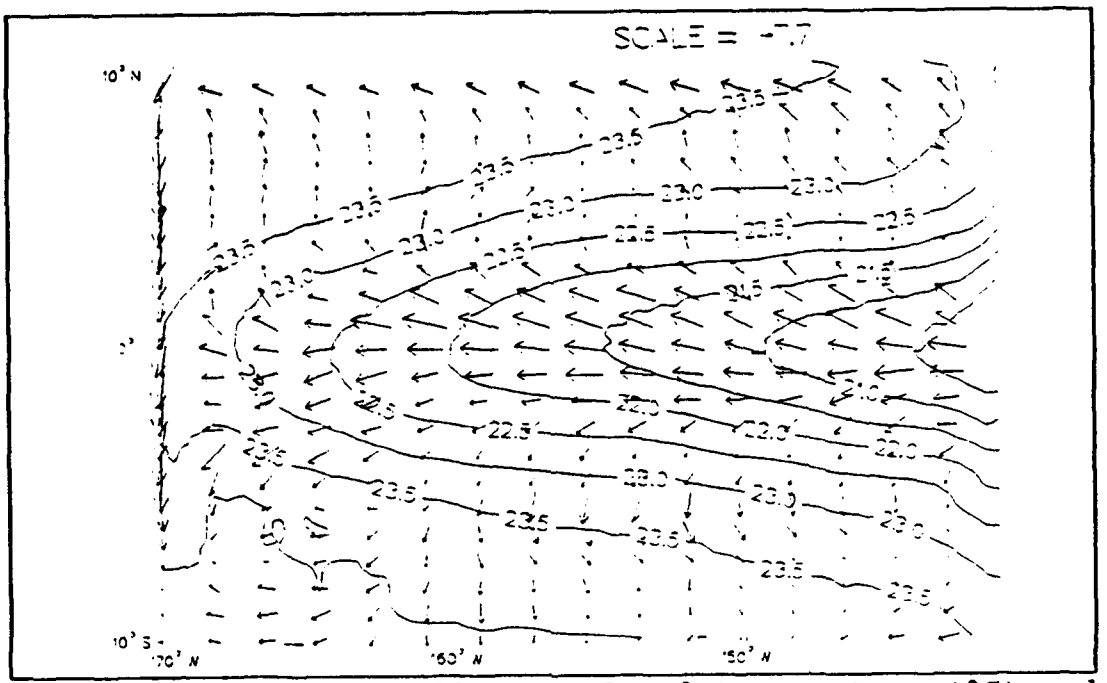

Figure 42. Model run S10 upper level temperature (°C) and currents (cm/s) on 27 February 1992. During the second cold tongue retreat.

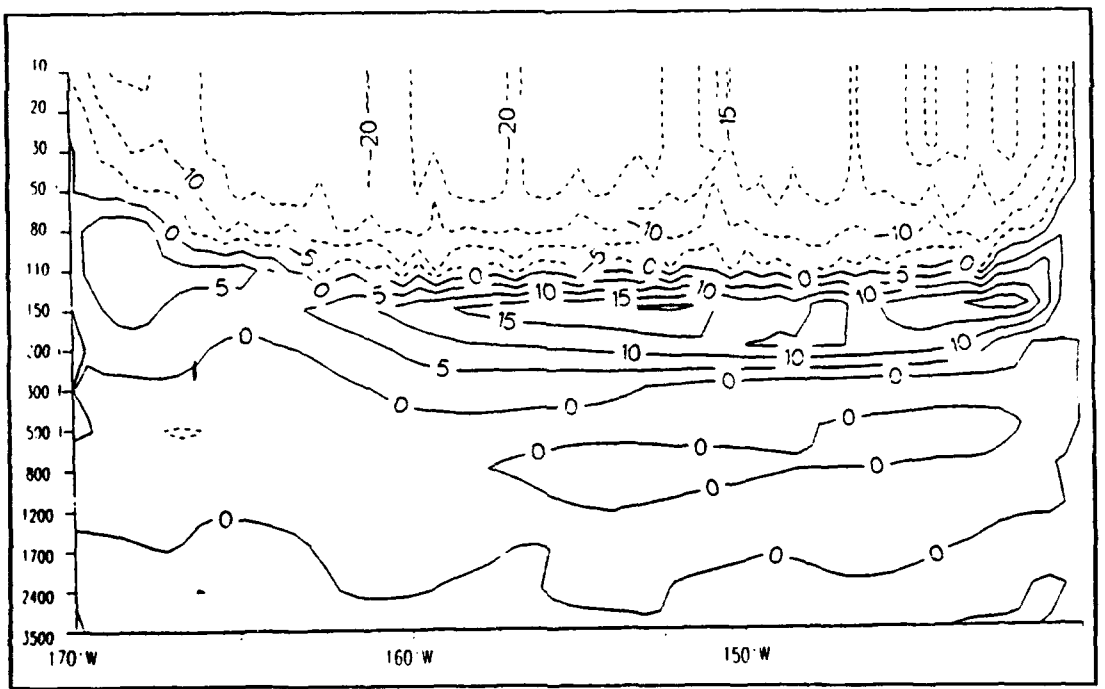

Figure 43. Depth-longitude cross section of model run S10 zonal currents (cm/s) along the equator on 27 February 1992. During the second cold tongue retreat. Dashed (solid) contours indicate westward (eastward) flow.

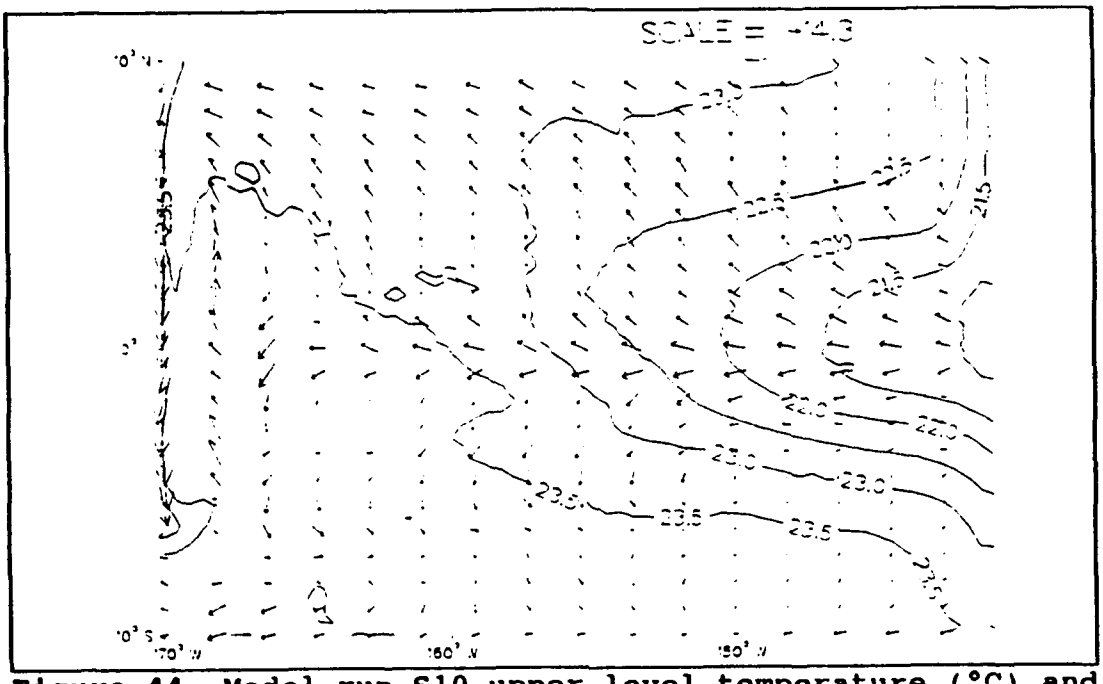

Figure 44. Model run S10 upper level temperature (°C) and currents (cm/s) on 31 December 1992. During the third cold tongue retreat.

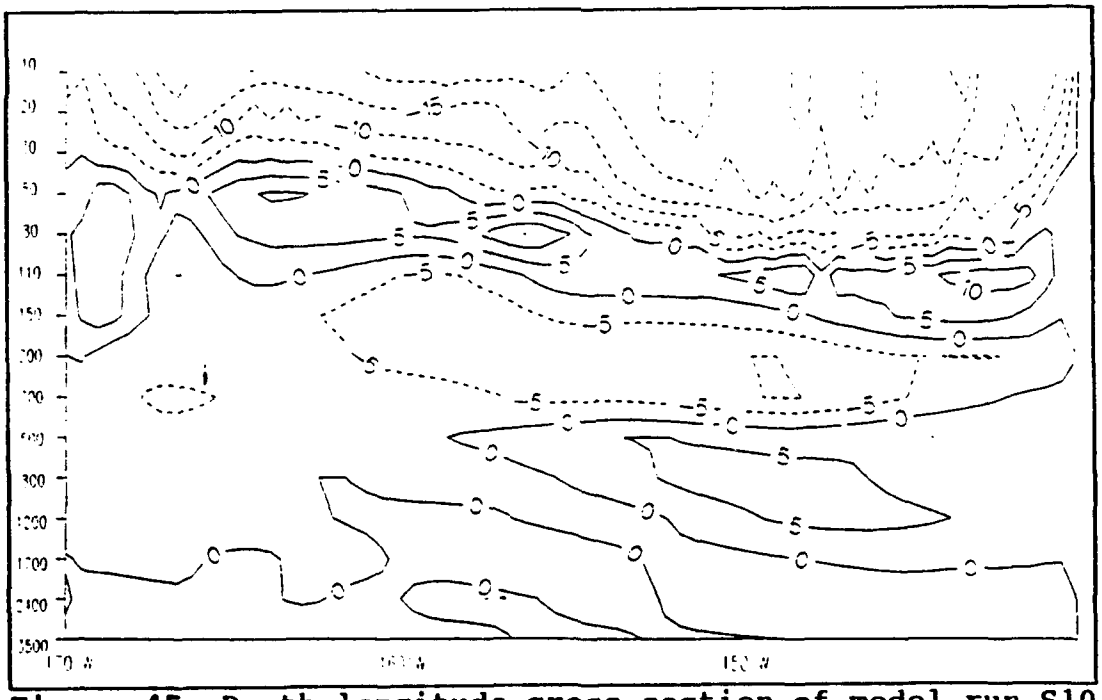

Figure 45. Depth-longitude cross section of model run S10 zonal currents (cm/s) along the equator on 31 December 1992. During the third cold tongue retreat. Dashed (solid) contours indicate westward (eastward) flow.

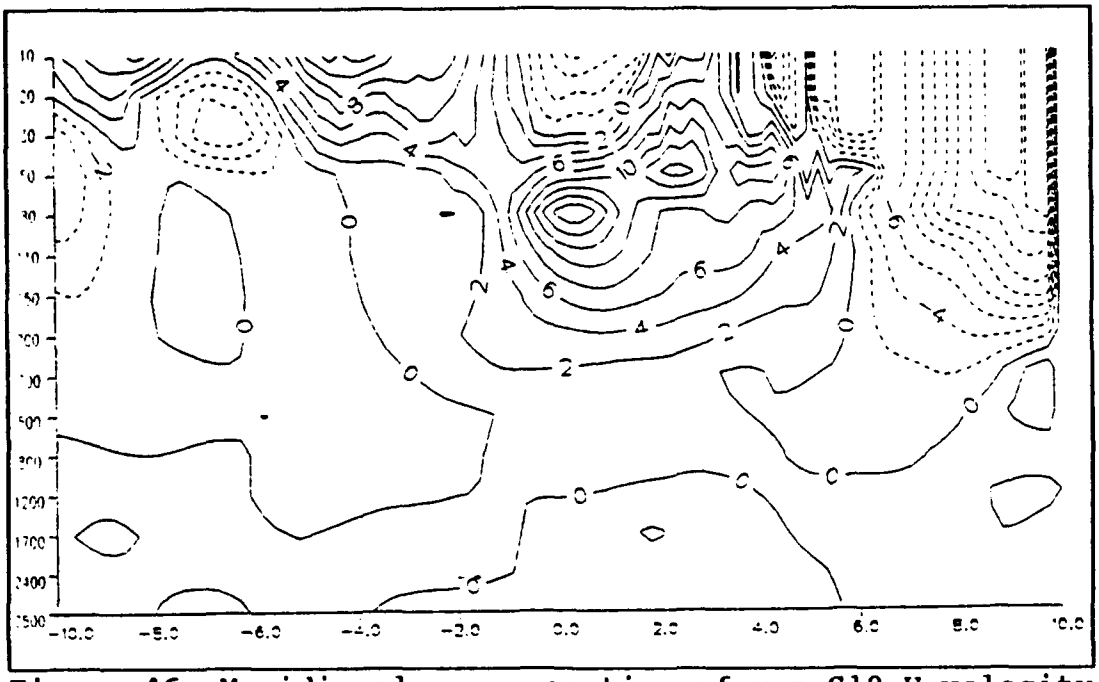

Figure 46. Meridional cross section of run S10 U velocity at 166°W on 13 November 1991, showing the merging of the NECC and EUC. Dashed (solid) contours indicate westward (eastward) flow. North is to the right.

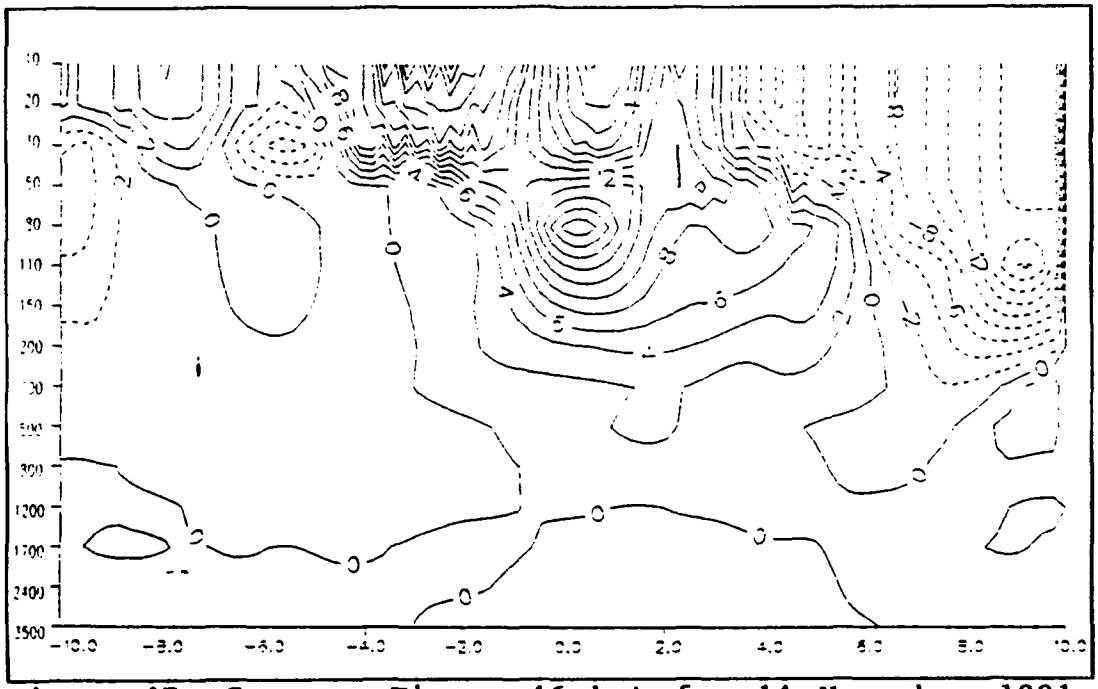

Figure 47. Same as Figure 46 but for 14 November 1991, showing completed merger of the EUC and NECC. Dashed (solid) contours indicate westward (eastward) flow. North is to the right.

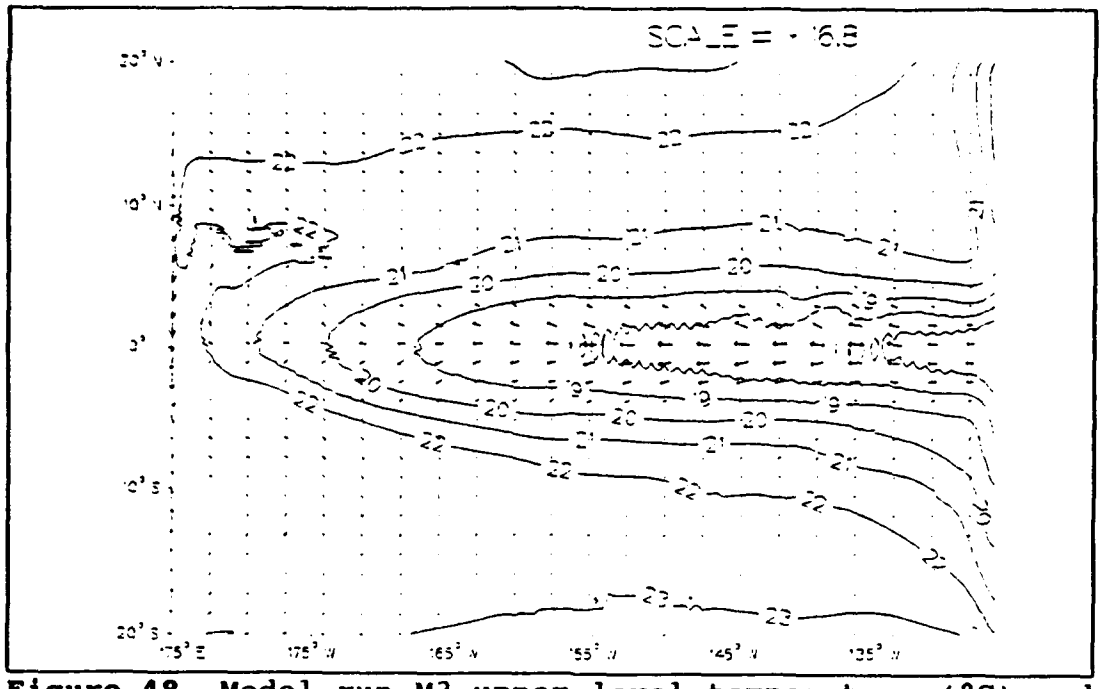

Figure 48. Model run M3 upper level temperature (°C) and currents (cm/s) at the end of the model run.

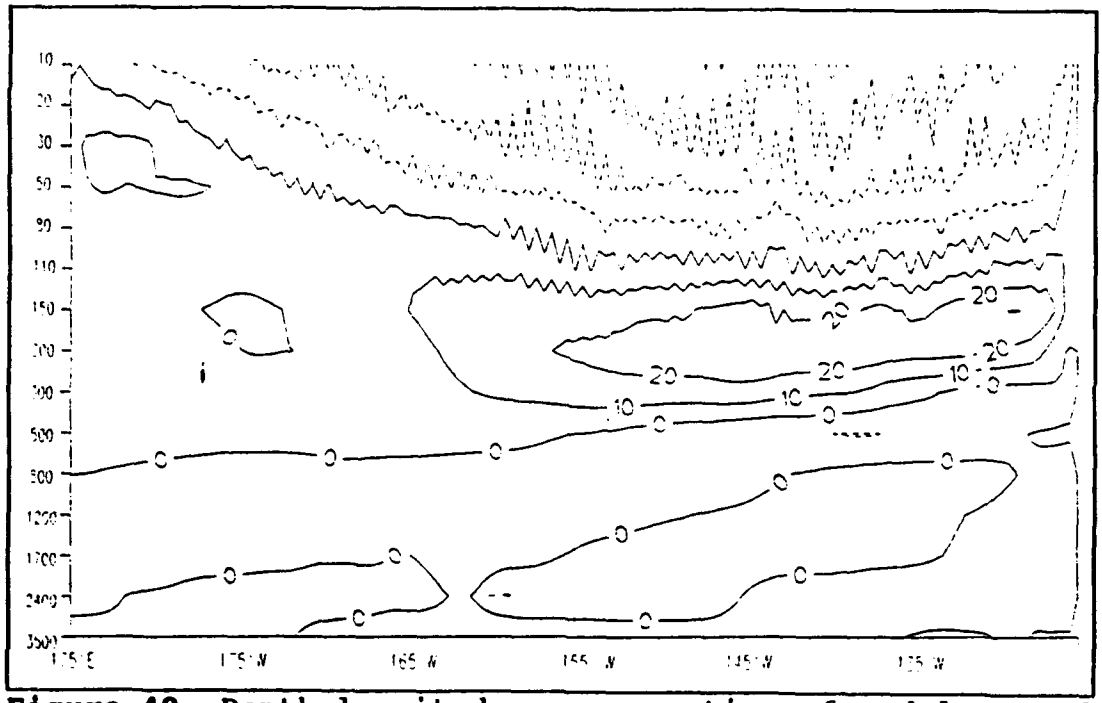

Figure 49. Depth-longitude cross section of model run M3 zonal currents (cm/s) along the equator at the end of the model run. Dashed (solid) contours indicate westward (eastward) flow.

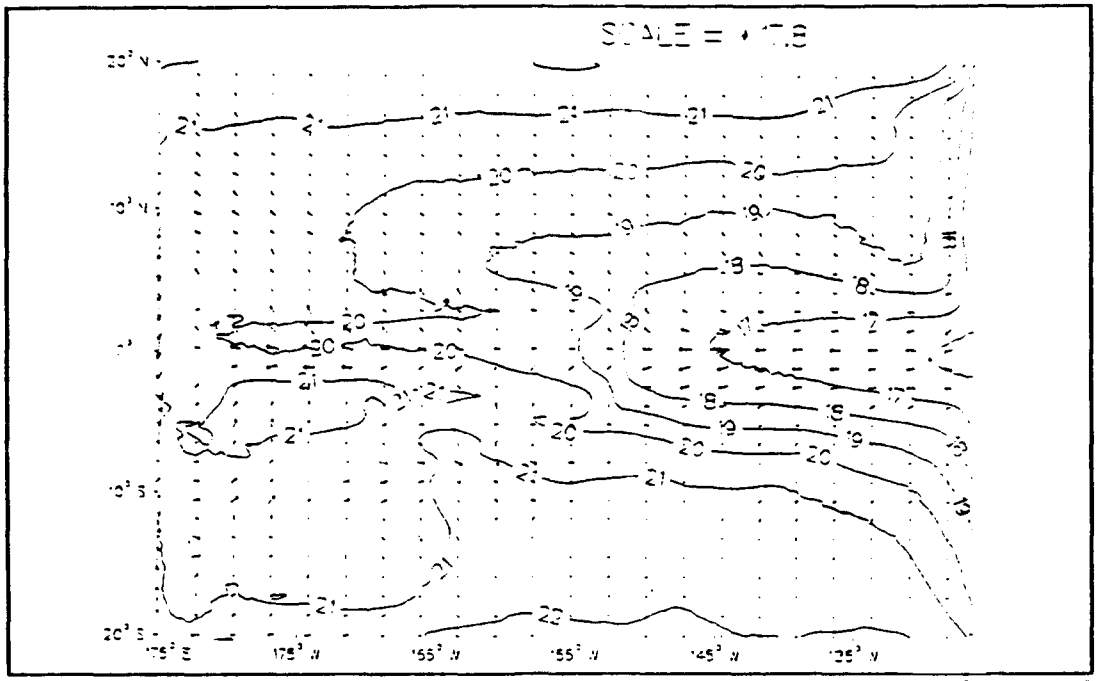

Figure 50. Model run M4 upper level temperature (°C) and currents (cm/s) on 11 March 1992. During the second cold tongue retreat.

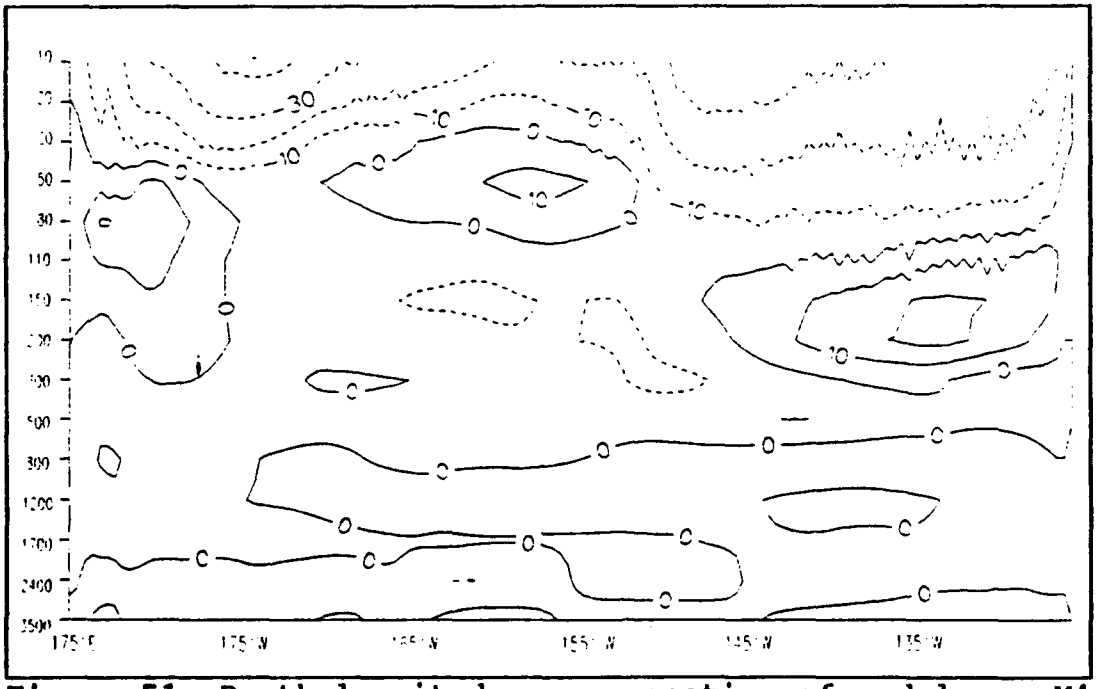

Figure 51. Depth-longitude cross section of model run M4 zonal currents (cm/s) along the equator on 11 March 1992. During the second cold tongue retreat. Dashed (solid) contours indicate westward (eastward) flow.

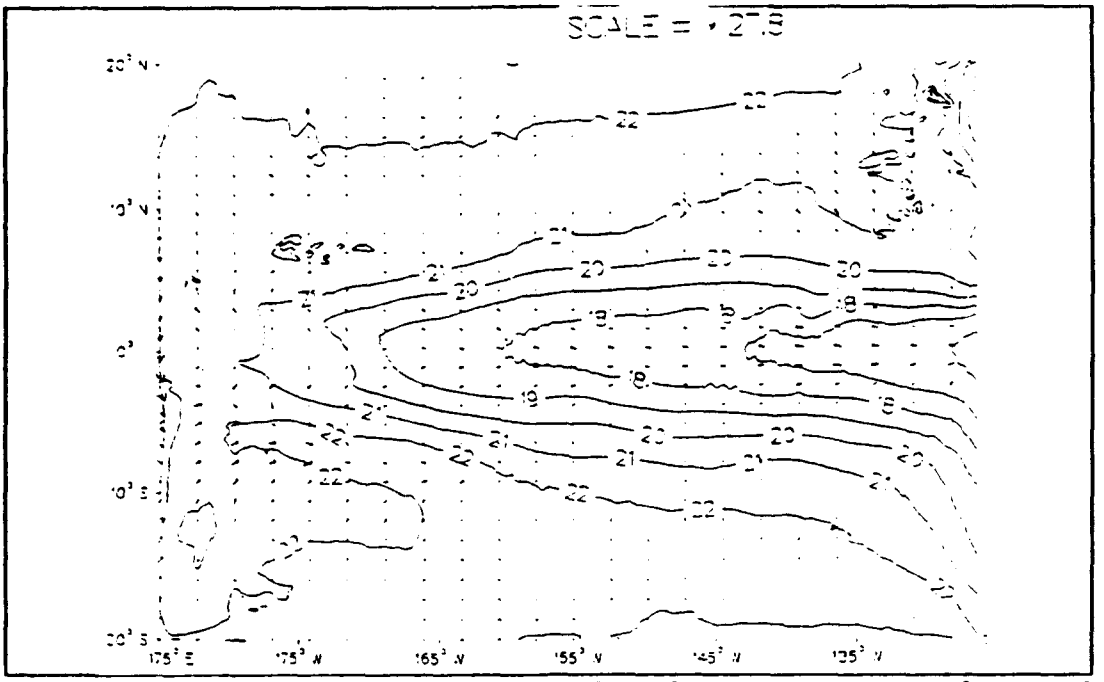

Figure 52. Model run M4 upper level temperature (°C) and currents (cm/s) on 31 December 1992. During the third cold tongue retreat.

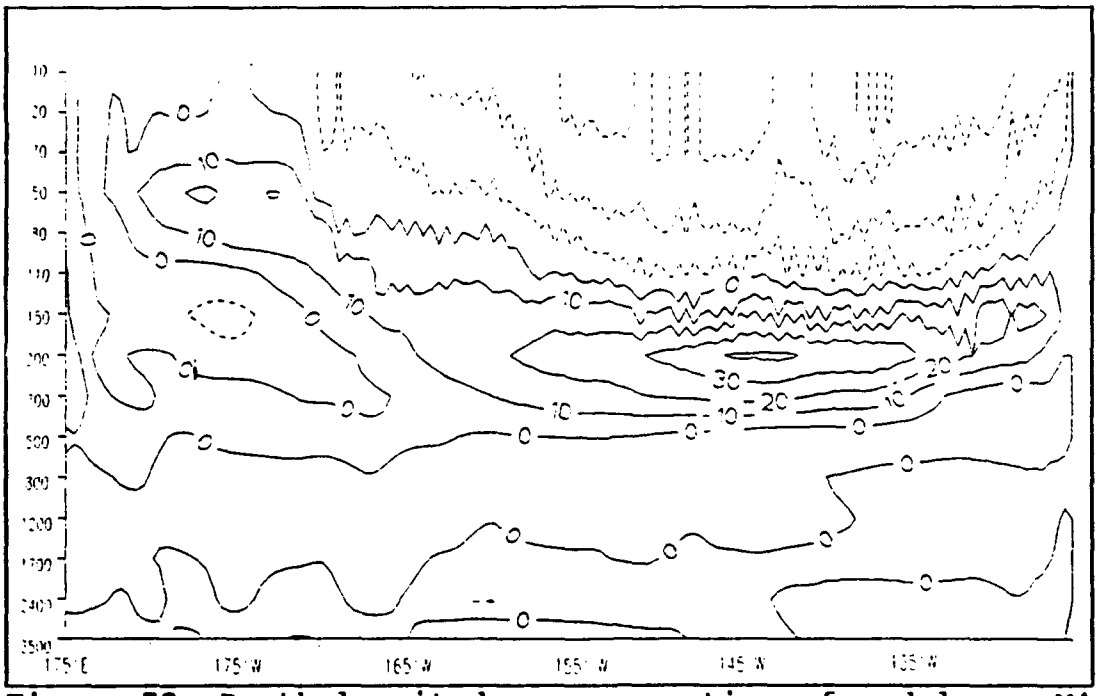

Figure 53. Depth-longitude cross section of model run M4 zonal currents (cm/s) along the equator on 31 December 1992. During the third cold tongue retreat. Dashed (solid) contours indicate westward (eastward) flow.

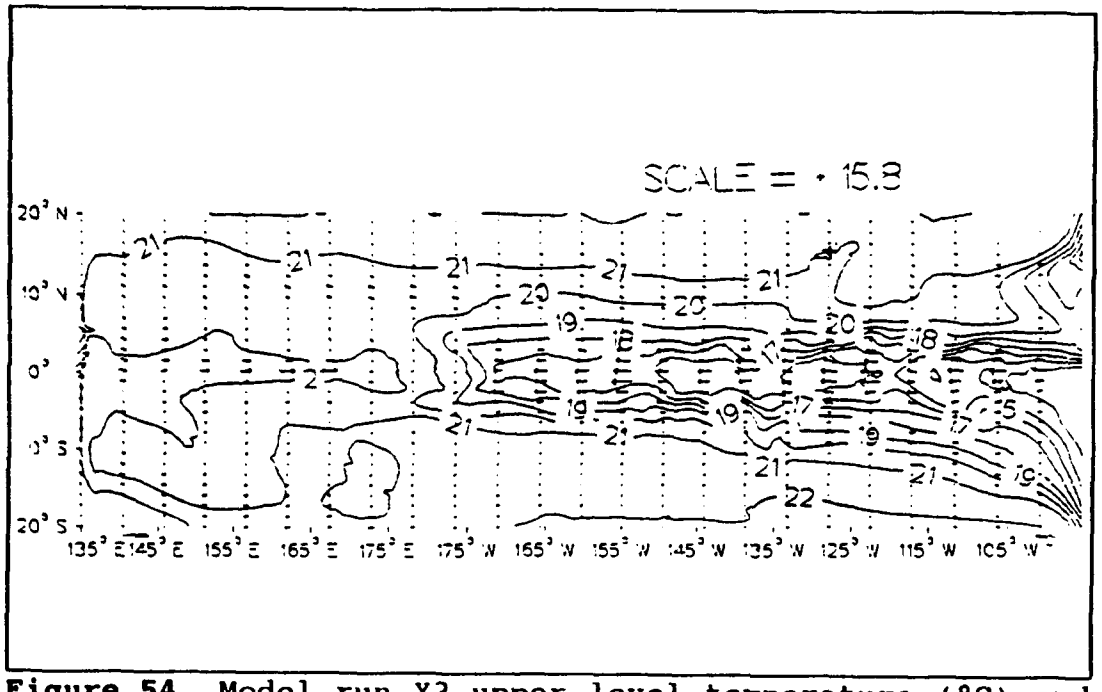

Figure 54. Model run X3 upper level temperature (°C) and currents (cm/s) at the end of the model run.

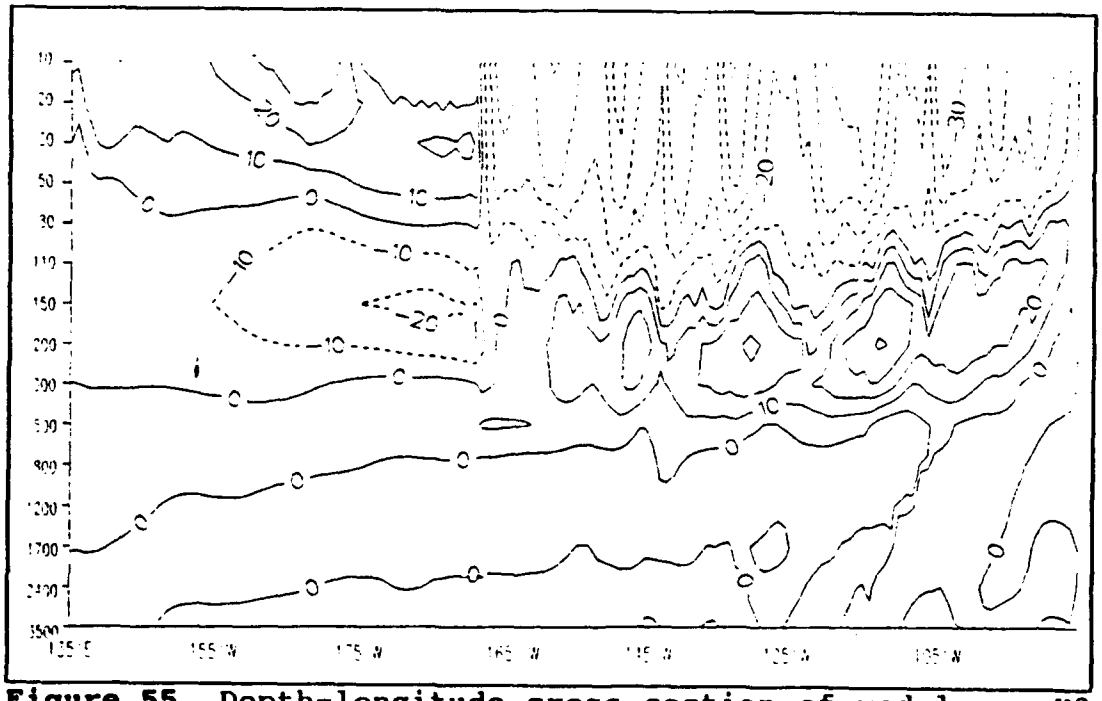

Figure 55. Depth-longitude cross section of model run X3 zonal currents (cm/s) along the equator at the end of the model run. Dashed (solid) contours indicate westward (eastward) flow.

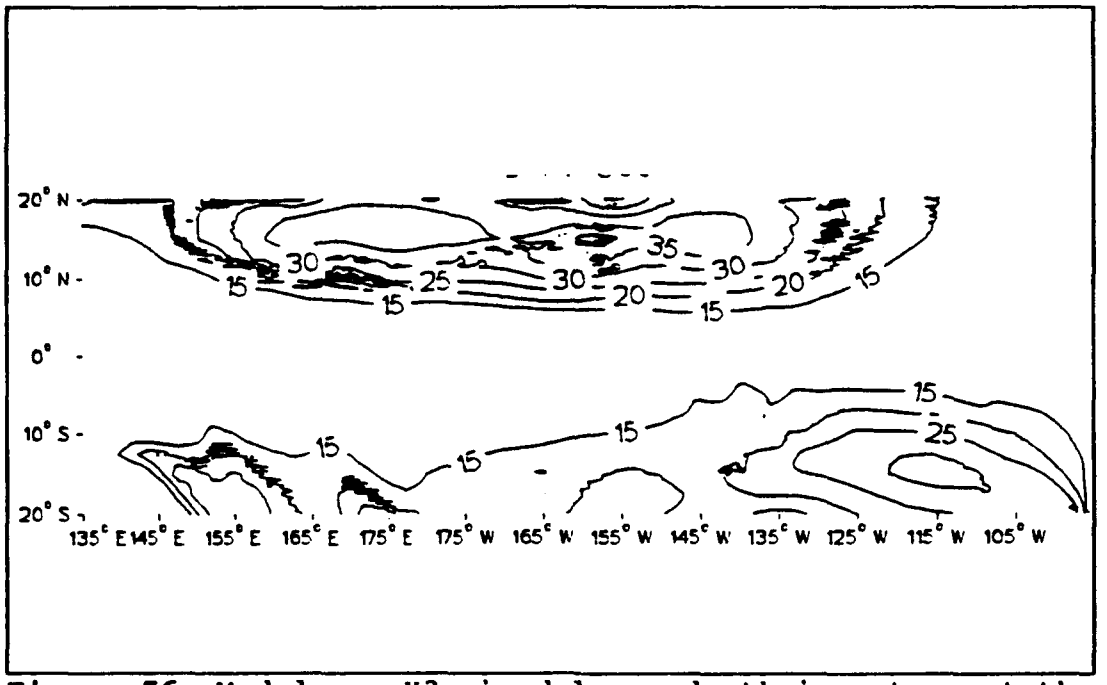

Figure 56. Model run X3 mixed layer depth in meters at the end of the model run.

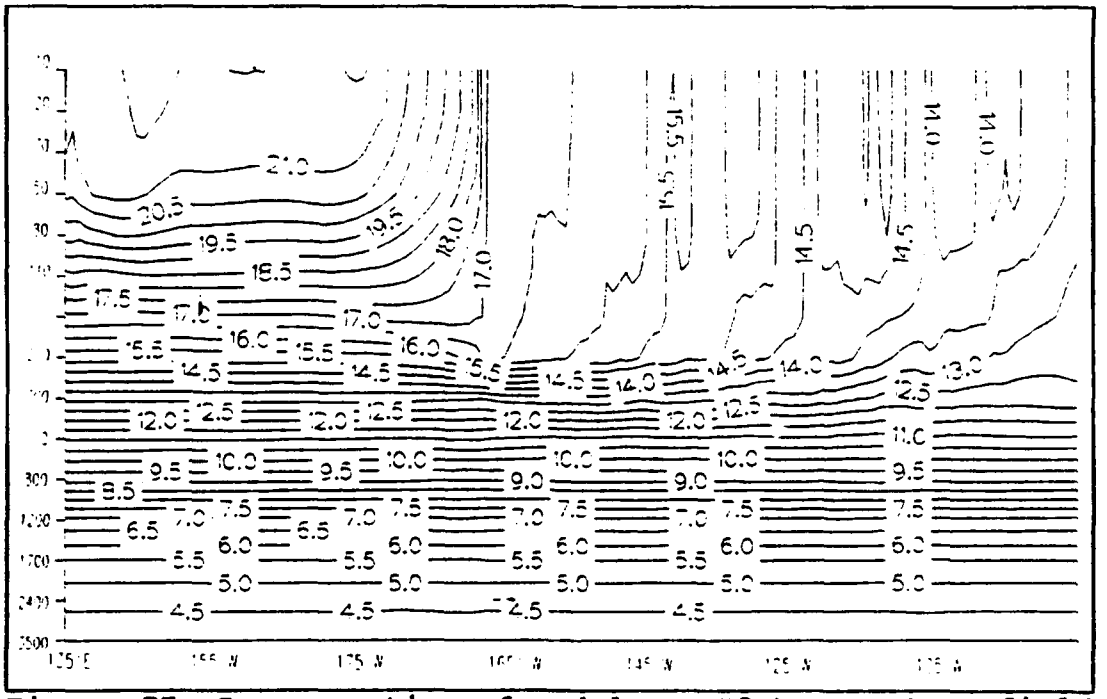

Figure 57. Cross section of model run X3 temperature field (°C) along the equator at the end of the model run.

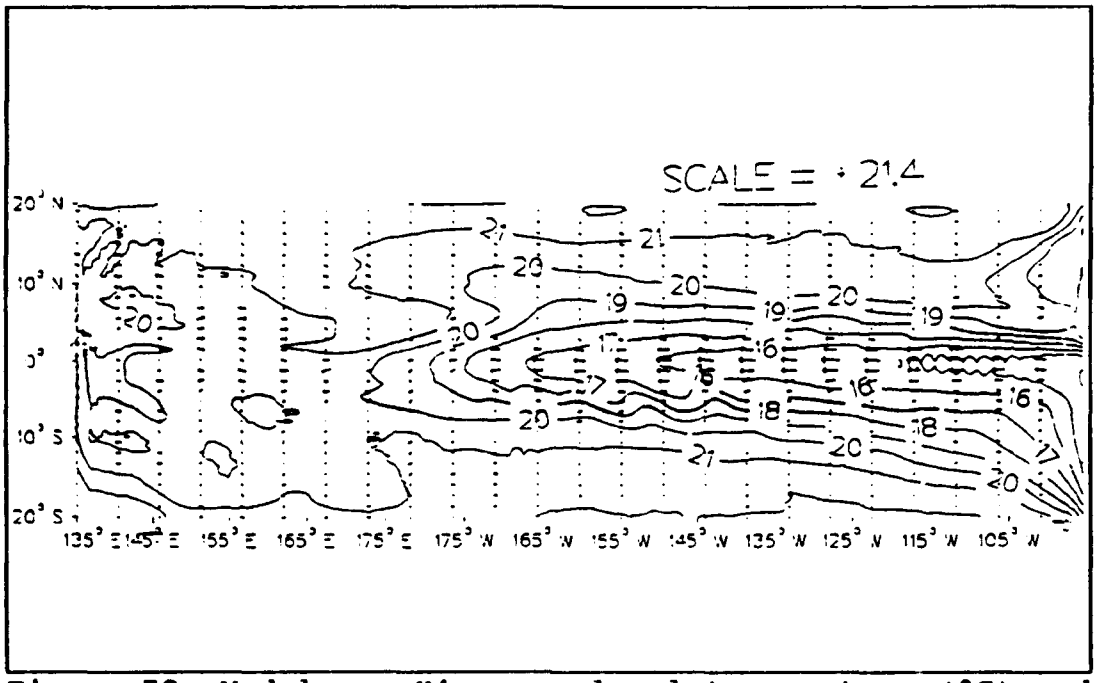

Figure 58. Model run X4 upper level temperature (°C) and currents (cm/s) on 29 August 1991, once the equatorial eastward surface current has disappeared.

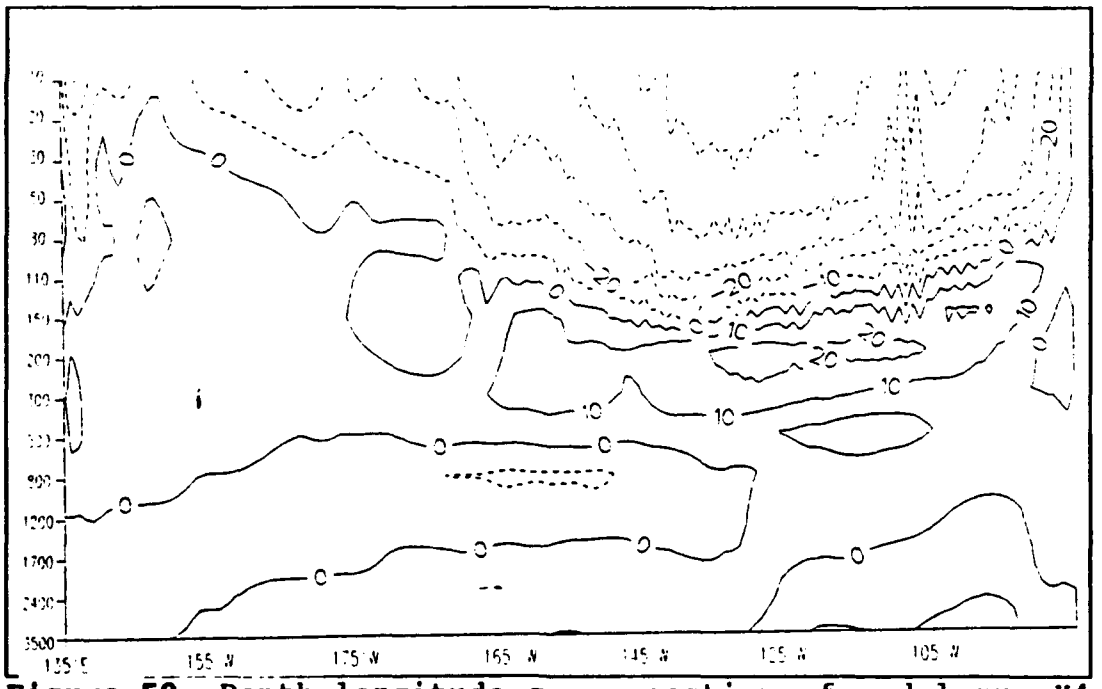

Figure 59. Depth-longitude cross section of model run X4 zonal currents (cm/s) along the equator on 29 August 1991, once the equatorial eastward surface current has disappeared. Dashed (solid) contours indicate westward (eastward) flow.

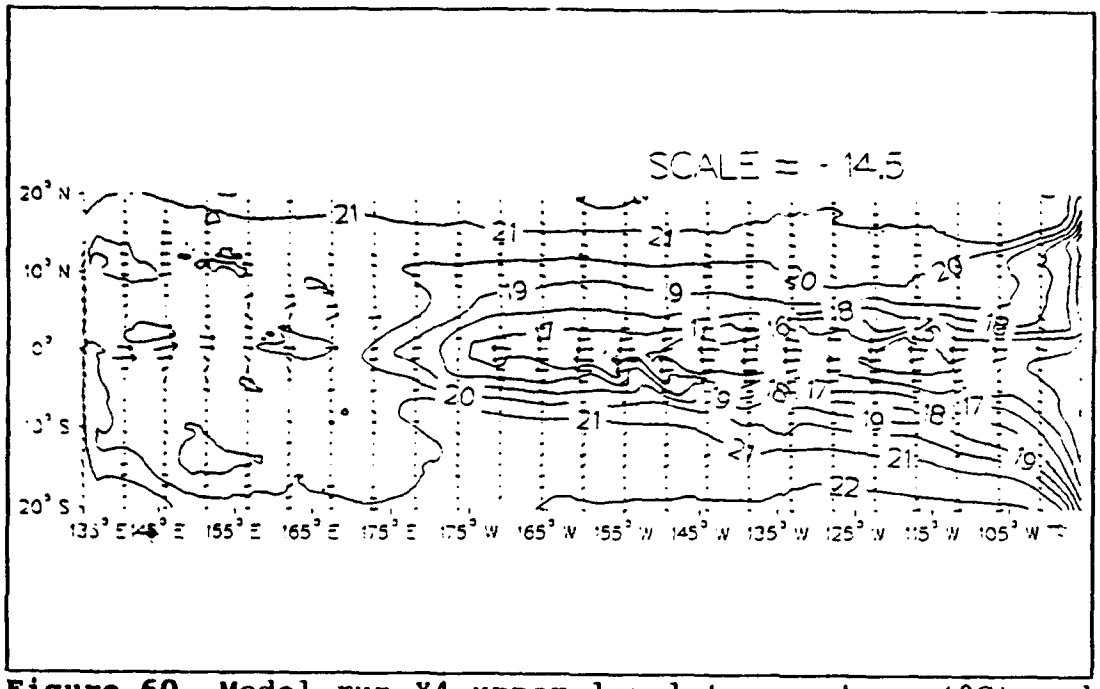

Figure 60. Model run X4 upper level temperature (°C) and currents (cm/s) on 26 March 1991, when the cold tongue has reached it's maximum extent before the first retreat.

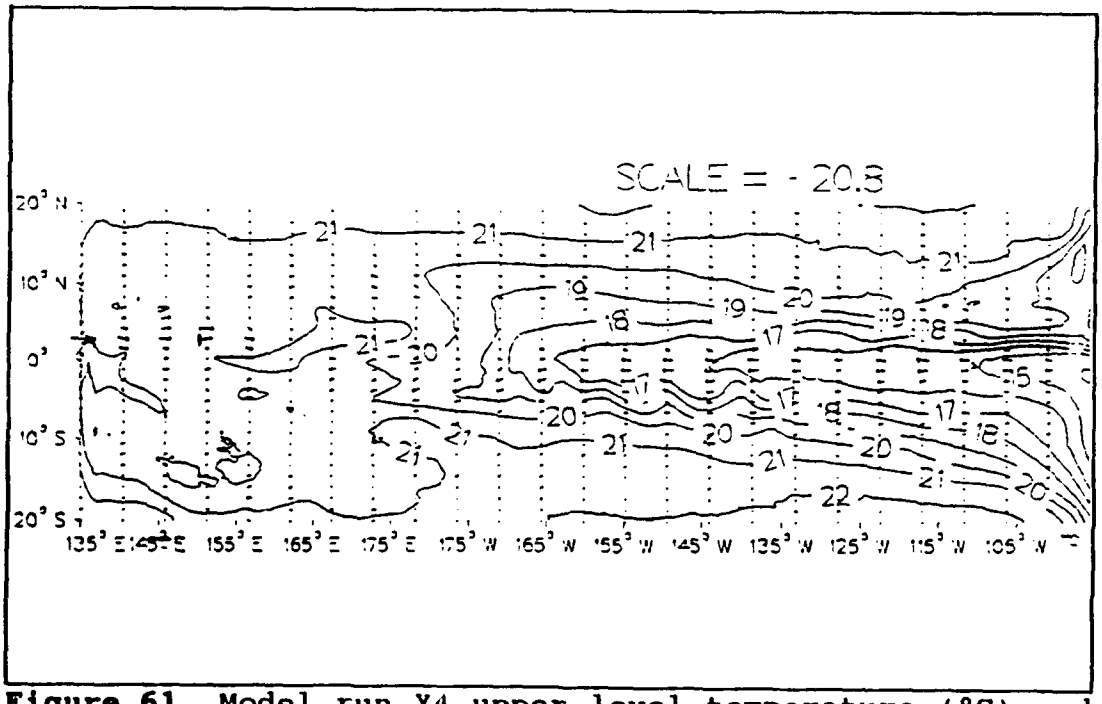

Figure 61. Model run X4 upper level temperature (°C) and currents (cm/s) on 12 July 1991. During the first cold tongue retreat.

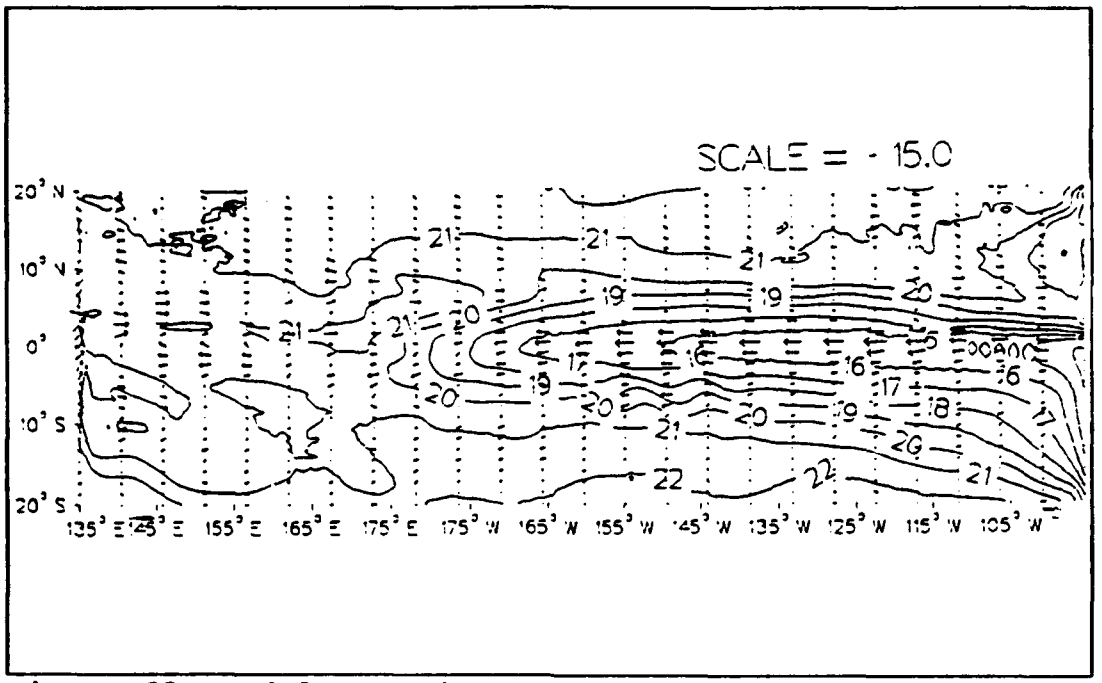

Figure 62. Model run X4 upper level temperature (°C) and currents (cm/s) on 16 October 1991. Time of greatest extent of the cold tongue.

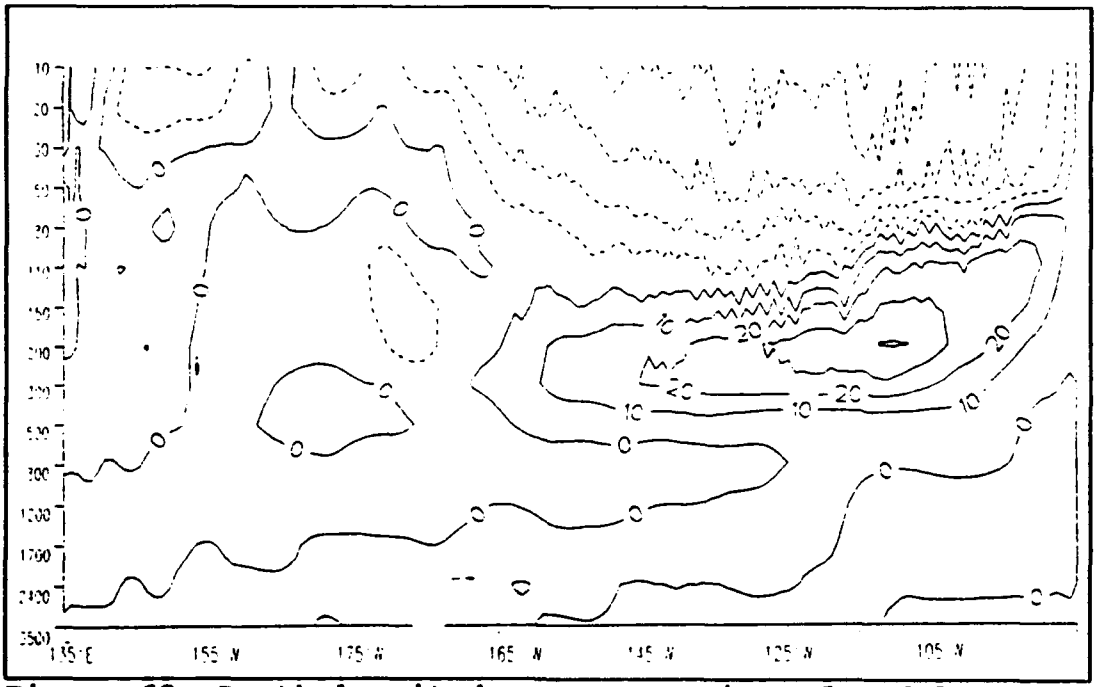

Figure 63. Depth-longitude cross section of model run X4 zonal currents (cm/s) along the equator on 16 October 1991. Time of greatest extent of the cold tongue. Dashed (solid) contours indicate westward (eastward) flow.

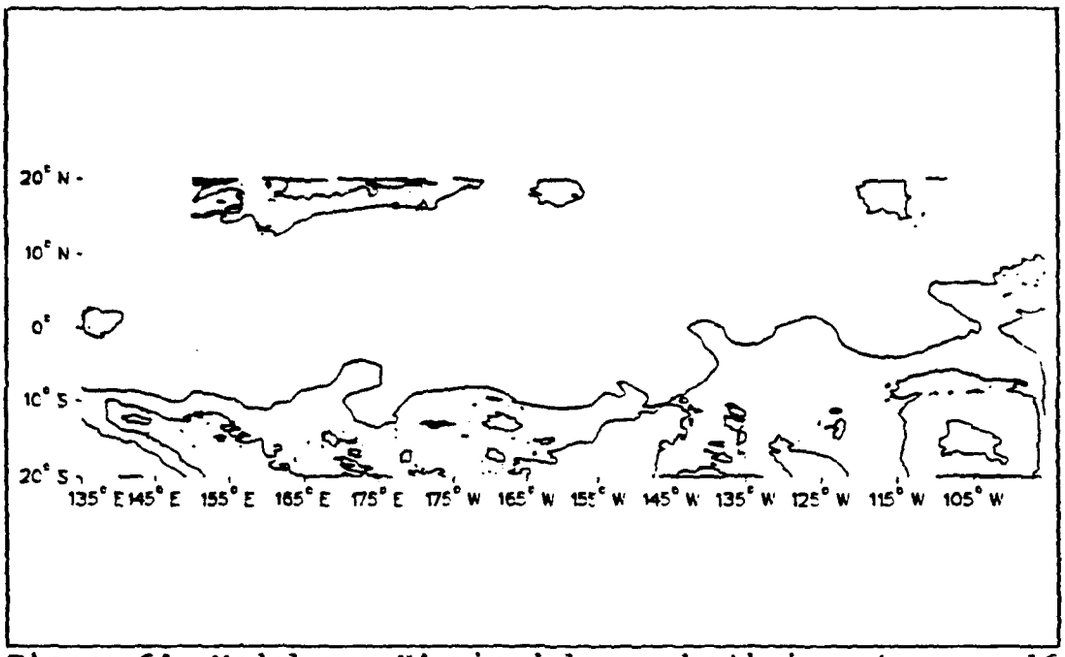

Figure 64. Model run X4 mixed layer depth in meters on 16 October 1991. Time of greatest extent of the cold tongue.

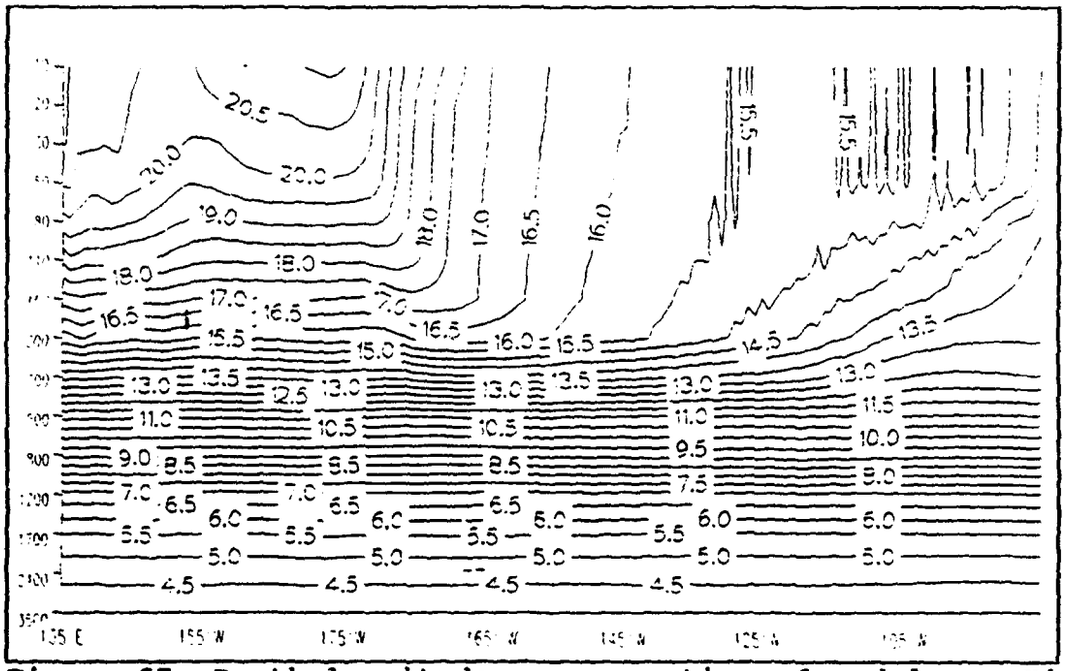

Figure 65. Depth-longitude cross section of model run X4 temperature field (°C) along the equator on 16 October 1991. Time of greatest extent of the cold tongue.

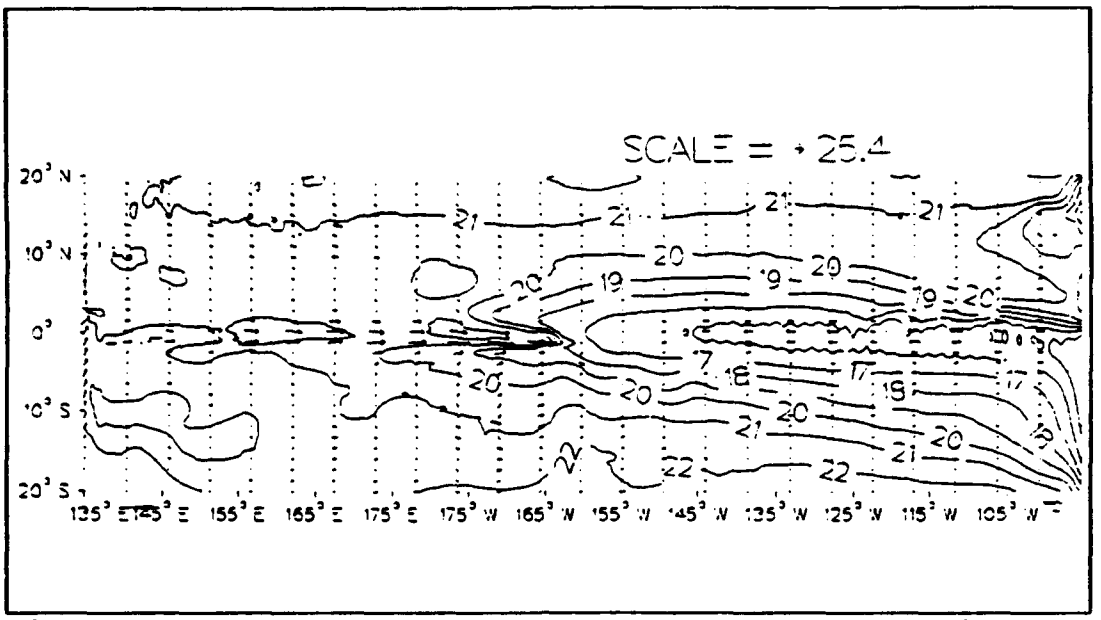

Figure 66. Model run X4 upper level temperature (°C) and currents (cm/s) on 11 December 1991. Note the strong eastward surface current in the equatorial western Pacific.

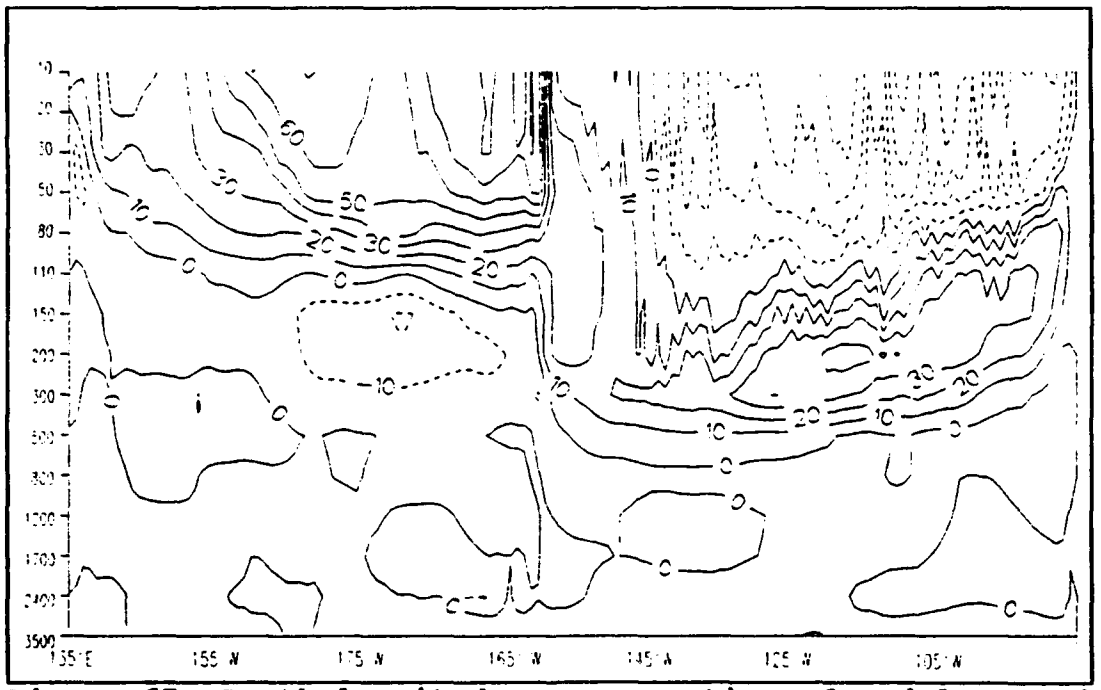

Figure 67. Depth-longitude cross section of model run X4 zonal currents (cm/s) along the equator on 11 December 1991. Note the eastward surface current in the equatorial western Pacific. Dashed (solid) contours indicate westward (eastward) flow.

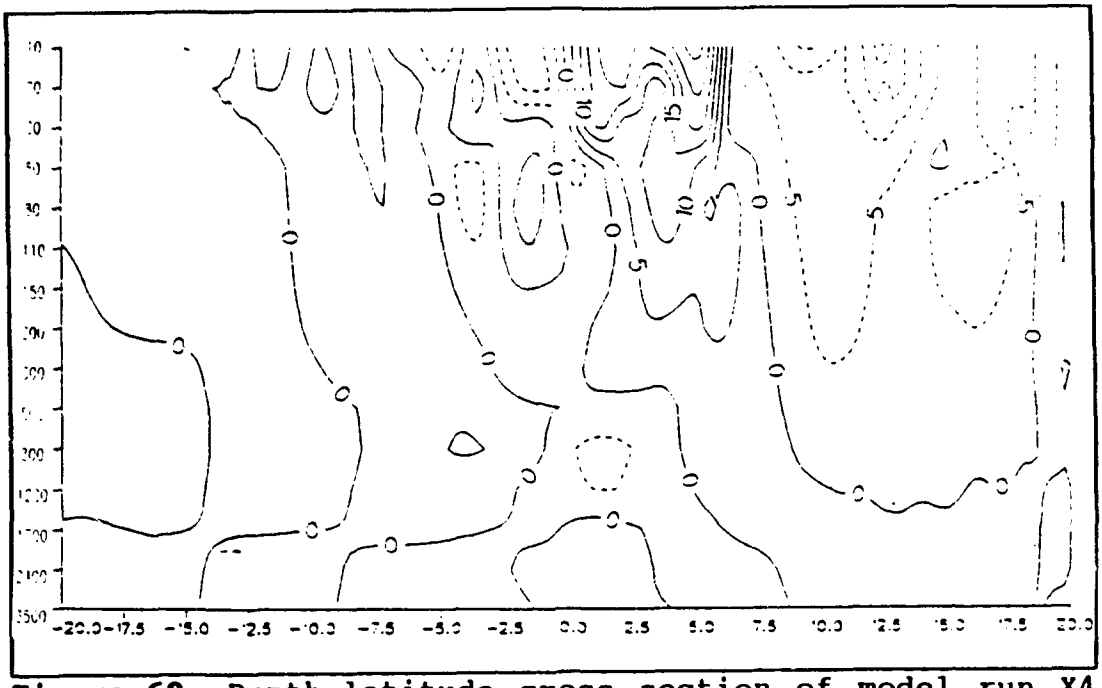

Figure 68. Depth-latitude cross section of model run X4 zonal currents (cm/s) at 165°E on 13 November 1991. Note the eastward surface current north of the equator. Dashed (solid) contours indicate westward (eastward) flow.

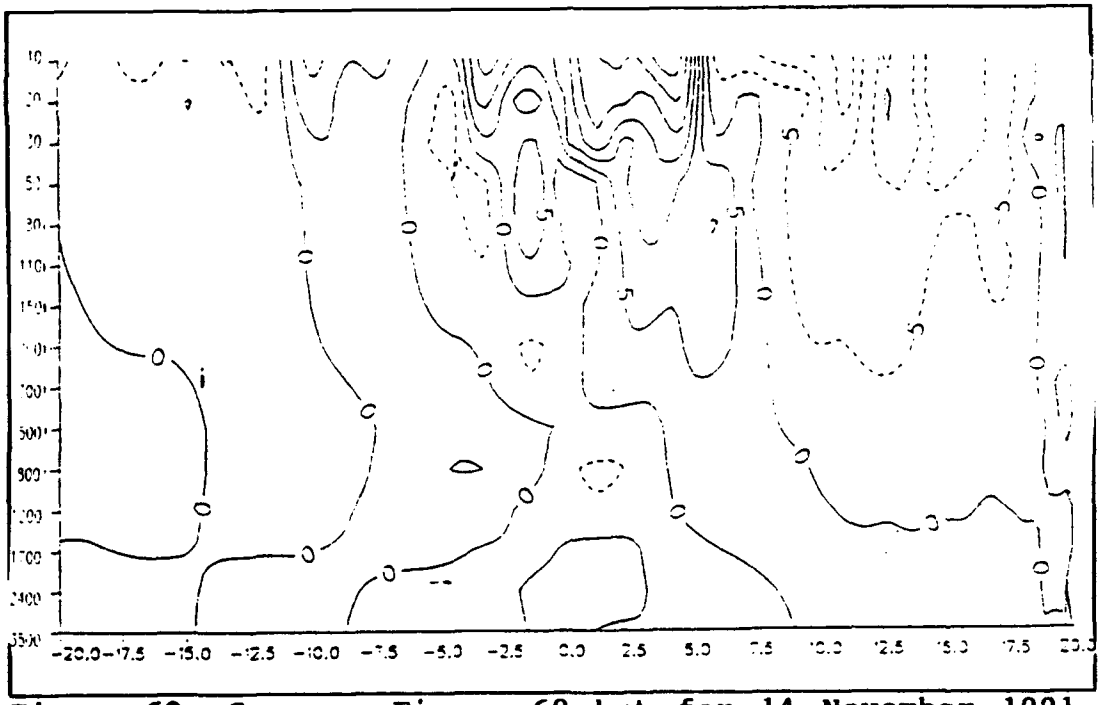

Figure 69. Same as Figure 68 but for 14 November 1991. Note the southward extension of the eastward surface current onto the equator. Dashed (solid) contours indicate westward (eastward) flow.

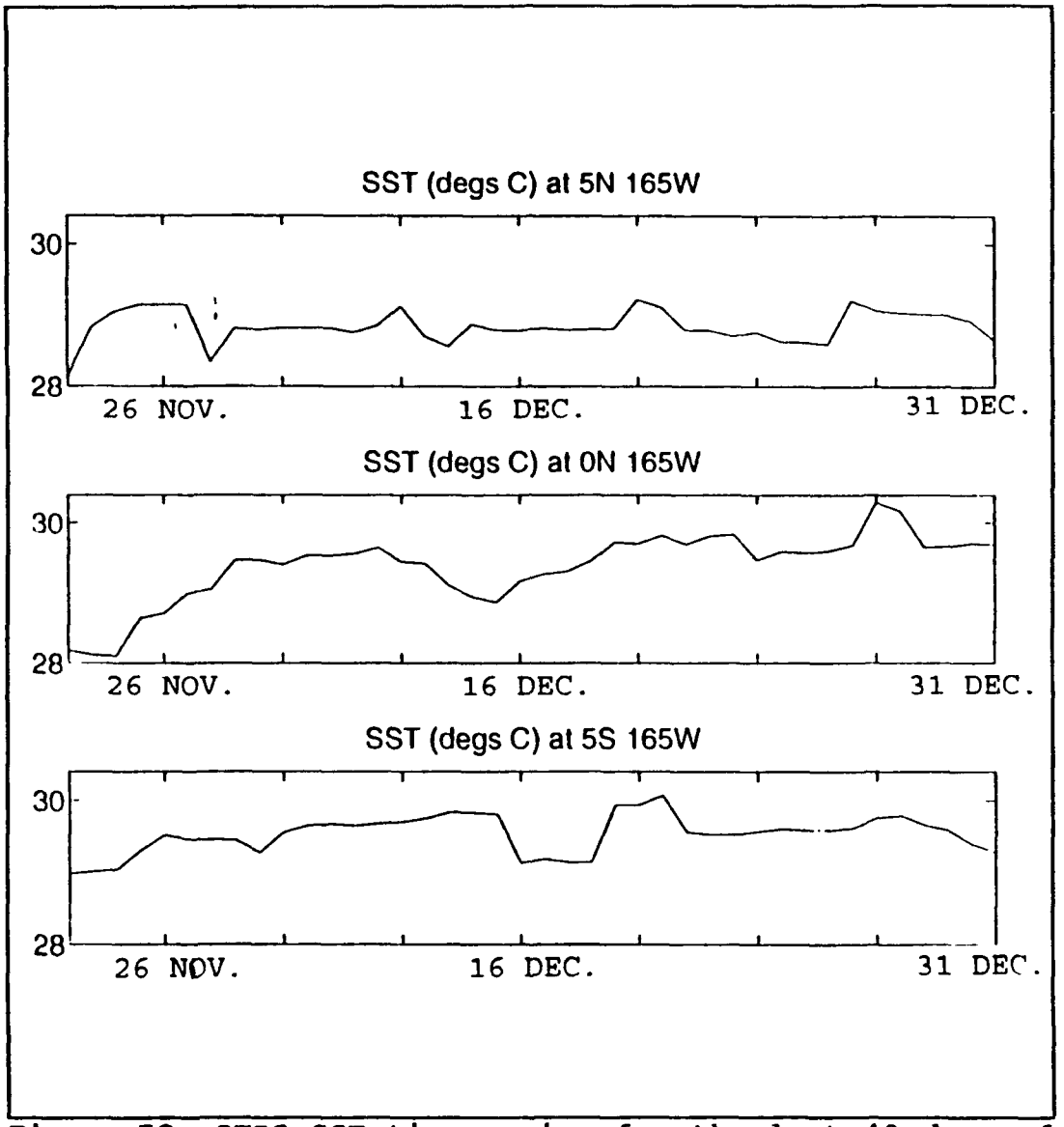

Figure 70. OTIS SST time series for the last 40 days of 1991 at three stations bisecting the equatorial warm tongue seen in model run X4 (Figure 66).

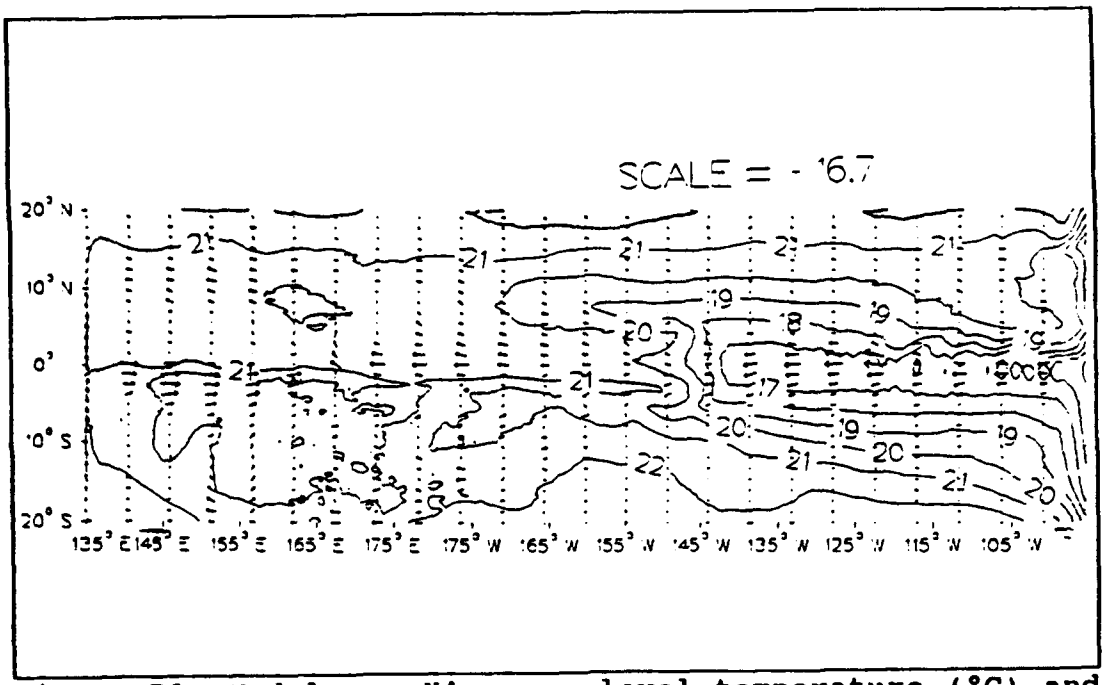

Figure 71. Model run X4 upper level temperature (°C) and currents (cm/s) on 13 March 1992. During the second cold tongue retreat.

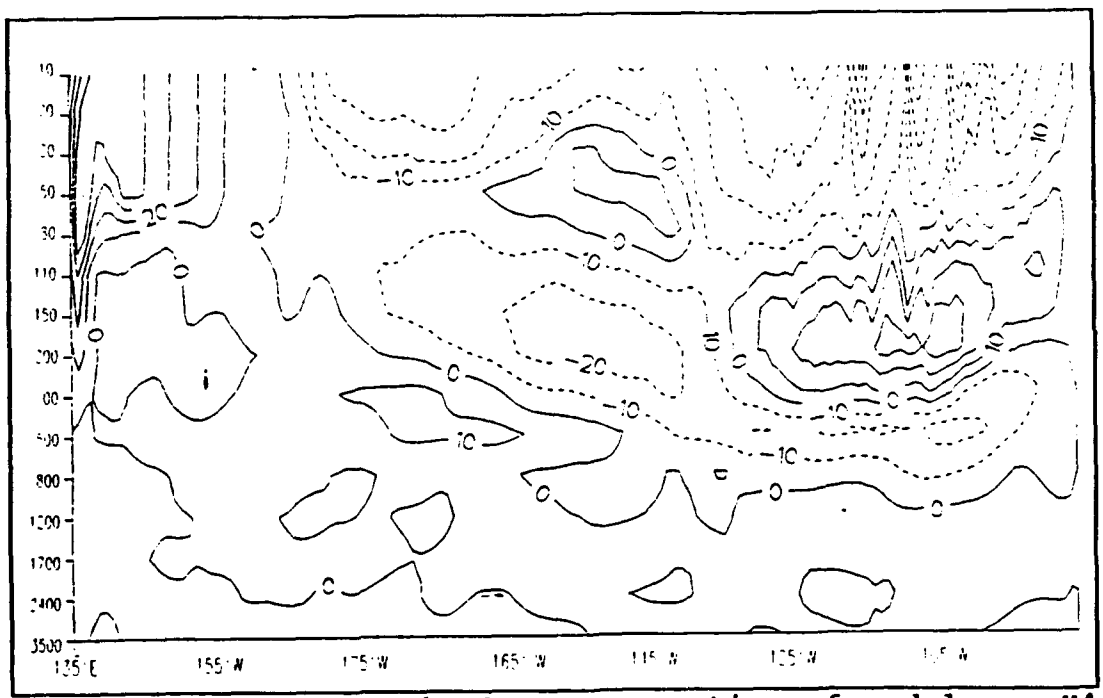

Figure 72. Depth-longitude cross section of model run X4 zonal currents (cm/s) along the equator on 13 March 1991. During the second cold tongue retreat. Dashed (solid) contours indicate westward (eastward) flow.

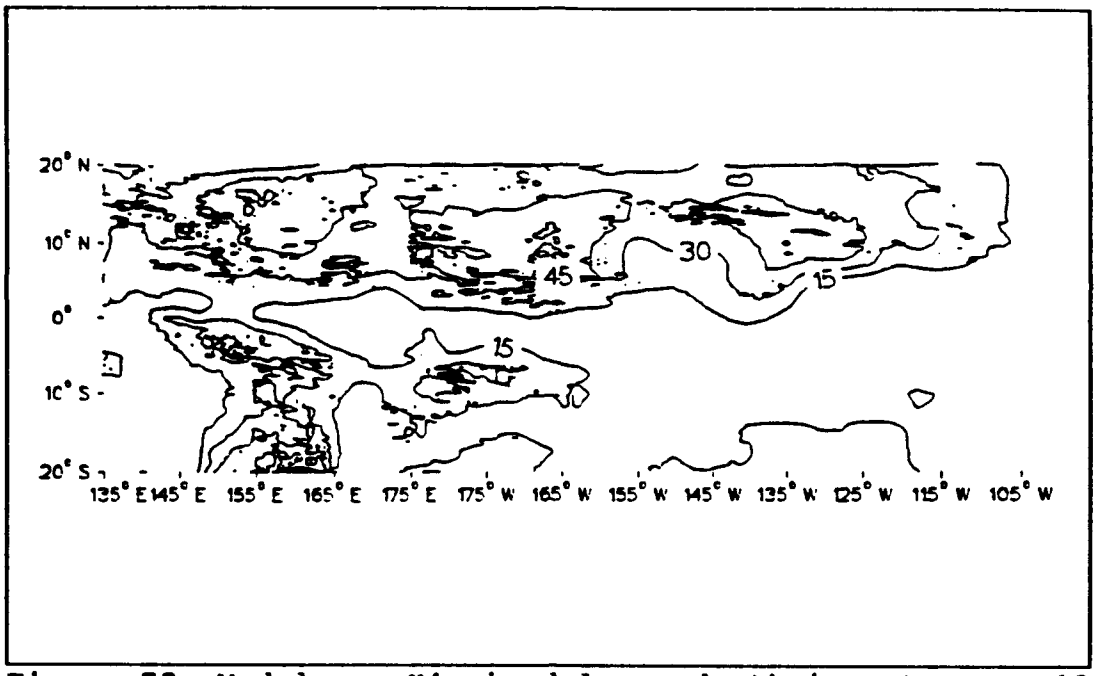

Figure 73. Model run X4 mixed layer depth in meters on 13 March 1992. During the second cold tongue retreat.

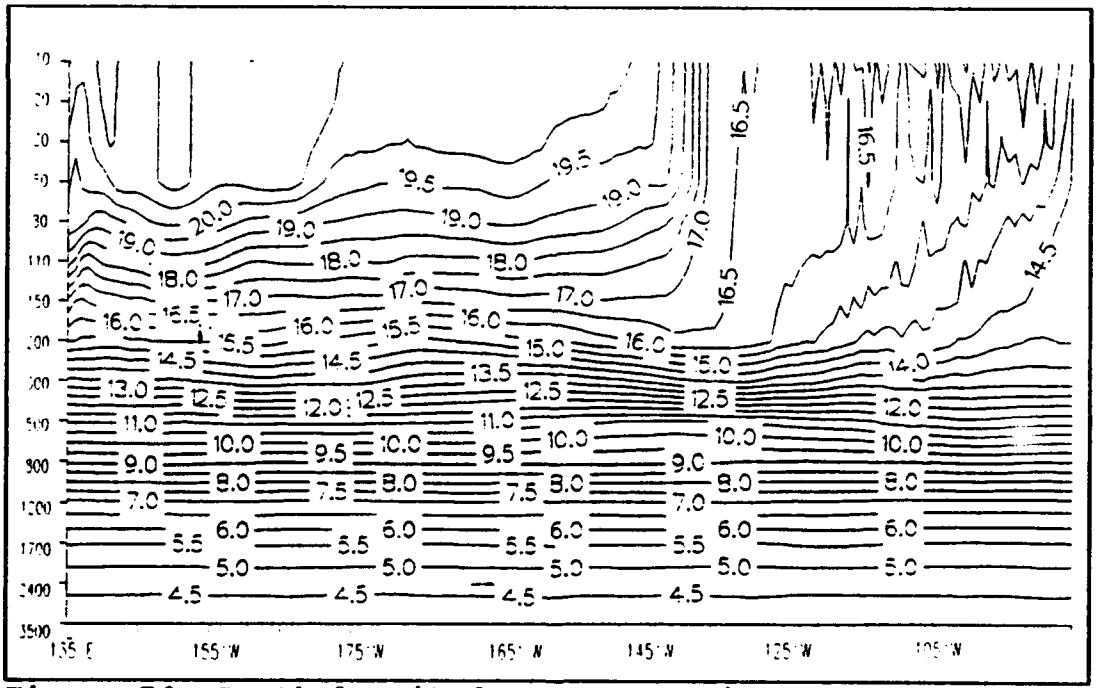

Figure 74. Depth-longitude cross section of model run X4 temperature field (°C) along the equator on 13 March 1992. During the second cold tongue retreat.

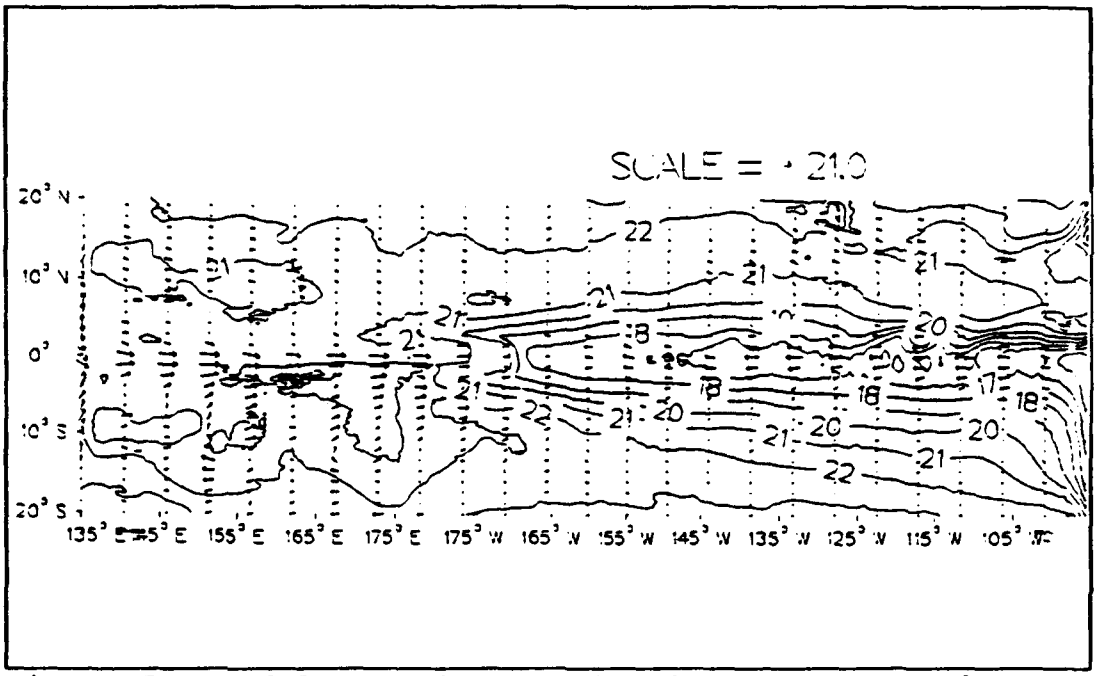

Figure 75. Model run X4 upper level temperature (°C) and currents (cm/s) on 31 December 1992. During the third cold tongue retreat.

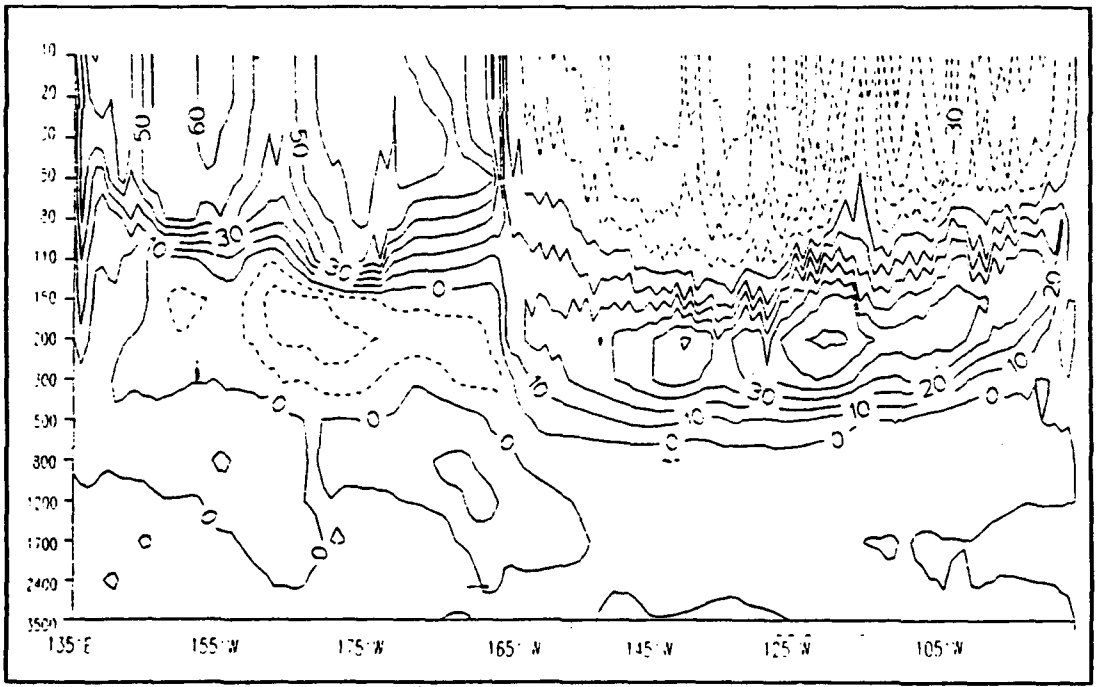

Figure 76. Depth-longitude cross section of model run X4 zonal currents (cm/s) along the equator on 31 December 1992. During the third cold tongue retreat. Dashed (solid) contours indicate westward (eastward) flow.

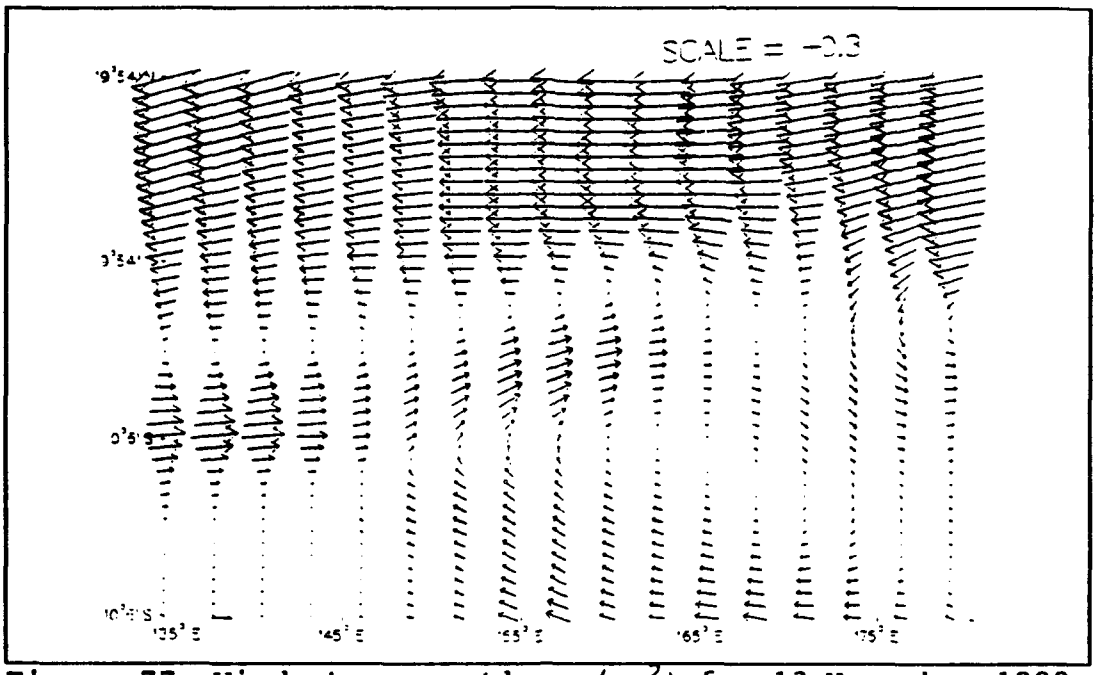

Figure 77. Wind stresses (dynes/cm^2) for 13 November 1992. Note weak typhoon Hunt at about 158°E, 8°N and the early stages of typhoon Gay located on the eastern edge of the figure at about 7°N.

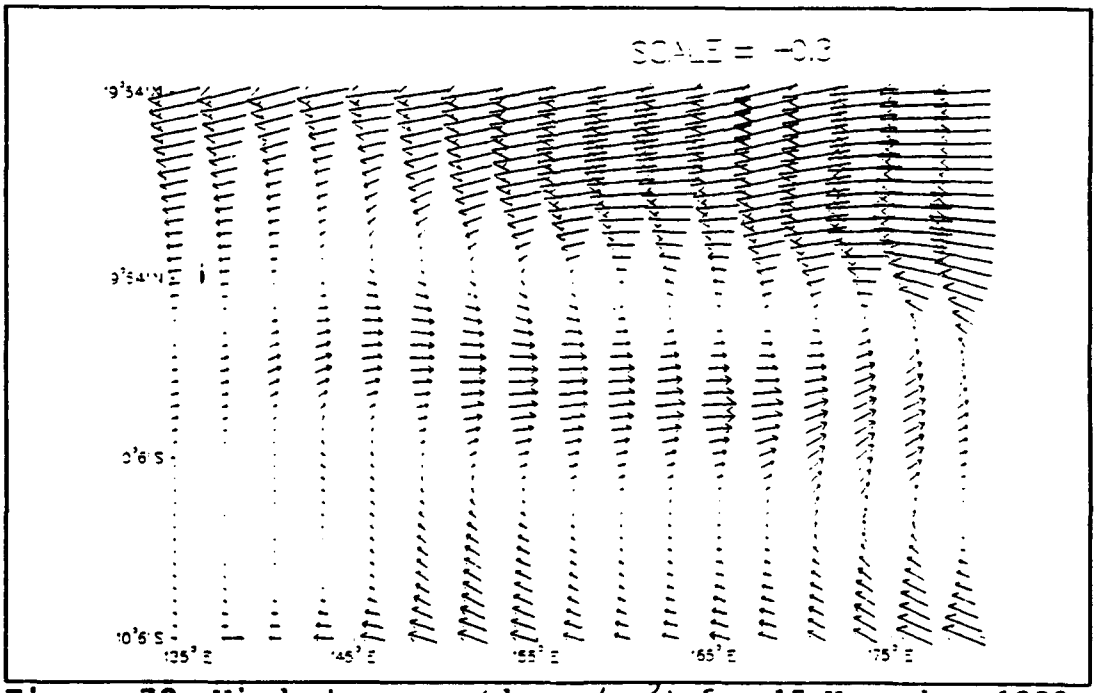

Figure 78. Wind stresses (dynes/cm^2) for 15 November 1992.

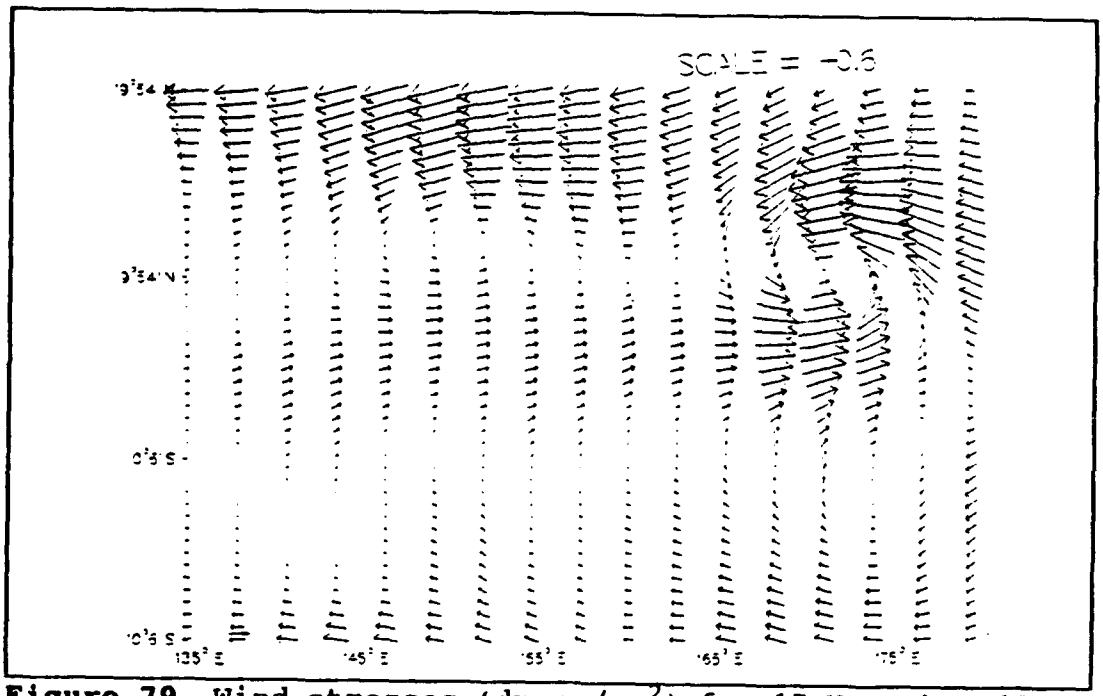

Figure 79. Wind stresses (dynes/cm^2) for 17 November 1992.

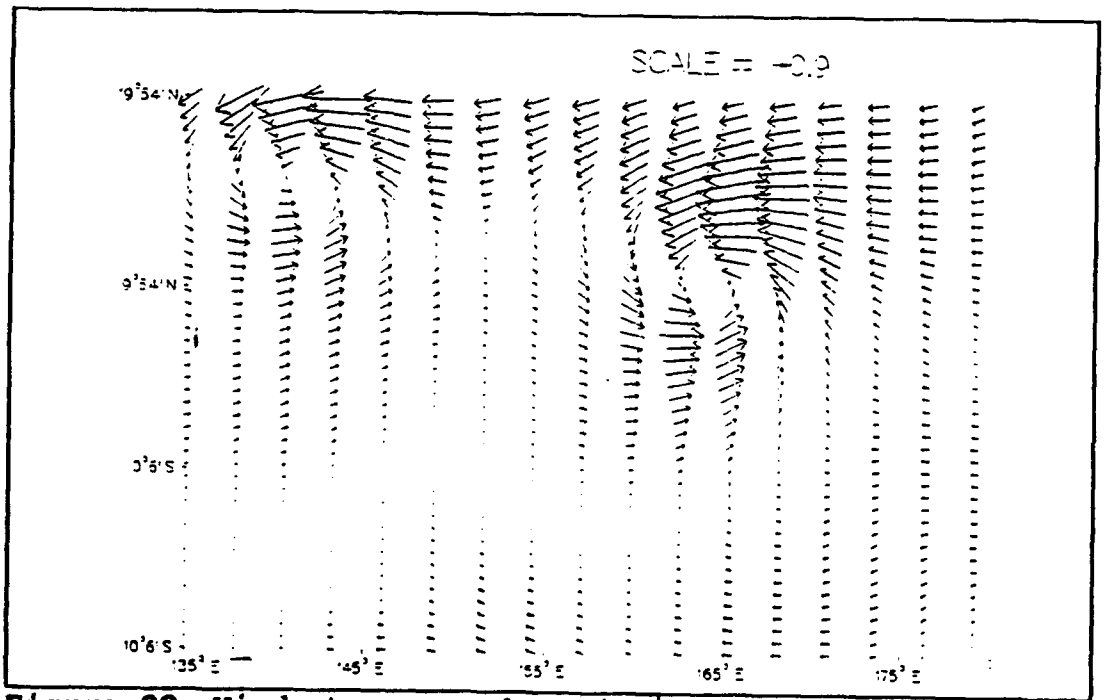

Figure 80. Wind stresses (dynes/cm^2) for 19 November 1992. Note typhoon Hunt in the northwest corner and typhoon Gay at about 165°E, 10°N.

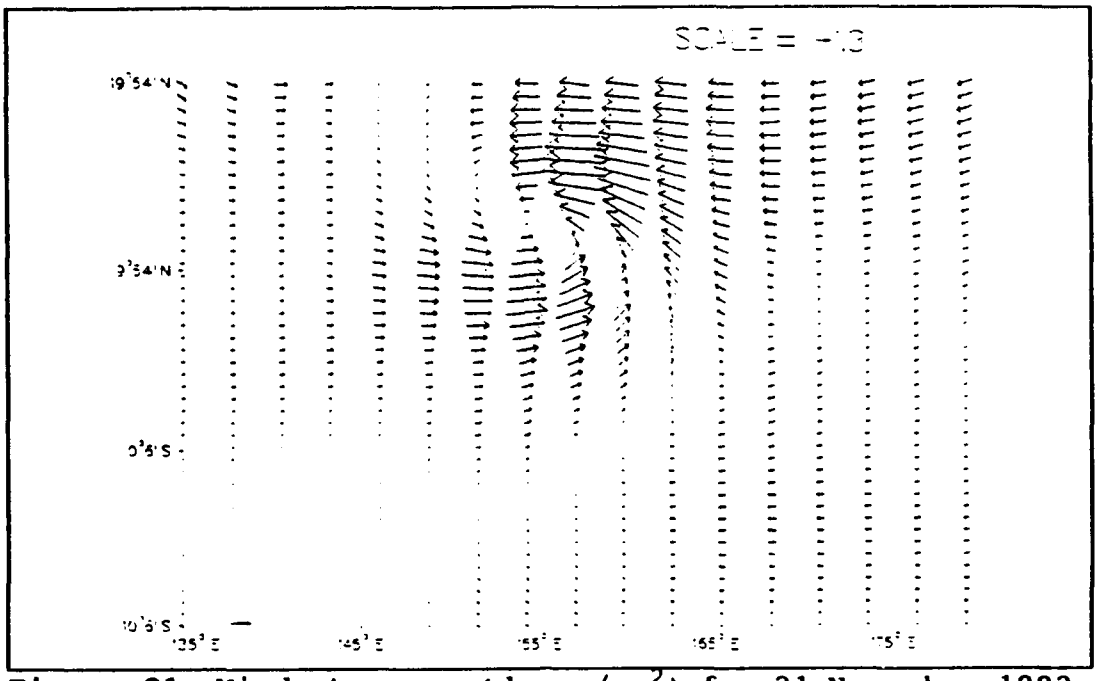

Figure 81. Wind stresses (dynes/cm^2) for 21 November 1992. Note typhoon Gay at about 156°E, 11°N.

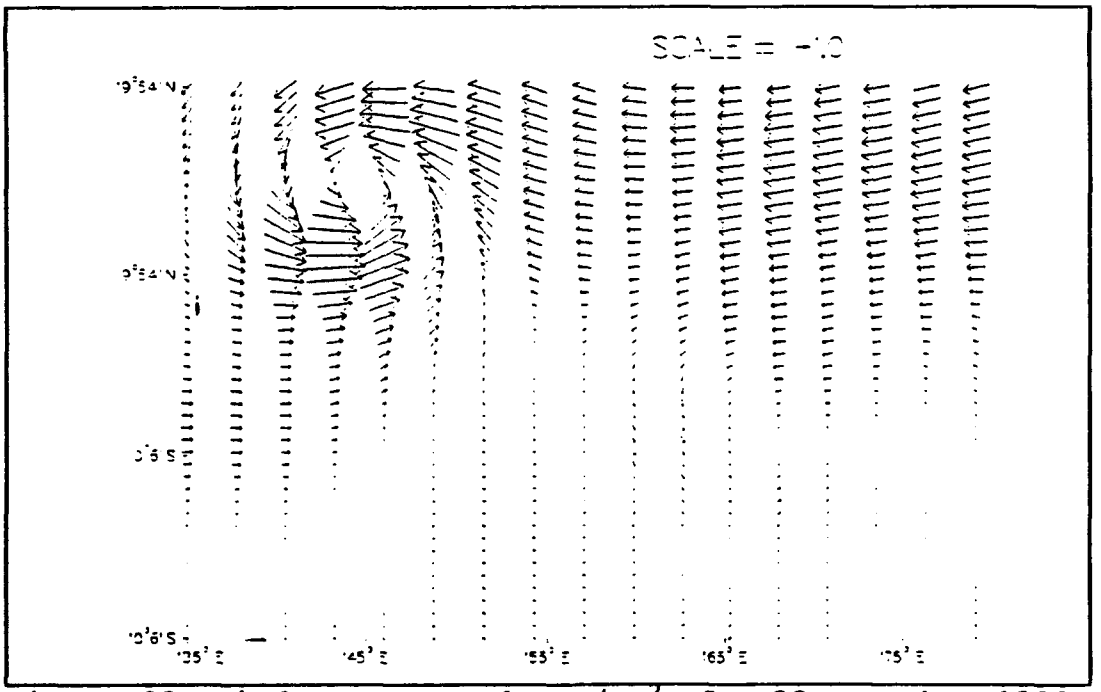

Figure 82. Wind stresses (dynes/cm^2) for 23 November 1992. Note typhoon Gay at about 143°E, 15°N.

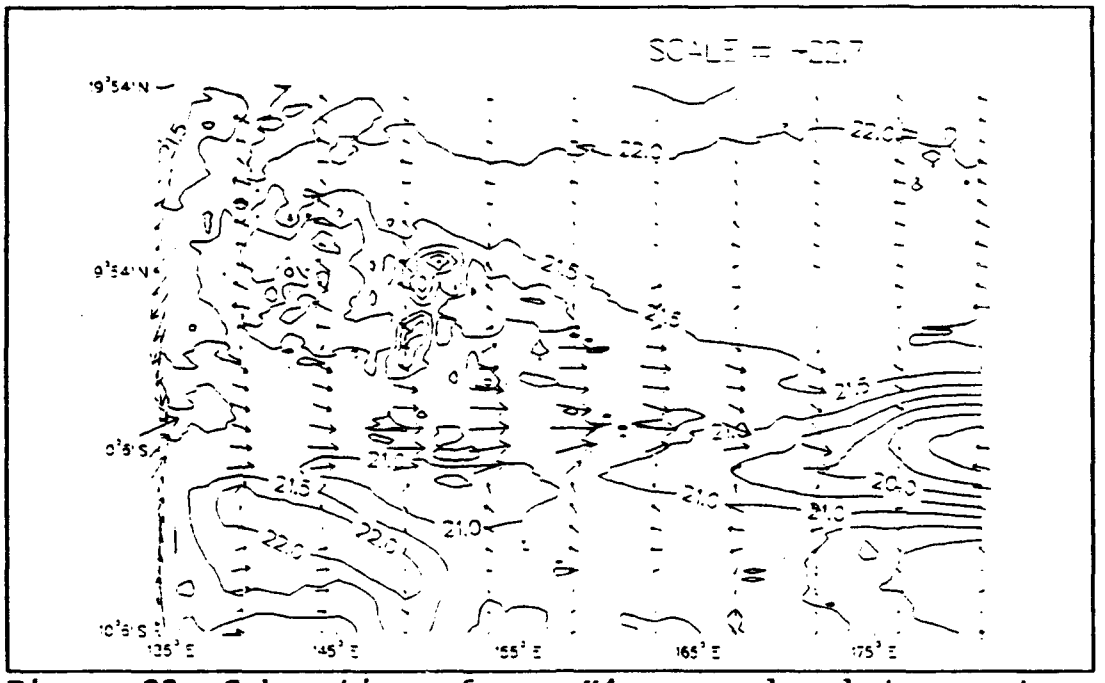

Figure 83. Subsection of run X4 upper level temperature (°C) and currents (cm/s) for 13 November 1992.

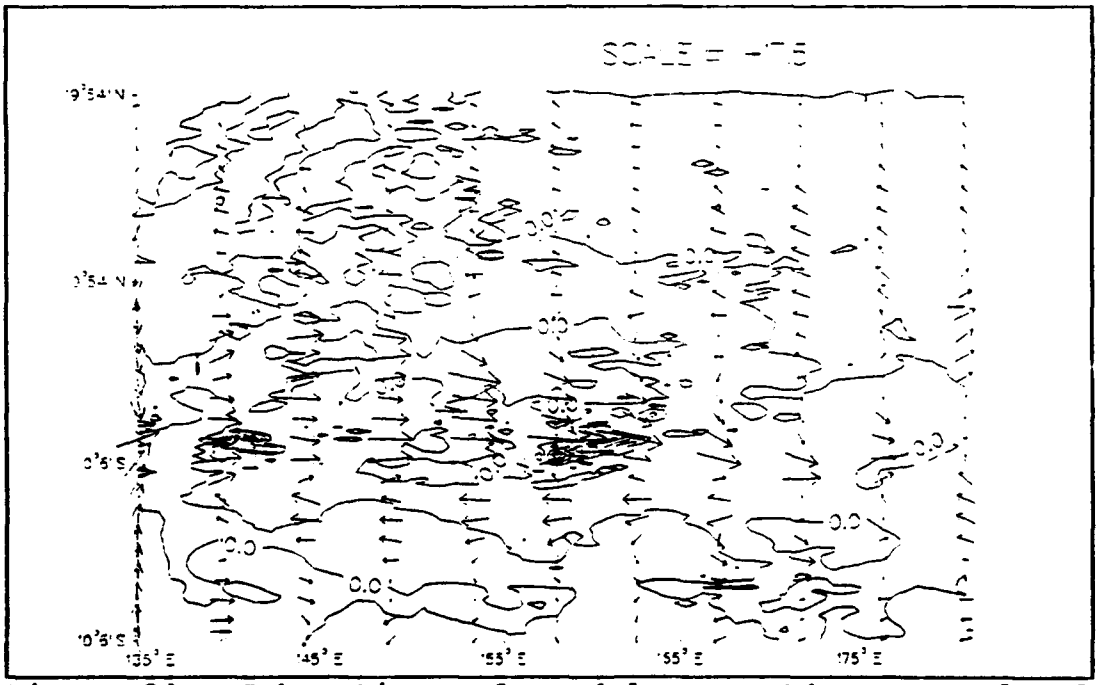

Figure 84. Subsection of model run X4 upper level temperature anomaly (°C) and currents (cm/s) for 15 November 1992. Dashed (solid) contours indicate cooler (warmer) temperatures. Contour interval is .5°C.

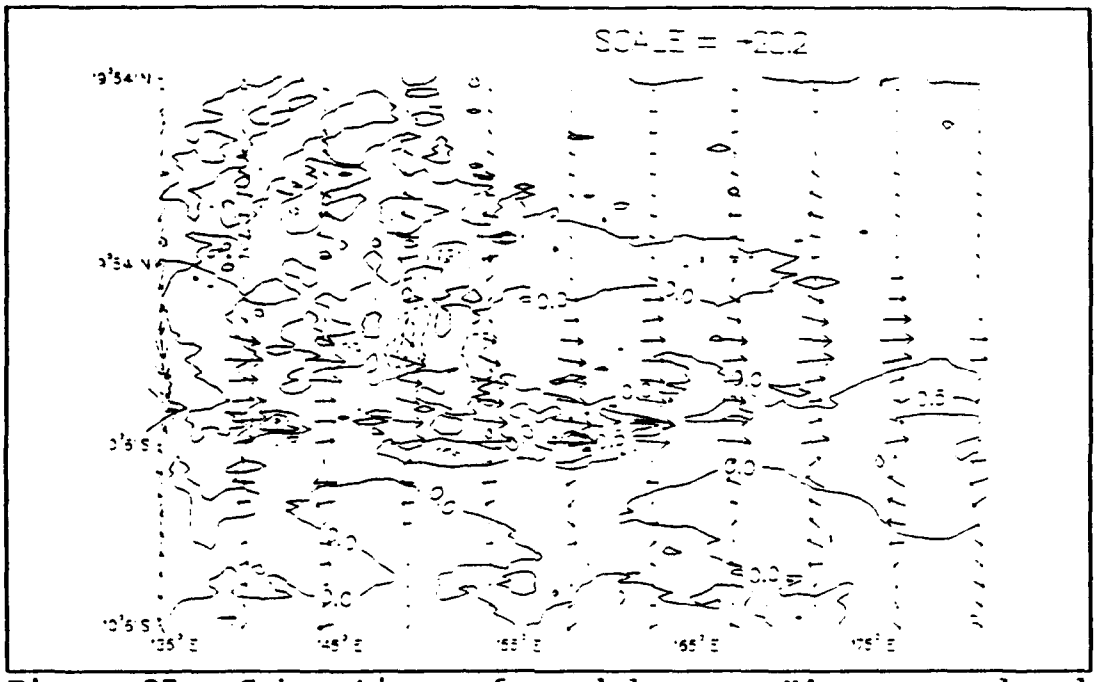

Figure 85. Subsection of model run X4 upper level temperature anomaly (°C) and currents (cm/s) for 17 November 1992. Dashed (solid) contours indicate cooler (warmer) temperatures. Contour interval is .5°C.

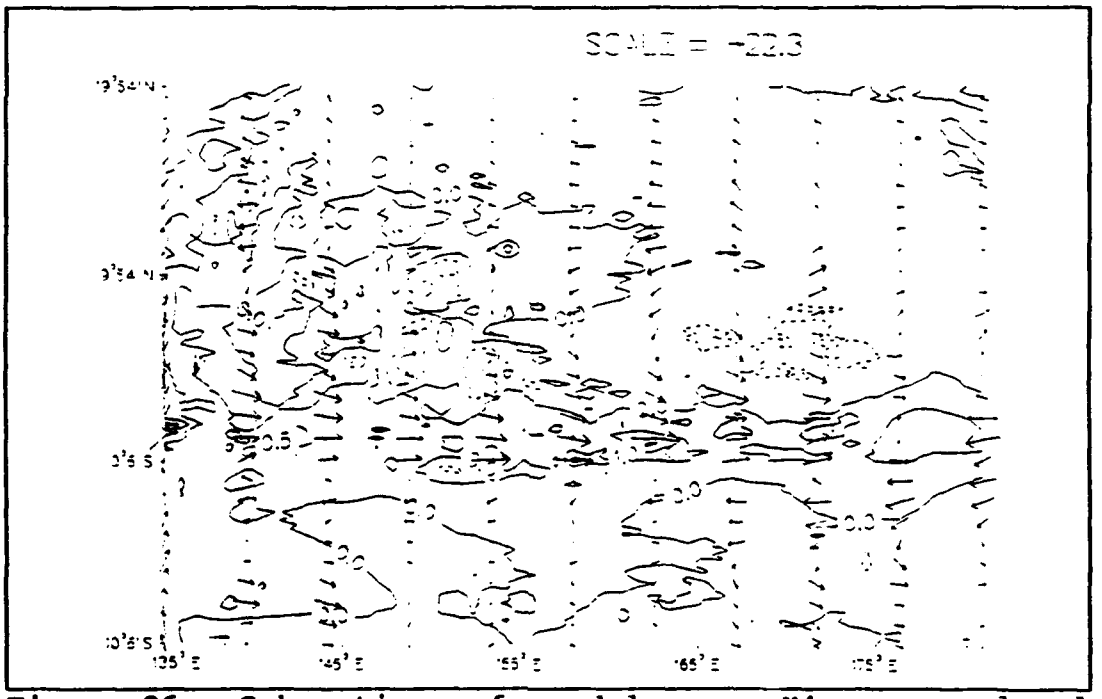

Figure 86. Subsection of model run X4 upper level temperature anomaly (°C) and currents (cm/s) for 19 November 1992. Dashed (solid) contours indicate cooler (warmer) temperatures. Contour interval is .5°C.

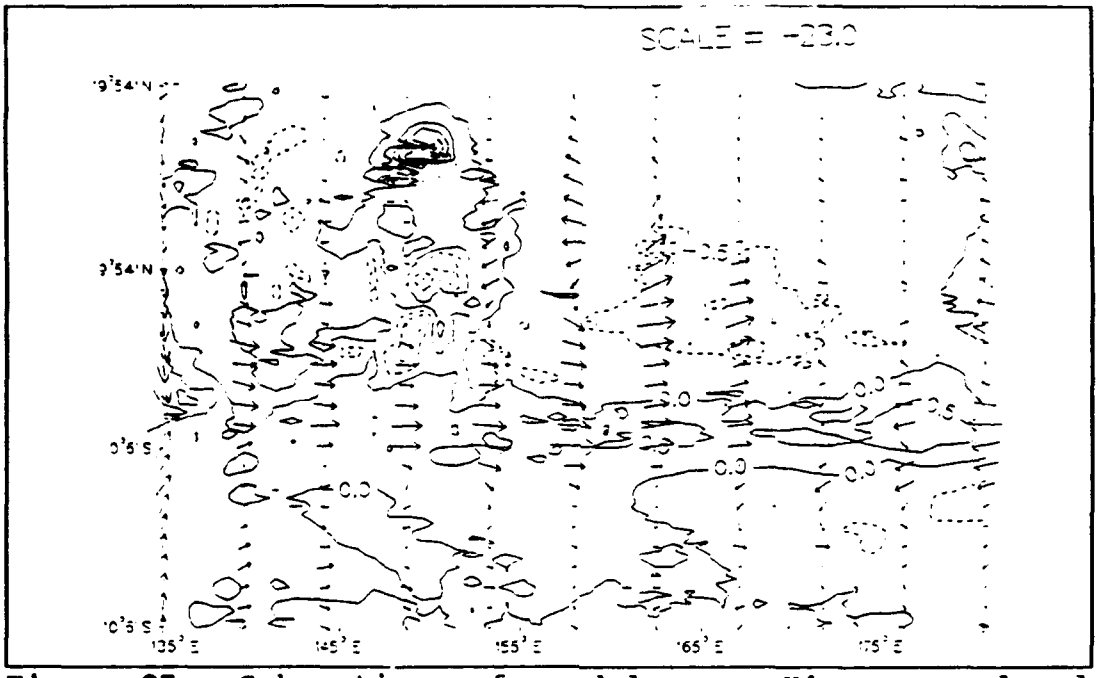

Figure 87. Subsection of model run X4 upper level temperature anomaly (°C) and currents (cm/s) for 21 November 1992. Dashed (solid) contours indicate cooler (warmer) temperatures. Contour interval is .5°C.

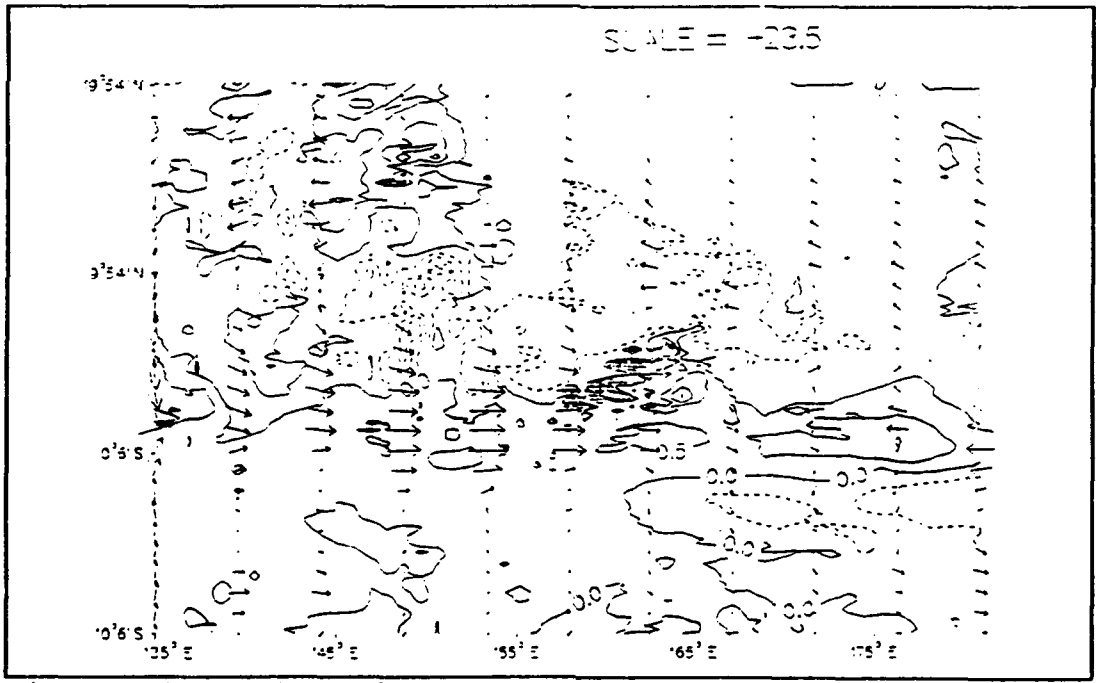

Figure 88. Subsection of model run X4 upper level temperature anomaly (°C) and currents (cm/s) for 23 November 1992. Dashed (solid) contours indicate cooler (warmer) temperatures. Contour interval is .5°C.

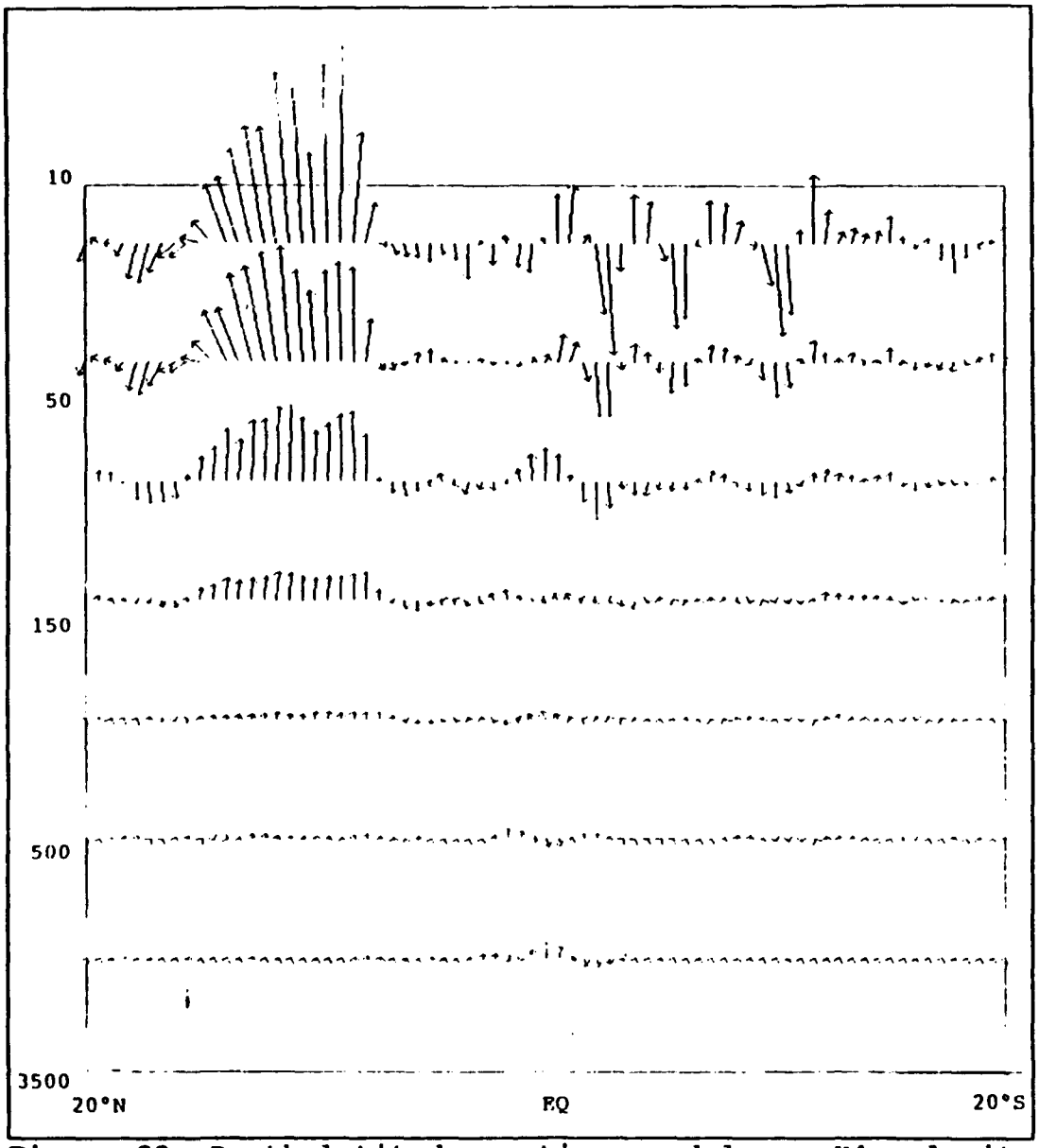

Figure 89. Depth-latitude section, model run X4 velocity field (cm/s) at 159°E on 21 November 92, in the region of upwelling near typhoon Gay. Vertical velocity exaggerated by factor of 86400. Longest vector equals vertical velocity of .2 m/day

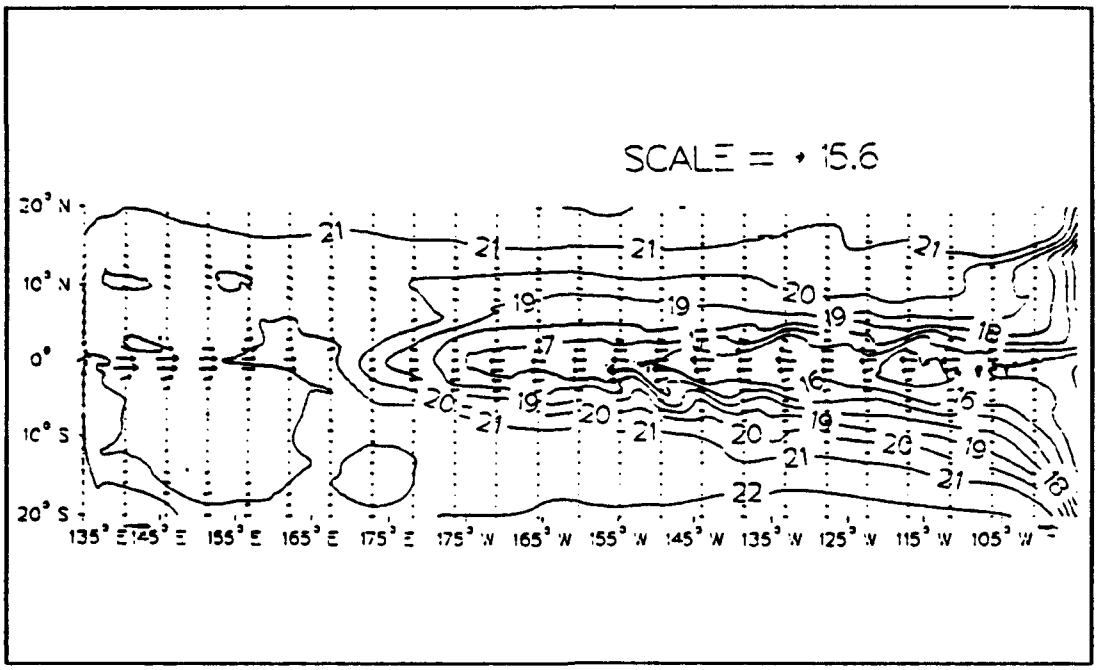

Figure 90. Model run X5 upper level temperature (°C) and currents (cm/s) on 26 March 1992. For comparison to model run X4 (Figure 60).

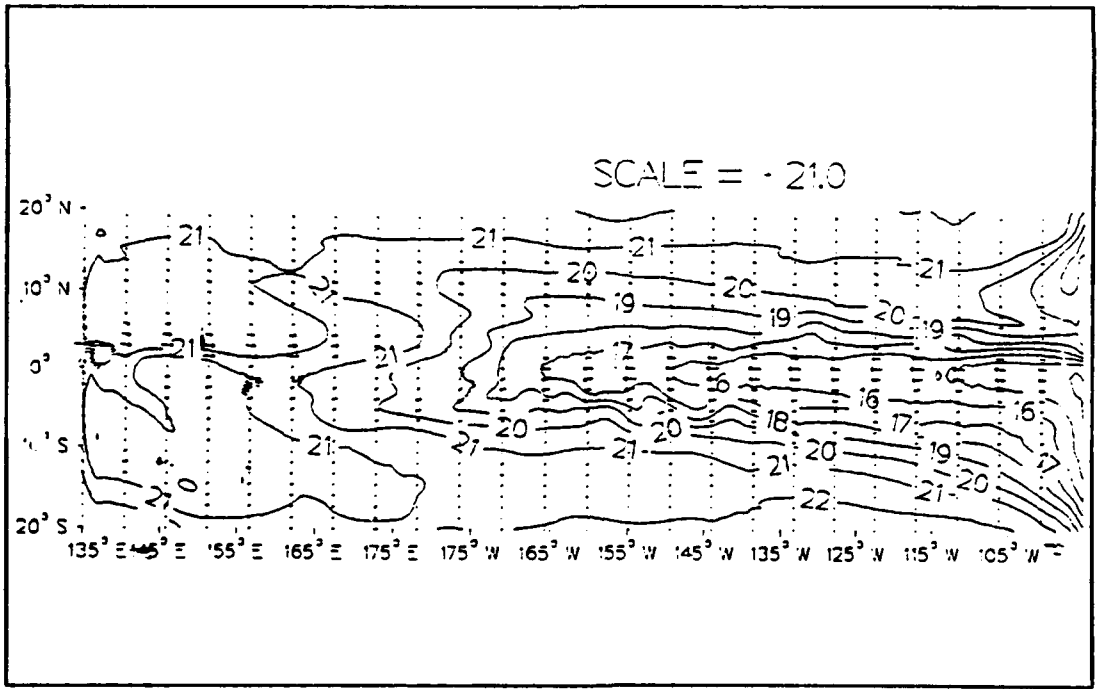

Figure 91. Model run X5 upper level temperature (°C) and currents (cm/s) on 12 July 1991. For comparison to model run X4 (Figure 61).

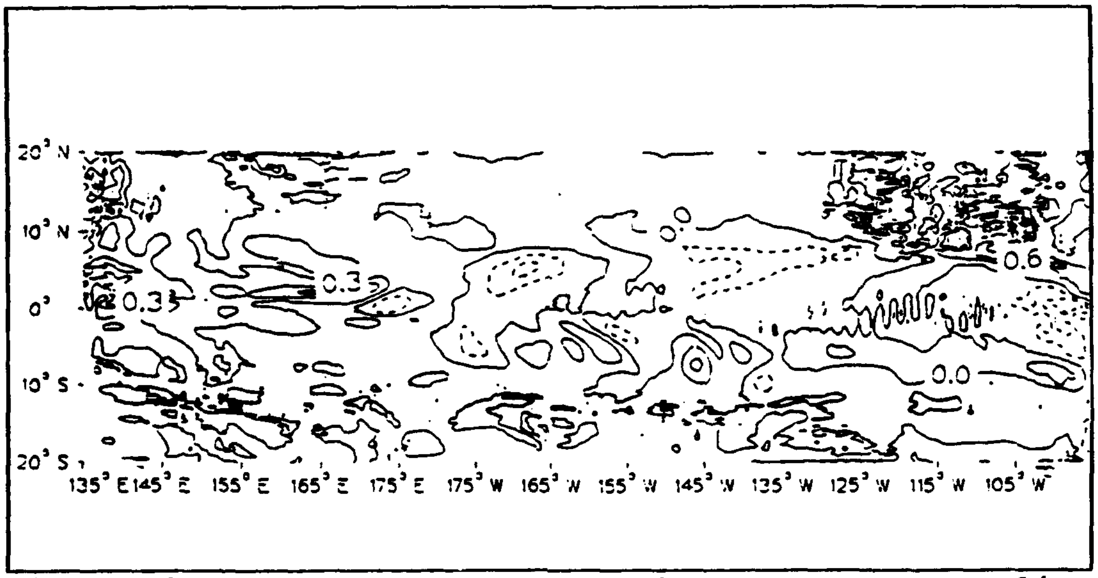

Figure 92. Model run X5 upper level temperature anomalies (°C) on 1 October 1991. Positive anomalies indicate model run X5 was warmer than X4. Dashed (solid) contours indicate cooler (warmer) temperatures. Contour interval is .3°C.

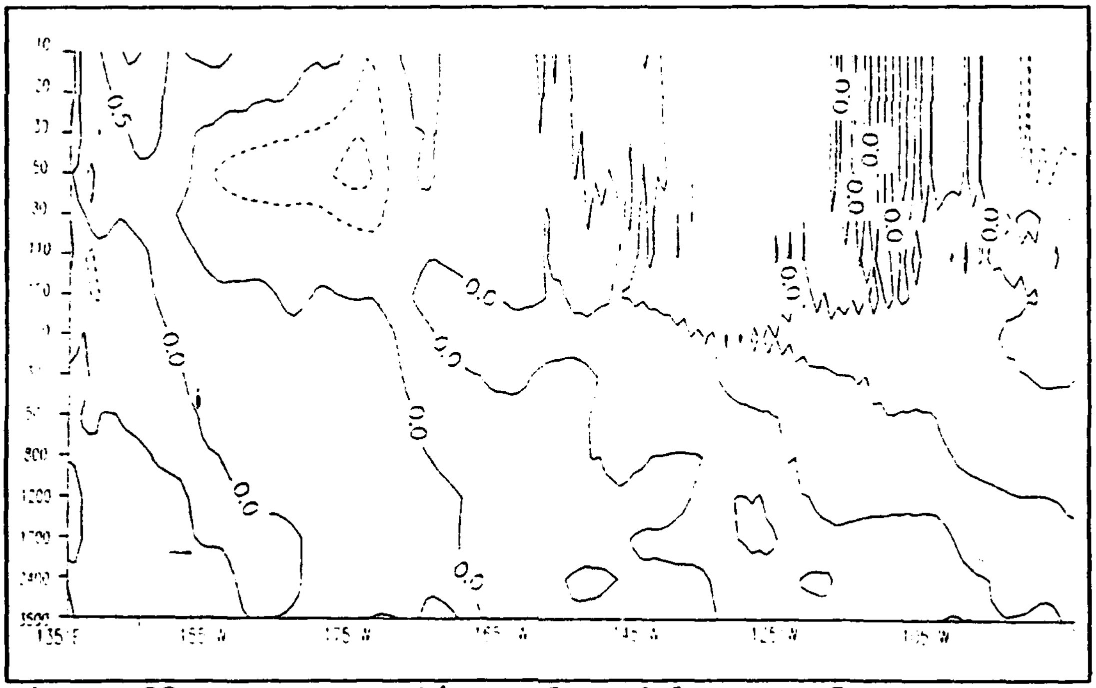

Figure 93. Cross section of model run X5 temperature anomalies (°C) on 1 October 1991. Positive anomalies indicate model X5 was warmer than X4. Dashed (solid) contours indicate cooler (warmer) temperatures. Contour interval is .5°C.

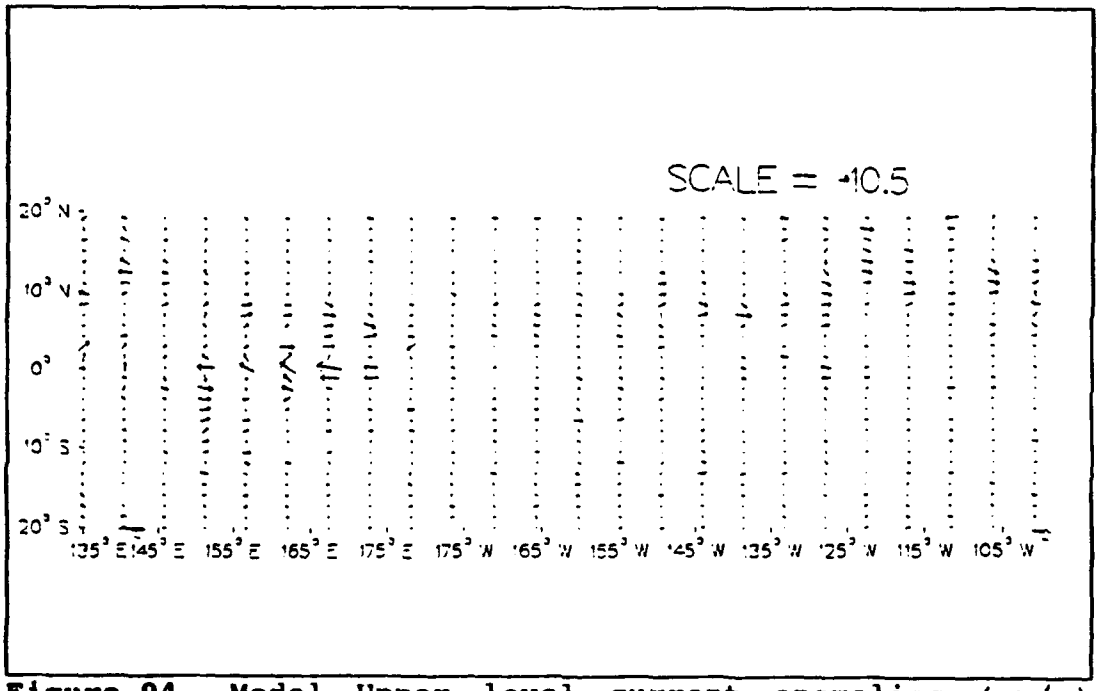

Figure 94. Model Upper level current anomalies (cm/s) showing the difference between model run X5 and X4 on 1 October 1991.

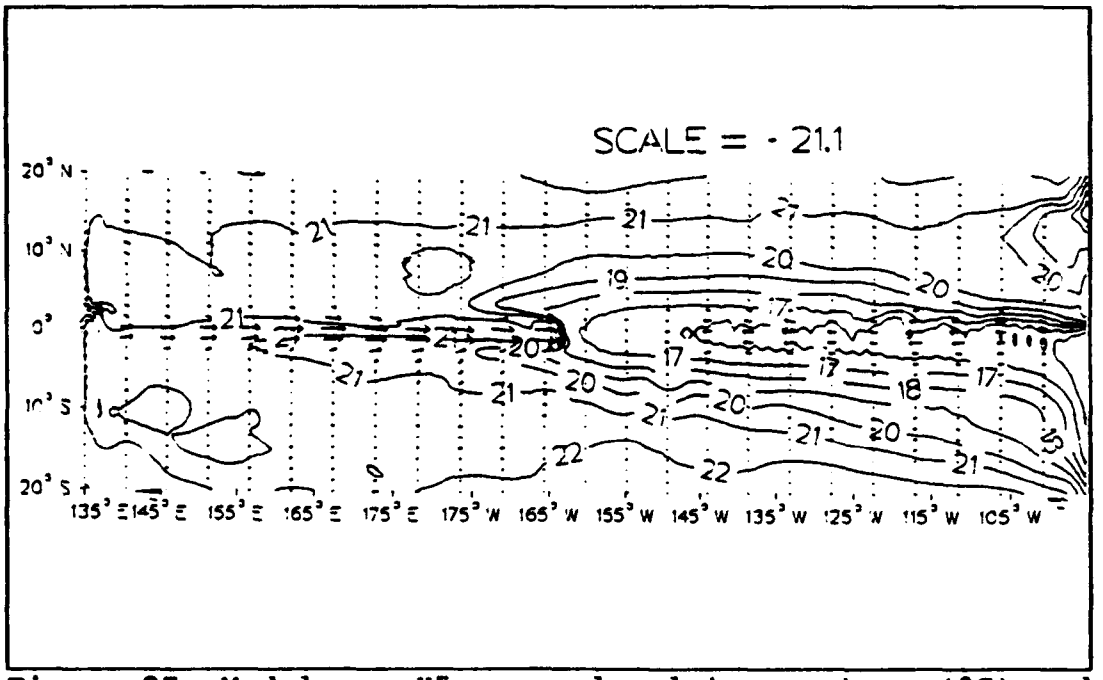

Figure 95. Model run X5 upper level temperature (°C) and currents (cm/s) on 11 December 1991. Showing the strong eastward surface current on the equator. Compare to run X4 (Figure 66).

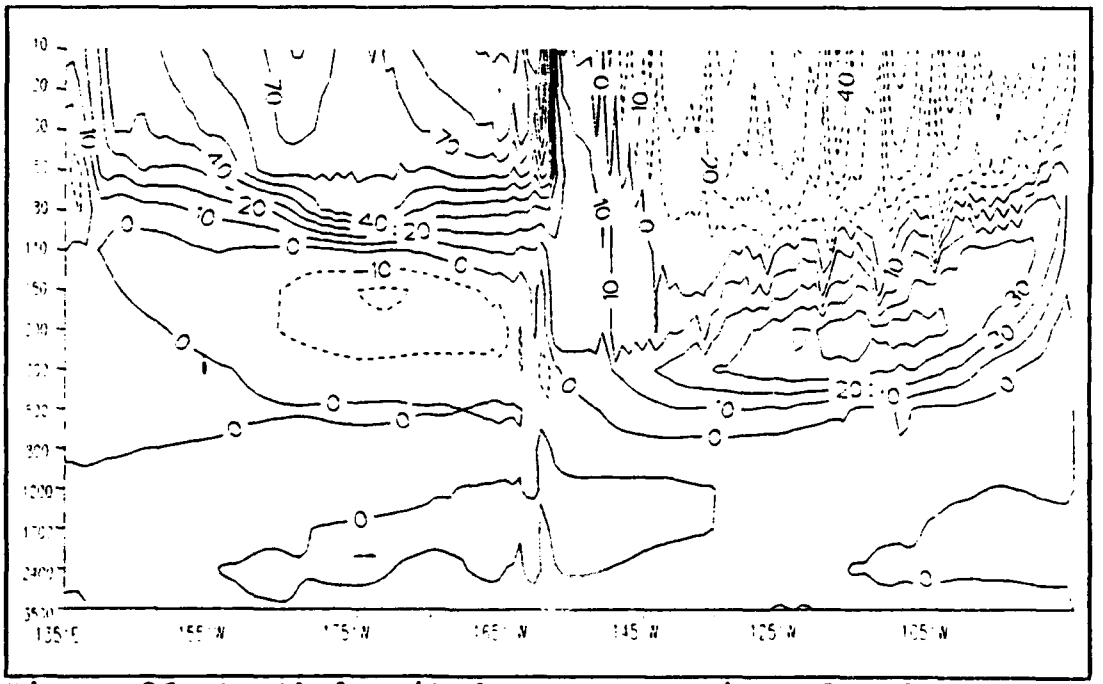

Figure 96. Depth-longitude cross section of model run X5 zonal currents (cm/s) along the equator on 11 December 1991. Compare to run X4 (Figure 67). Dashed (solid) contours indicate westward (eastward) flow.

IV. SUMMARY

A. DISCUSSION

In this study, a tropical ocean general circulation model with an imbedded mixed layer has been used to investigate the tropical Pacific ocean's response to daily varying winds and westerly wind bursts.

The model was tested using several different basin sizes with the larger basin sizes giving the most realistic results. The smaller basin size runs did develop the same major features as the larger runs and were very useful for studying small scale or short time frame effects. The increases in basin size led to faster current speeds, with the EUC reaching a maximum speed in run X4 of greater than 70 cm/s. This is still slower than the observed speeds of approximately 150 cm/s (Pond and Pickard 1983) but is a large improvement over the speeds (about 30 cm/s) seen in the small basin runs.

The runs with the largest domain size (runs X3, X4, and X5) and with two years of daily varying wind stress for 1991-1992 developed three retreats of the cold tongue. The first retreat was a weak event compared to the later two retreats. This weak retreat may have been associated with passage of a weak Kelvin wave across the model domain that was created by

strong westerly wind bursts in March through May of 1991 (cf. Phoebus and Kindle 1993).

The second major retreat of the cold tongue corresponds well with the mature phase in December 1991 - May 1992 of the 1991-92 El Niño. This retreat can again be tied to an increase in westerly wind bursts in the western Pacific during September - November of 1991. Westerly wind bursts continued to occur near the equator in the western Pacific into early 1992. These westerly winds bursts provided the forcing needed to advect warm water to the east.

The third retreat of the model's cold tongue came at the end of 1992 and coincided with the resurgence of the El Niño. This last retreat started later and developed slower than the one a year earlier. Wind stress data from 1993 was not available to see if this equatorial warming in the model at the end of 1992 would have developed as the observed El Niño did.

The model also developed several other features that correspond well with observed phenomena in the Pacific ocean. The model developed tropical instability waves along the equator during the spin-up phase of the model runs. These waves were also present in the variable wind forced runs, but varied in intensity with the strength of the NECC and the SECC. The size and seasonality of these waves match well with similar observed waves.

The model's response to individual westerly wind bursts was checked by looking at the model's response to the strong typhoons that moved through the model's domain. The model developed regions of decreased upper level temperatures in the wake of the typhoons due to increased mixing and upwelling.

The model quite clearly shows the importance of the westerly wind bursts that are associated with tropical cyclones that form near the equator. The cold tongue retreat at the end of 1991 was associated with several typhoons that moved through the western Pacific during October and November. In particular typhoons Yuri and Tia in November 1991 provided the major westerly wind burst forcing for the the model's cold tongue retreat. In November 1992, typhoons Hunt and Gay produced extremely strong westerly winds on the equator that appear to have initiated the retreat of the model's cold tongue at the end of 1992.

Comparisons of model runs X4 and X5 showed that the daily variations in the wind stresses used for this study played an important role in developing both the small scale and transient features, and in developing the basin wide temperature patterns. The temperature differences between these two runs showed that the smoothed winds tended to cause more upwelling and advection of cold water to the west in the eastern half of the model domain, leading to colder eastern Pacific SST's. This is due to the lack of westerly wind bursts in the eastern Pacific that would tend to decrease the

upwelling or advect warm water to the east. The smoothed winds also tended to reduce the amount of warm water advected out of the western Pacific leading to higher SST's in this region. Again, this is caused by the lack of westerly wind bursts that would advect the water to the east. Only during the El Niño period do the westerly wind bursts become strong enough and persistant enough to show up in the average fields as westerly winds.

B. CONCLUSIONS

The model's response to the inclusion of the daily fluctuating winds from NOGAPS gave very encouraging results and allowed the model to develop a realistic El Niño-like response. Comparisons of the model runs forced with daily varying wind stresses and those forced with smoothed wind stresses showed that these differences in forcing produced significant short term, small scale differences in the upper ocean currents and temperatures. In addition, these forcing differences led, over several months of model integration, to intraseasonal, basin wide differences in the currents and temperatures. The runs with daily varying wind stresses also indicate that individual tropical cyclone forcing events play a major role in the model's development of cold tongue retreats and warming of the central and eastern Pacific. Thus, the model's simulation of the 1991-1992 El Niño was enhanced by the use of realistic daily varying wind stresses.

The model's response to the winds is even more impressive given the many simple forcing parameterizations used (e.g., the surface heat flux). For example, the model was able to develop a retreat of the cold tongue without complex temperature and salinity forcing. This highlights the role of westerly wind bursts in the development of an El Niño-like response.

The model's development of an El Niño-like response also shows the usefulness of this model in the study of this major climatological event. The NOGAPS wind forcing data could be obtained and applied to the model on a monthly basis to verify early indications of an El Niño.

Mismatches between the model's upper level temperatures and the observed SST pattern in the ocean are probably the major flaws in the model's depiction of the tropical Pacific. The development in the model of a more realistic subtropical gyre circulation for the return of water to the eastern Pacific should make the long narrow cold tongue in the model more closely resemble the observations.

The model did not properly resolve the deep currents and jets that have been observed in the tropics due to the lack of detailed resolution in the deep ocean. The model also did not develop realistic western boundary currents due to the lack of bottom topography and realistic coastlines. The proper modeling of these features would improve the character of the model results. However, their inclusion should not change the

major features observed in the model's response. This is in partdue to the efforts that were made in this study to reduce the effect either one of these features would have on the upper levels in the central Pacific which is the primary area of focus in this study.

C. RECOMMENDATIONS

Several options for improving the model results are being investigated, and additional efforts to improve the model domain are needed. The inclusion of realistic coastlines and bottom topography should improve the model's results. The north and south boundaries need to be moved further from the equator so the north and south subtropical gyres are properly represented. This increase in the domain should improve the model's upper level temperature field in comparison to observations.

However, the model used for runs X3, X4, and X5 can still be used to investigate many phenomena associated with El Niño. The inclusion of a spatially and temporally varying heating parameter would allow the determination of how variable heating modifies the model's simulation of El Niño. Comparison of the model's results with and without this heating would give an indication of the relative importance of the wind and heating in developing and maintaining an El Niño.

Model runs using monthly climatological winds interpolated to daily values need to be done to determine baseline

variations of the model fields. A comparison of these fields with the results of model run X5 would highlight the importance of the differences in the average wind field in El Niño years versus non-El Niño years. This model run would also provide a more realistic spin-up run for use in later model runs.

Several efforts were made to include biharmonic diffusion in the model to replace the current Laplacian diffusion. The model is unstable when run with both ixed layer physics and biharmonic diffusion. Further work in this area is needed to determine a method of using biharmonic friction with the mixed layer physics.

I was able to identify individual tropical cyclones that played an important part in initiating and maintaining the cold tongue retreat. However, no effort has been made to try to identify specific events that lead to the preconditioning of the cold tongue prior to these events. The identification of individual events that led to the stronger easterlies that created the proper conditions for the cold tongue retreat would be a significant step forward in understanding El Niño.

The model output also needs to be thoroughly analyzed using the same type of statistical methods applied to the observational data by Cooper (1992) and Kent (1993). This work would provide a better way of comparing the model data to the observations than just using visual comparisons. This

would allow a more careful verification of the model's wave patterns and other temporal and spatial variations.

LIST OF REFERENCES

Adamec, D., R. L. Elsberry, R. W. Garwood, R. L. Haney, 1981: An Embedded Mixed-Layer Ocean Circulation Model. Dyn. Atmos. Oceans, **6**, 69-96.

Charnock, H. and Philander, S. G. H., 1989: The Dynamics of the Coupled Atmosphere and Ocean. A Royal Society Discussion, University Press, 315 pp.

Chu, P. C?S., 1988: Extratropical Forcing and the Burst of Equatorial Westerlies in the Western Pacific: A Synoptic Study. J. Metecr. Soc. Japan, **66**, 549-564.

Cooper, G. A., 1992: Local and Remote Response of the Equatorial Pacific Ocean to Westerly Wind Bursts: An Observational Study. Master's Thesis, Naval Postgraduate School, Monterey, California, 103 pp.

Delcroix, T., J. Picuat, and G. Eldin, 1991: Equatorial Kelvin and Rossby Waves Evidenced in the Pacific Ocean Through GEOSAT Sea Level and Surface Current Anomalies. J. Geophys. Res., **96**, 3249-3262.

Garwood, R. W., Jr., 1977: An Oceanic Mixed Layer Model Capable of Simulating Cyclic States. J. Phys. Oceanogr., **7**, 455-468.

Giese, B. S. and D. E. Harrison, 1990: Aspects of Kelvin Wave Response to Episodic Wind Forcing. J. Geophys. Res., **95**, 7289-7312.

Giese, B. S. and D. E. Harrison, 1991: Eastern Equatorial Pacific Response to Three Composite Westerly Wind Types. J. Geophys. Res., **96**, 3239-3248.

Ginis, I. edited by R. L. Elsberry, 1993: Global Perspectives on Tropical Cyclones Chapter 6, Interaction of Tropical Cyclones with the Ocean. Work in progress.

Goerss J. S. and P. A. Phoebus, 1993: Multivariant Optimum Interpolation Analysis of Meteorological Data at Fleet Numerical Oceanography Center. NRL/FR/7531-92-9413., 58 pp.

Halpern, D., R. A. Knox, and D. S. Luther, 1988: Observations of 20-day Period Meridional Current Oscillations in the Upper Ocean Along the Equator. J. Phys. Oceanogr., **18**, 1514-1534.

Haltiner, G. J. and R. T. Williams 1980: Numerical Prediction and Dynamic Meteorology. John Wiley and Sons, 477 pp.

Haney, R. L., 1971: Surface Thermal Boundary Condition for Ocean Circulation Models. J. Phys. Oceanogr., 4, 241-248.

Haney, R. L., 1974: A Numerical Study of the Response of an Idealized Ocean to Large-Scale Heat and Momentum Flux. J. Phys. Oceanogr., 4, 145-167.

Harrison, D. E. and B. S. Giese, 1991: Episodes of Surface Westerly Winds as Observed From Islands in the Western Tropical Pacific. J. Geophys. Res., 96, 3221-3237.

Harrison, D. E. and P. S. Schopf, 1984: Kelvin-Wave Induced Anomalous Advection and the Onset of Surface Warming in El Niño Events. Mon. Wea. Rev., 112, 923-933.

Harvey, R. R., and W. C. Patzert, 1976: Deep Current Measurements Suggest Long Waves in the Eastern Equatorial Pacific. Science, 193, 883-885.

Hibbard B., Paul B., Santek D., Battaiola A., and Maria-Francoise V., 1993: VIS 5D Software. Space Science and Engineering Center at the University of Wisconsin-Madison.

Keen, R. A., 1982: The Role of Cross-Equatorial Tropical Cyclone Pairs in the Southern Oscillation. Mon. Wea. Rev., 110, 1405-1416.

Kent, J. E. 1993: Air - Sea Interaction Patterns in the Equatorial Pacific. Master's Thesis, Naval Postgraduate School, Monterey, California, 210 pp.

Kousky, V. E. 1991: Climate Diagnostic Bulletin (May-September 1991), Climate Analysis Center, U.S. Department of Commerce, Washington, D. C., 91/5-91/9.

Kousky, V. E. 1992a: Climate Diagnostic Bulletin (October 1991-June 1992), Climate Analysis Center, U.S. Department of Commerce, Washington, D. C., 91/10-92/6.

Kousky, V. E. 1992b: Climate Diagnostic Bulletin (October 1992-January 1993), Climate Analysis Center, U.S. Department of Commerce, Washington, D. C., 92/10-93/1.

Kousky, V. E. 1992c: Climate Diagnostic Bulletin (September), Climate Analysis Center, U.S. Department of Commerce, Washington, D. C., May. 92/9.

Latif, M., 1986: Tropical Ocean Circulation Experiments. J. Phys. Oceanogr., **17**, 246-263.

Legeckis, R., 1977: Long Waves in the Eastern Equatorial Pacific Ocean: A View From a Geostationary Satellite. Science, **197**, 1179-1181.

Luther, D. S., D. E. Harrison, and R. Knox, 1983: Zonal Winds in the Central Equatorial Pacific and the Onset of El Niño. Science, **222**, 327-330.

McCreary, J. P., 1976: Eastern Tropical Ocean Response to Changing Wind Systems: With Application to El Niño. J. Phys. Oceanogr., **6**, 632-645.

McCreary, J. P. and D. L. T. Anderson, 1984: A Simple Model of El Niño and the Southern Oscillation. Mon. Wea. Rev., **112**, 934-946.

McCreary, J. P. and D. L. T. Anderson, 1991: An Overview of Coupled Ocean-Atmosphere Models of El Niño and the Southern Oscillation. J. Geophys. Res., **96**, 3125-3150.

McPhaden, M. J., H. P. Freitag, S. P. Hayes, B. A. Taft, S. Chen, and K. Wyrtki, 1988: The Response of the Equatorial Pacific Ocean to a Westerly Wind Burst in May, 1986. J. Geophys. Res., **93**, 10589-10603.

Miller, A. J., J. M. Oberhuber, N. E. Graham, and T. P. Barnett, 1992: Tropical Pacific Ocean Response to Observed Winds in a Layered General Circulation Model. J. Geophys. Res., **97**, 7317-7340.

Pickard G. L. and W. J. Emery, 1990: Descriptive Physical Oceanography. Pergamon Press, 320 pp.

Philander, S. G. H., 1981: The Response of Equatorial Oceans to a Relaxation of the Trade Winds. J. Phys. Oceanogr., **11**, 176-189.

Philander, S. G. H., N. C. Lau, R. C. Pacanowski, and M. J. Nath, 1989: Two Different Simulations of the Southern Oscillation and El Niño With Coupled Ocean-Atmosphere General Circulation Models. The Dynamics of the Coupled Atmosphere and Ocean. University Press, 315 pp.

Philander, S. G. H., W. J. Hurlin, and A. D. Seigel, 1987: Simulation of the Seasonal Cycle of the Tropical Pacific Ocean. J. Phys. Oceanogr., **17**, 1986-2002.

Phoebus, P. A. and J. C. Kindle, 1993: The Pacific Ocean Response to Equatorial Westerly Wind Events Analyzed by a Global Data Assimilation System. Paper presented at IAMAP-IAHS 1993, Yokohama, Japan, July 11-23, 1993.

Pond, S. and G. L. Pickard, 1983: Introductory Dynamical Oceanography. Pergamon Press, 329 pp.

Rasmusson, E. M. and T. H. Carpenter, 1982: Variations in Tropical Sea Surface Temperature and Surface Wind Fields Associated With the Southern Oscillation/El Niño. Mon. Wea. Rev., **110**, 354-384.

Riehl, H., 1979: Climate and Weather in the Tropics. Academic Press, 611 pp.

Semtner, A. J. and W. R. Holland, 1980: Numerical Simulation of Equatorial Ocean Circulation. Part I: A Basic Case in Turbulent Equilibrium. J. Phys. Oceanogr., **10**, 667-693.

Webster, P. J. and R. Lukas, 1992: TOGA COARE: The Coupled Ocean-Atmosphere Response Experiment. Bull. Amer. Meteor. Soc., **73**, 1377-1416.

Whitney, C. S., 1992: Modeling the Tropical Ocean Response to Westerly Wind Forcing. Master's Thesis, Naval Postgraduate School, Monterey, California, 126 pp.

Wyrtki, K., 1975: El Niño -- The Dynamic Response of the Equatorial Pacific Ocean to Atmospheric Forcing. J. Phys. Oceanogr., **5**, 572-584.

INITIAL DISTRIBUTION LIST

		No.Copies
1.	Defense Technical Information Center Cameron Station Alexandria, VA 22304-6145	2
2.	Librarian, Code 52 Naval Postgraduate School 411 Dyer Rd. RM 104 Monterey, CA 93943-5101	2
3.	Department of Meteorology Code MR/HY Naval Postgraduate School 589 Dyer Rd. Rm 252 Monterey, CA 93943-5114	1
4.	Department of Oceanography Code OC/CO Naval Postgraduate School 833 Dyer Rd. Rm 331 Monterey, CA 93943-5122	1
5.	Prof. J. T. Murphree (Code MR/Me) Department of Meteorology Naval Postgraduate School 589 Dyer Rd. Rm 252 Monterey, CA 93943-5114	1
6.	Prof. R. W. Garwood (Code OC/Gd) Department of Oceanography Naval Postgraduate School 833 Dyer Rd. Rm 331 Monterey, CA 93943-5122	1
7.	Ms. A. Guest (Code OC/Gt) Department of Oceanography Naval Postgraduate School 833 Dyer Rd. Rm 331 Monterey, CA 93943-5122	1
8.	LT Charles A. Weddle Naval Oceanography Command Box 31 FPO AE 09645-5000	1

9. Director Naval Oceanography Division — 1
Naval Observatory
34th and Massachusetts Avenue NW
Washington, DC 20390

10. Commander — 1
Naval Oceanography Command
Stennis Space Center, MS 39529-5000

11. Superintendent — 1
Naval Research Laboratory
7 Grace Hopper Ave. Stop 2
Monterey, CA 93943-5502

12. Dr. Ron Gelaro — 1
Naval Research Laboratory
7 Grace Hopper Ave. Stop 2
Monterey, CA 93943-5006

13. Patricia Phoebus — 1
Naval Research Laboratory
7 Grace Hopper Ave. Stop 2
Monterey, CA 93943-5006